INVESTIGATION OF SPRAY COOLING SCHEMES FOR DYNAMIC THERMAL MANAGEMENT

Vishnu Vardhan Reddy Yata

Thesis Prepared for the Degree of

MASTER OF SCIENCE

UNIVERSITY OF NORTH TEXAS

May 2017

APPROVED:

Huseyin Bostanci, Major Professor
Haifeng Zhang, Committee Member
Zhenhua Huang, Committee Member
Enrique Barbieri, Chair of the Department of
    Engineering Technology
Costas Tsatsoulis, Dean of the College of
    Engineering
Victor Prybutok, Vice Provost of the Toulouse
    Graduate School

Yata, Vishnu Vardhan Reddy. *Investigation of Spray Cooling Schemes for Dynamic Thermal Management*. Master of Science (Engineering Technology), May 2017, 101 pp., 4 tables, 45 figures, 48 numbered references.

This study aims to investigate variable flow and intermittent flow spray cooling characteristics for efficiency improvement in active two-phase thermal management systems. Variable flow spray cooling scheme requires control of pump input voltage (or speed), while intermittent flow spray cooling scheme requires control of solenoid valve duty cycle and frequency. Several testing scenarios representing dynamic heat load conditions are implemented to characterize the overall performance of variable flow and intermittent flow spray cooling cases in comparison with the reference, steady flow spray cooling case with constant flowrate, continuous spray cooling. Tests are conducted on a small-scale, closed loop spray cooling system featuring a pressure atomized spray nozzle. HFE-7100 dielectric liquid is selected as the working fluid. Two types of test samples are prepared on 10 mm x 10 mm x 2 mm copper substrates with matching size thick film resistors attached onto the opposite side, to generate heat and simulate high heat flux electronic devices. The test samples include: (i) plain, smooth surface, and (ii) microporous surface featuring 100 μm thick copper-based coating prepared by dual stage electroplating technique. Experimental conditions involve HFE-7100 at atmospheric pressure and 30°C and ~10°C subcooling. Steady flow spray cooling tests are conducted at flow rates of 2 - 5 ml/cm².s, by controlling the heat flux in increasing steps, and recording the corresponding steady-state temperatures to obtain cooling curves in the form of surface superheat vs. heat flux. Variable flow and intermittent flow spray cooling tests are done at selected flowrate and subcooling conditions to investigate the effects of dynamic

flow conditions on maintaining the target surface temperatures defined based on reference

steady flow spray cooling performance.

ACKNOWLEDGEMENTS

TABLE OF CONTENTS

LIST OF TABLES

LIST OF FIGURES

NOMENCLEATURE AND ABBREVIATIONS

A   Area of heater surface, cm^2

CHF   Critical heat flux, W/cm^2

c_p Specific heat at constant pressure, J/kg-K

DC   Duty cycle, %

h   Heat transfer coefficient, $kW/m^{2o}C$

h_{fg} Latent heat of vaporization, $kJ/kg°C$

HTC   Heat transfer coefficient, $kW/m^{2o}C$

I   Current, A

k   Thermal conductivity, $W/m°C$

K_p Proportional gain

MS-E   Microporous Surface - Electroplated

PID   Proportional-Integral-Derivative

q"   Heat flux, W/cm^2

Q   Total volumetric flow rate of spray

RS   Reference surface

T_{avg} Average temperature, °C

T_{sat} Saturation temperature, °C

T_{surf} Surface temperature, °C

T_{in} Inlet temperature, °C

T_i	Integral time constant
T_d	Derivative time constant
TC	Thermocouple
V	Voltage, V
x	TC to spray surface distance in heater wall, m
ΔT_{sat}	Surface superheat, °C
ΔT_{sub}	Degree of subcooling ($T_{sat} - T_{in}$)
ρ_f	Liquid density, kg/m^3
η	Efficiency

CHAPTER 1

INTRODUCTION

Thermal management is necessary for the efficient and reliable operation of many devices and systems used in computing, power electronics and electro-optics applications such as computer chips, insulated gate bipolar transistors, solid state lasers, phased-array radar sensors, directed energy weapons, signal processing systems, hypersonic flight structures and high Mach engines. Certain challenging applications require thermal management technologies that are capable of removing high heat fluxes up to 1000 W/cm^2 and some of the systems need to be operated with in a few ^{0}C and medium temperature range for that device to function safely.

Today's electronics industry is aiming towards the light-weight and compact systems, where there is a need of efficient heat removal techniques. Apart from this, space technologies are in need of efficient thermal management techniques with reduced mass and size that are capable of handling high heat loads with fine temperature control that can be operated in any orientation. If proper thermal management technique is not equipped with these systems, there is high chance for temperature related failures to occur, where these failures may be temporary but in some cases it is permanent. In order to avoid these failures, there is a necessity of implementing proper thermal management technologies.

The need for high heat flux cooling techniques is driven very much by the microelectronics and semiconductor industry. In accordance with Moore's law, advancements in the semiconductor industry allow the device size to shrink and increase the transistor density, switching speeds to double every one and half to two years as illustrated in Figure 1.

Correspondingly, the heat dissipation from the chip increase in proportion if there is no change

in the semiconductor technology.
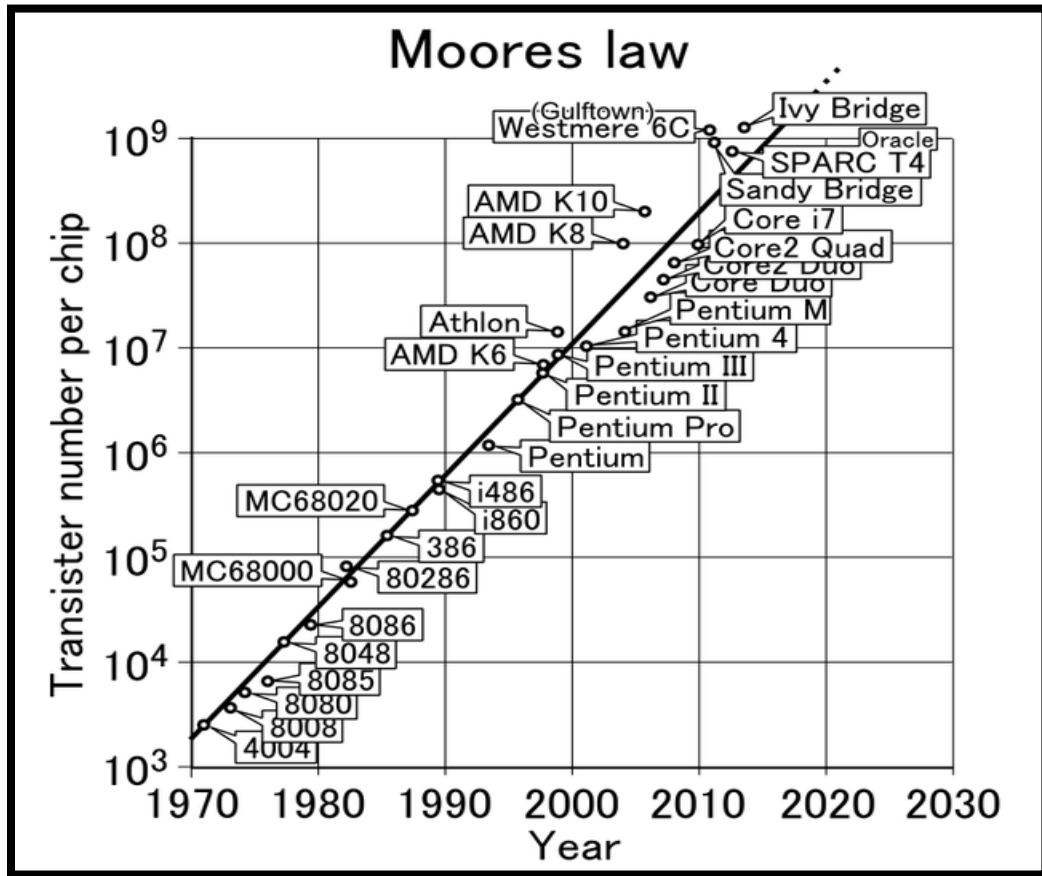
Figure 1: Graph showing number of transistors increasing in a chip yearly [1].

A recent report [2] released by Semiconductor Industry Association (SIA), titled

International Technology Roadmap for Semiconductors 2.0 (ITRS), mention that, by 2040

computing needs more amount of electricity than the world can produce. Due to the continued

efforts by the manufacturers to pack the transistors closer and closer, managing the thermal

output is becoming hard [3]. Unless a method is developed to decrease the thermal loss and

increase the transistor efficiency, there will be a time where dense processors will draw more power to function properly.

In order to overcome all the problems outlined above, there is a need to develop a thermal management technology that can increase the lifetime of the electronic components maintaining the designed efficiency levels. The operating efficiency and the stability of the electronic devices depends on how effectively the heat can be removed from the system. Over the two decades several emerging cooling techniques have been developed for specific applications, but the cooling characteristics of each technique is limited to specific applications.

Table 1 summarizes the existing thermal management technologies including their respective mode of heat transfer, HTC and CHF.

Table 1: Heat transfer capability of various cooling techniques [4], [5]

Heat Transfer Mode	Cooling Technology or Method	Heat Transfer Coefficient (W/cm^2.K)	Critical Heat Flux (W/cm^2) up to
Single Phase	Free Air convection (Finned heat sink)	$0.0005 - 0.05$	15
Single Phase	Forced Air convection (Heat Sink with a Fan)	$0.001 - 0.025$	35
Two Phase	Jet Impingement with water	Up to 20	1000
Two Phase	Microchannel boiling	10 -20	275
Two Phase	Spray cooling with water	$20 - 40$	1200

The choice of an appropriate cooling technique depends on the specific application and the critical system factors which must be satisfied, such as maximum permissible heat flux, heat dissipation potential, reliability considerations, packaging concerns and overall power consumption. Studies show that not only the cooling requirements of the chip have to be met but also their junction temperature needs to be maintained at certain range. Excessive temperatures can melt joints, cause oxidation, and induce thermal stress causing failure of the device. Thus, an appropriate cooling technique is to be preferred in order to sustain the chip with more reliability.

Several thermal management technologies, such as liquid jet impingement cooling, microchannel cooling, and spray cooling, are promising alternatives to accommodate challenging applications. When these technologies are compared based on parameters like removal of high heat fluxes, system mass, volume and power consumption, spray cooling appears to be the most promising.

Spray cooling is one of the active thermal management technologies using external energy to increase the heat transfer rate. Some of the advantages of spray cooling are HTC's up to 500,000 W/m^2K, (or even higher with water or ammonia on enhanced surfaces), high CHF up to 1000 W/cm^2 for water & ammonia, up to 200 W/cm^2 with dielectric liquids like HFE-7100 [6]. Two phase spray cooling can remove high amounts of heat due to latent heat of vaporization; it also uses the coolant effectively, creates uniform surface temperature, avoids temperature overshoot during transition to nucleate boiling regime, and provides the ability to scale-up for large surfaces.

Dynamic flow spray cooling schemes have recently been an area of interest to improve cooling efficiency. Steady flow continuous spray cooling systems are designed to use a flow rate that could satisfy maximum heat load conditions, and dynamic flow is an area of interest in the thermal management of varying heat load conditions such as cold starts, and pulsing power cycles. Continuous spray cooling uses large amounts of coolant liquid with these varying heat loads. Thus, in order to eliminate this issue, researchers have adopted the usage of a miniature solenoid valve to control two major parameters: duty cycle and frequency of spray. By controlling these two parameters with respect to the heat load, cooling efficiency could be improved to a maximum extent thus decreasing the excess use of coolant liquid.

Use of control systems increase in all areas of technology. PID controller is one of them, which is a control loop feedback mechanism commonly employed in industrial control systems. Such feedback mechanism can also be considered to control the surface temperature based on the predefined set point. This can be used to create a variable flow by controlling the pump speed (RPM) based on a set point, and eventually can save pumping power and coolant, and improve the overall efficiency of the spray cooling system.

1.1 Research Objectives

This study aims to experimentally investigate spray cooling schemes for dynamic thermal management, with the following specific research objectives:

1) To investigate spray cooling performance on both plain and microporous surfaces using *steady-flow*, continuous spray.

2) To investigate the spray cooling performance on both plain and microporous surfaces using *dynamic-flow* spray involving (i) *variable-flow*, and (ii) *intermittent-flow* spray conditions.

CHAPTER 2

LITERATURE REVIEW

2.1 Steady Flow Spray Cooling

Spray cooling is carried out by forcing a liquid stream through a small orifice which leads it into a dispersion of fine droplets. These droplets are then directed to impact the heated surface, forming thin discs and interact with each other giving rise to thin liquid film, or it can be evaporated if the spray is dilute. In case of thin film formation, the sprayed liquid flows radially towards that liquid film on the heated surface and absorbs large amount of heat because of several heat transfer mechanisms, including forced convection due to the incoming spray droplets, boiling through surface and secondary nucleation, and the evaporation at the liquid film surface (Figure 2). The performance of the spray cooling process can be further improved to address the terrestrial and space applications. This can be achieved by improving the spray characteristics and heat transfer capability through the novel surfaces.

Bostanci et al. [7] conducted spray cooling experiments using ammonia to investigate the effect of enhanced surfaces on HTC, and this research concluded that, microstructured surfaces offered up to 81% increase in HTC.
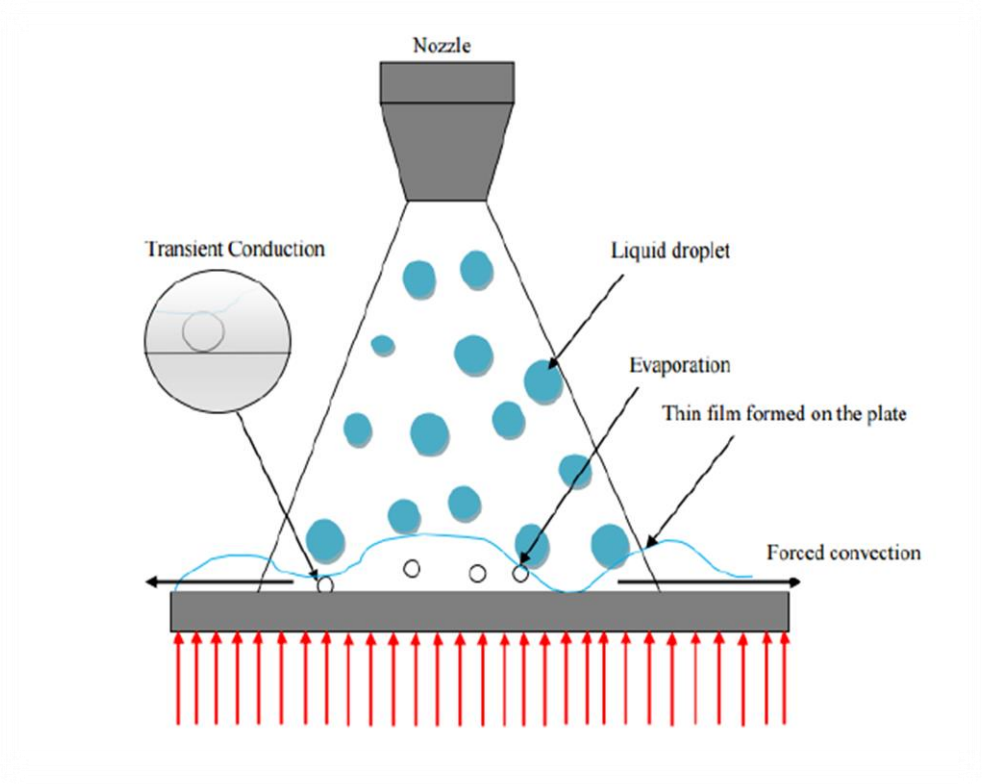
Figure 2: Schematic illustration of spray cooling [8].

There are many types of coolants [9] that are being tested for specific applications. Water has the highest heat removing capability due to its high latent heat of vaporization, but also has a high boiling point and is not very compatible with electronic packages at the end user level. Other refrigerant fluids that can be considered are Fluorinerts (FC- 72, FC-87, HFE-7100 and HFE-7000), performance fluids (PF-5052, PF-5060 and PF-5070) and hydro fluorocarbons HFCs (R134a, R143a and R1234yf). These fluids have low boiling points.

Mudawar et al. [10] conducted tests in pool boiling, flow boiling, micro and mini channel heat sinks, jet impingement, and detachable heat sinks. He explained that these cooling technologies are capable of removing heat fluxes over 100 W/cm^2 with the dielectric liquids

possess relatively poor heat transfer properties. For all coolants, forced convection can greatly improve the heat transfer characteristics when compared to natural convection; however in order to attain superior properties phase change of the liquid is needed. Phase change plays a key role in attaining better heat transfer properties, but it is difficult to implement this to single phase liquid cooling systems. Phase change cooling helps to predict the CHF so that a factor of safety can be assigned to heat dissipation of the device and this CHF can be improved by surface enhancement, subcooling, and high coolant velocity.

Lin et al. [11] found that heat flux increases with the increase in volumetric flux for a given surface superheat and CHF increases with the increase in volumetric flux or pressure drop. In a closed loop spray cooling system, if the vapor is non condensable, it affects the overall heat transfer at lower heat fluxes because of high thermal resistance to condensation heat transfer. CHF is caused by the inability of the liquid to reach the hot surface.

El-Genk and Bostanci [12] conducted saturation boiling experiments using HFE-7100 and concluded that CHF and nucleate boiling heat transfer decreases with the increase of inclination angle, this is due to the increase in vapor accumulation near the surface.

Phase change heat transfer contribution was studied by Kim et al. [13] they conducted spray cooling experiments using a single nozzle with a varying amount of dissolved gas and found that effective subcooling of the liquid increased with the presence of dissolved gas increasing the CHF. Due to the presence of non-condensable gas, it was observed that there is a shift in the saturation temperature of the liquid increasing the subcooling level of the liquid being sprayed.

9

Experiments were conducted by Moreira et al. [14] to find the effect of inclination angle on secondary atomization using water and isooctane droplets on stainless surfaces and observed that the secondary droplet diameters are influenced by the larger inclination angles, but this effect is negligible for smaller inclination angles. It was also observed that particularly at the inclination angle of 90° large secondary droplets stay for longer periods of time and these large secondary droplets are swept away at lower inclination angles due to gravitational forces.

Besides spray characteristics, another key research focus towards improving spray cooling performance has been enhanced heat transfer surfaces. Among various types of surface enhancement techniques, microporous surfaces have recently received particular interest in thermal management technologies. Microporous surfaces act as extended surfaces and dissipate more heat thus making the thermal management process more efficient. When a liquid is sprayed on these surfaces, it utilizes the entire surface area which is more than the regular plain surface.

Kim et al. [15] conducted spray cooling experiments with water on the microporous coating surfaces and observed that these surfaces enhanced the heat removal rate due to the capillary pumping action through the microporous cavities connecting each other. Apart from this, the evaporative spray cooling increased the heat transfer coefficient up to 400% relative to that of the uncoated surface cooled by dry air, and this enhancement was maintained at high heat fluxes by using microporous surfaces.

El-Genk and Ali [16] investigated saturation boiling of PF-5060 dielectric liquid on copper micro-porous surfaces with different thicknesses, and the nucleate boiling results showed better

performance with dielectric liquids on micro- and macro-structured surfaces. Values of CHF are 40–70% higher and more than 17 times those reported on plane surfaces.

Yang et al. [17] conducted spray cooling experiments on plain and microporous coated copper surfaces and found that the boiling incipience temperature is low on microporous coated surfaces when compared with the plain surface. At higher flowrates CHF decreased with subcooling for both surfaces, this is likely due to the limited contact time of liquid droplets with the surface. The CHF increased by 50% to 80% on the microporous coated surfaces when compared with plain surface. At low flow rates, subcooling resulted in higher heat fluxes and CHF throughout the nucleate boiling regime.

Yang et al. [18] in an another research investigated the performance of microporous coated surfaces in nucleate pool boiling and observed that under all tested conditions microporous surfaces showed lower boiling incipience than the plain copper surface. The HTC increased by 50% to 270% from its initial value on the microporous coated surfaces. The CHF was increased by 33% to 60% on the microporous surfaces compared to the plain copper surfaces.

Kandlikar et al. [19] in their research found that pool boiling performance is a characteristic of the surface morphology. After developing different microporous coated surfaces using a dual-stage electroplating process, it was observed that in the second stage at lower current densities, pure copper without any oxides was deposited. When tested it was concluded that microporous coated surfaces with the time duration more than 2500 seconds in the second stage of electroplating showed no significant effect on the pool boiling performance.

You et al. [20] developed microporous coated copper surfaces using dual stage electroplating surfaces with different high current densities and a fixed low current density. When pool boiling experiments were performed using R-123 and FC-72 HTC's were increased by 600% to 700% and CHF by 40% to 70%. Microporous surface prepared with a high current density of 0.5A and a low current density of 0.05A showed better performance over other microporous coated surfaces and the plain copper surfaces.

Jaikumar and Kandlikar [21] studied pool boiling performance on sintered open microchannels and concluded that the surface with a maximum HTC of 565 kW/m²°C showed a better performance with an enhancement of 782% over plain surface.

Xie et al. [22] investigated the effect of different heater surfaces under acceleration in spray cooling and observed that the porous tunnel surface exhibited the best heat transfer capability over the flat and straight fin surfaces. Flowrates and the nozzle heights has the same effect on the spray cooling performance. However, higher flowrates do not always improve the heat flux.

Bica et al. [23] tested micro structured surfaces to study the thermal and fluid dynamics of impacting single droplets. He observed that the micro-textured surfaces improve the cooling performance of the droplets over the plain surfaces, and also promote the increase of the thermal induced atomization. This further gives rise to larger secondary droplets, ejected away from the test surface with a larger momentum.

2.2 Variable Flow Spray Cooling

Wang et al. [24] implemented control systems to investigate novel spray cooling on sintered porous copper. Fuzzy-PID controller is adopted to control the pump to maintain the working temperature of the applications in a safe range. The simulation results conclude that Fuzzy-PID achieved faster response and smaller overshoot than the PID.

Myung and Kim [25] explained a method for tuning the PID controller based on a model reference to control the steam temperature. This was carried out by a simple parameter identification method and validating the simulation results.

Ding et al. [26] implemented PID controls to control the junction temperature of IGBT with high heat flux using water spray cooling system. This research concludes that, the junction temperature of the IGBT component is controlled much better by a Fuzzy PID controller than a conventional PID. This method can control the junction temperature of up to 150°C at 129.96 W.

Reddy and Sai [27] designed a Fuzzy gain scheduler for controlling super heater temperature in power plant. This research concludes that simulation and experimental results showed good performance when compared to PID controller in dynamic and steady state characteristics of all loops. PID controller has given a response with lower rise time and it offers a high settling time and oscillations with peak overshoot. Fuzzy gain scheduler can eliminate these large oscillations providing smooth operation with lower settling time.

2.3 Intermittent Flow Spray Cooling

Intermittent spray cooling characteristics have recently been an area of interest to improve cooling efficiency. Continuous spray cooling systems are designed to use a flow rate that

13

could satisfy maximum heat load conditions and intermittent spray cooling is an area where the heat load conditions vary such as cold starts, and pulsing power cycles. Continuous spray cooling uses a large amount of coolant liquid with these varying heat loads, so in order to eliminate this researchers have adopted the use of miniature solenoid valve to control two major parameters namely duty cycle and frequency of spray. By controlling these two parameters with respect to the heat load, cooling efficiency could be improved to a maximum extent, decreasing the excess use of coolant liquid. There are two research groups in this area have made significant contributions.

Moreira and Panao [28] in their initial work on spray cooling with pulsed sprays, conducted experiments with injection times of 5/10 milliseconds and injection frequencies in the range of 10-30 Hz, maintaining the target surface at a constant temperature before injection started. When the spray impacts onto the target surface, a decrease in the wall temperature occurred for wetted conditions. It was observed that the HTC is higher for these conditions and decreases with an increase in temperature up to the Leiden frost regime, indicating its dependence on the heat transfer regimes affected by the spray droplets at impact region.

Experiments conducted by Moreira and Panao [29] concluded that local heat transfer was increased with increase in frequency in the region of 10-20 Hz and decreased with the further increase in frequency. They also concluded that the heat transfer mechanism in nucleate boiling regime is one of thin film boiling.

In their experimental study on two-phase cooling with multiple intermittent sprays, Moreira and Panao [30] discovered that there is no influence of frequency of injection and

surface temperature on spray characteristics before the impact. Heat transfer process in multiple intermittent sprays is governed by axial velocity of the droplets from the injector and the flux density of droplets. Heat transfer increases with the increase in the flowrate and injection frequency. Multiple pulses avoid thicker films and increase the vapor removal rate improving the efficiency of spray cooling.

Moreira et al. [31] in their research on intermittent spray cooling observed that for some short pulse durations of 5 milliseconds and low frequencies of injection the cooling efficiency increased at the CHF condition. The lag time between successive injections decreases with the increase in frequency of injection, thus increasing the interaction of each injection with the next enhancing the heat transfer at the nucleate regime.

Moreira and Panao [32] conducted intermittent spray cooling experiments to control the surface temperature of a heat generating device. They have concluded that the frequency of injection does not have any significant effect on the spray characteristics. With the increase in the duty cycle keeping the frequency constant, they have found that there was an improvement in the system's thermal response and a higher cooling power. The duty cycle was identified as a dominant parameter enabling accurate control of the spray cooling process. Shorter duty cycles are suggested for a finer control of surface temperature and larger duty cycles for a fast thermal response. Apart from this, low injection pressures and a shorter impingement distances give better performance. When the results are compared with the continuous spray tests, it was observed that there was a potential to save up to 90% of the coolant maintaining similar efficiency levels.

In their research Moreira et al. [33] conducted intermittent spray cooling experiments using a miniature solenoid valve along with multiple jet sprays, and concluded that shorter times between the consecutive injection cycles allows a better distribution of mass flow rates to keep the surface wetted for cooling purposes. Increasing the number of impinging jets leads to the higher heat transfer rates but lower cooling efficiencies. Multijet sprays are most promising in developing the intelligent thermal management techniques.

Tay and Somasundaram [34] conducted both steady state continuous spray and intermittent spray cooling to study the effect of different parameters such as heat flux, flow rate and set point temperature on the fluctuation of surface temperature, valve frequency, HTC, on-off periods, and observed that the temperature fluctuations are minimized only when the surface temperature is at a sufficient superheat, due to the cushioning effect provided by the evaporation or boiling of the liquid film present on the surface during spray off period. Additionally they concluded that the duty cycle increases with increase in the heat flux and with decrease in the set point.

In their experimental study, Tay and Somasundaram [35] observed that the system reaches a time dependent state in intermittent spray cooling. For the considered case, there was a 58% coolant savings for the variable heat flux application. Intermittent spray conditions are fully observed when the ambient temperature was very low in the two-phase regime. It was also found that the intermittent spray cooling has better efficiency when compared with the continuous sprays.

Majaron et al. [36] in their experimental study on intermittent spray cooling related to dermatological laser treatment, found that the highest cooling rates were observed at moderate duty cycle levels. On the other hand, lower duty cycles allow a considerable reduction in the average rate of heat extraction.

CHAPTER 3

EXPERIMENTAL SETUP AND PROCEDURE

This chapter explains the experimental setup and the procedure used in the current research. Detailed description of experimental setup, working fluid, test conditions and procedures are provided in separate sections. This chapter concludes with the uncertainty analysis of the measurements.

3.1 Steady Flow Spray Cooling Setup

Figure 3 represents the schematic view of continuous spray cooling setup. The major components of the experimental setup consist of a spray chamber, a reservoir chamber, a condenser, test heater, temperature and pressure sensors, a gear pump, cartridge heaters, two DC power supplies, and a computer controlled data acquisition system (DAQ). The working fluid (HFE-7100) is contained in the reservoir. This coolant is then circulated through the system using a gear pump. The coolant flows through the filter and the flow meter, and then enters the spray chamber and is sprayed on the heater. As the coolant interacts with the heater surface, phase change occurs and the resulting liquid-vapor mixture flows into the condenser where the vapor gets condensed and stored back into the reservoir. This closed loop cycle continues to operate for each single test.
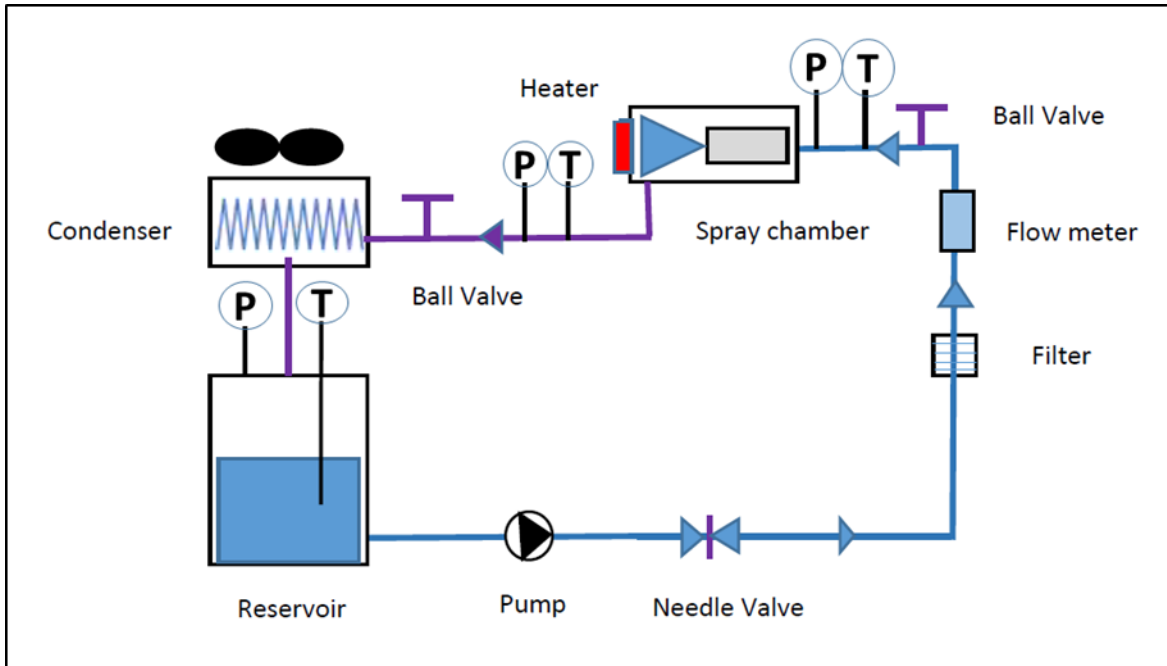
Figure 3: Schematic view of the steady flow spray cooling setup.

Figure 4 shows the reservoir chamber, and is made of polycarbonate material (having outer diameter of 3.5", inner diameter of 3", and height of 4.5") and contains the working fluid (HFE-7100). The top and bottom of this chamber is covered by two stainless steel lids of respective dimensions. The transparent polycarbonate shell provides a clear vision of the scene inside the chamber. The two stainless steel lids are fixed on the top and bottom of the polycarbonate shell and is held tightly using 3 sets of stainless steel bolts and nuts. In order to prevent the leakage of the coolant HFE-7100 in both liquid and vapor form during the tests and even in the idle stage, two O-rings of respective sizes are placed on both top and bottom lids with one ring set on each.
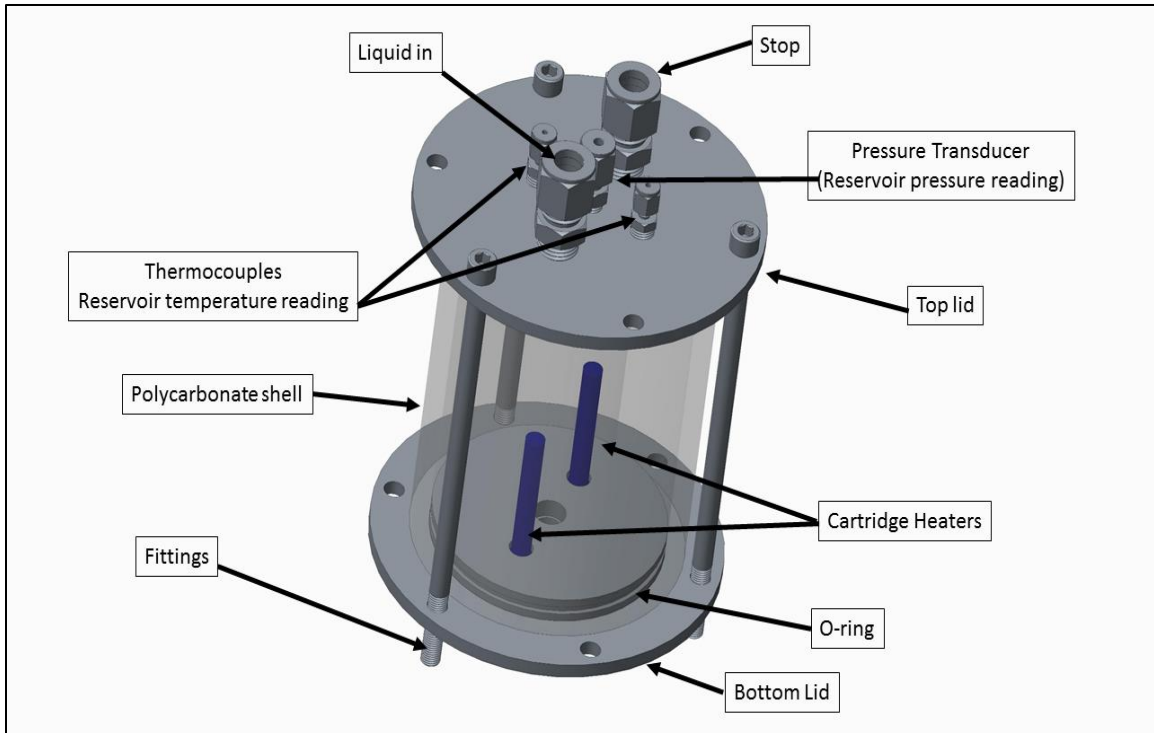
Figure 4: 3D model of the reservoir chamber (created using Creo 2.0).

The top lid has provisions to accommodate two temperature sensors (thermocouples to monitor the temperature of the liquid pool), one pressure sensor (pressure transducer to monitor the pressure of the reservoir when the system is in both on and off conditions), two fittings (to connect the tubing from condenser to carry the condensed coolant back to the reservoir, and to provide a port to fill the coolant). The bottom lid has provisions to accommodate two cartridge heaters (to create the desired test conditions through a temperature controller), and one fitting (to connect the tubing to a gear pump). The gear pump used in this setup is rated to take up to 12 volts and is used to circulate the coolant in the system. It helps to control the pressure and flowrate of the liquid. These two operating parameters help obtain the fine atomization of the liquid depending on the nozzle size. After the pump, a needle valve is installed to do fine

adjustments to the liquid flow rate. A filter of 80-micron size is then fixed to the tubing after the needle valve, and serves the purpose of removing small particulates from the liquid stream before they reach to the nozzle. A flowmeter (a variable area rotameter from Brook's Instruments) with a stainless steel float was installed in the system after the filter. This instrument is used to monitor the flowrate of the coolant in the closed loop cycle. Two ball valves were assembled in between the flowmeter and the spray chamber, one valve is fixed to the stainless steel tubing after the flowmeter followed by the other valve fixed to the tee joint that serves as a port for evacuation of air from the system. Next comes the spray chamber and the heater. Another ball valve is used in-between the condenser and the spray chamber. The condenser used in the system features stainless steel tubing and copper fins. With the help of two fans, this condenser serves to condense the vapor formed during the spray cooling process by rejecting the heat from the coolant to the ambient air. Condensed coolant then proceeds back to the reservoir.

Stainless steel tubing of size 1/4" outer diameter is used from the bottom lid of the reservoir chamber to the inlet of the spray chamber. Stainless steel tubing of size 3/8" is used from the exit of the spray chamber to the inlet of the condenser. The increase in the size of the tubing after the spray chamber is to accommodate the two phase coolant which expands in volume. A 1/4" Teflon tubing is used from the exit of the condenser to the top lid of the reservoir chamber. The entire reservoir chamber and the tubing from the reservoir to the inlet of the spray chamber is insulated to avoid heat loss from the coolant in the sub cooling tests to maintain the inlet temperature of the spray chamber near reservoir temperature.

The spray chamber, shown in Figure 5, consists of an inlet manifold including a strainer, exhaust manifold including a spray nozzle, and a spacer which accommodates a test heater. All parts of the spray chamber are made of stainless steel. When the gear pump circulates the coolant, it enters the inlet manifold of the spray chamber and passes through the strainer, which acts as a second filter in the spray chamber before entering the nozzle. The spray nozzle (a TG0.5 type pressure atomized nozzle from Spraying Systems Company) has an orifice size of 0.61 mm. When the coolant passes through this nozzle a full cone spray is generated at the outlet of the nozzle which further projects onto the test heater and the two phase coolant generated in the exhaust manifold of the spray chamber exits into the condenser through the opening from the bottom of the exhaust manifold.

The heater is mounted on to a spacer which separates the heater from the exhaust manifold and provides spacing for spray do develop and cover the proper area. This spacer has a 1 cm^2 opening which allows spray to expose 1 cm^2 area of the heater. The inlet manifold, exhaust manifold, and the spacer are fixed using four stainless steel screws with end threading one at each corner of the spray chamber. The test heater is fixed to the spacer using four smaller screws. Three O-rings of respective sizes are placed in the provisions provided on the inlet manifold, exhaust manifold, and spacer before fixing the screws for the spray chamber and the heater, to avoid the leakage of the coolant in both liquid and vapor state.
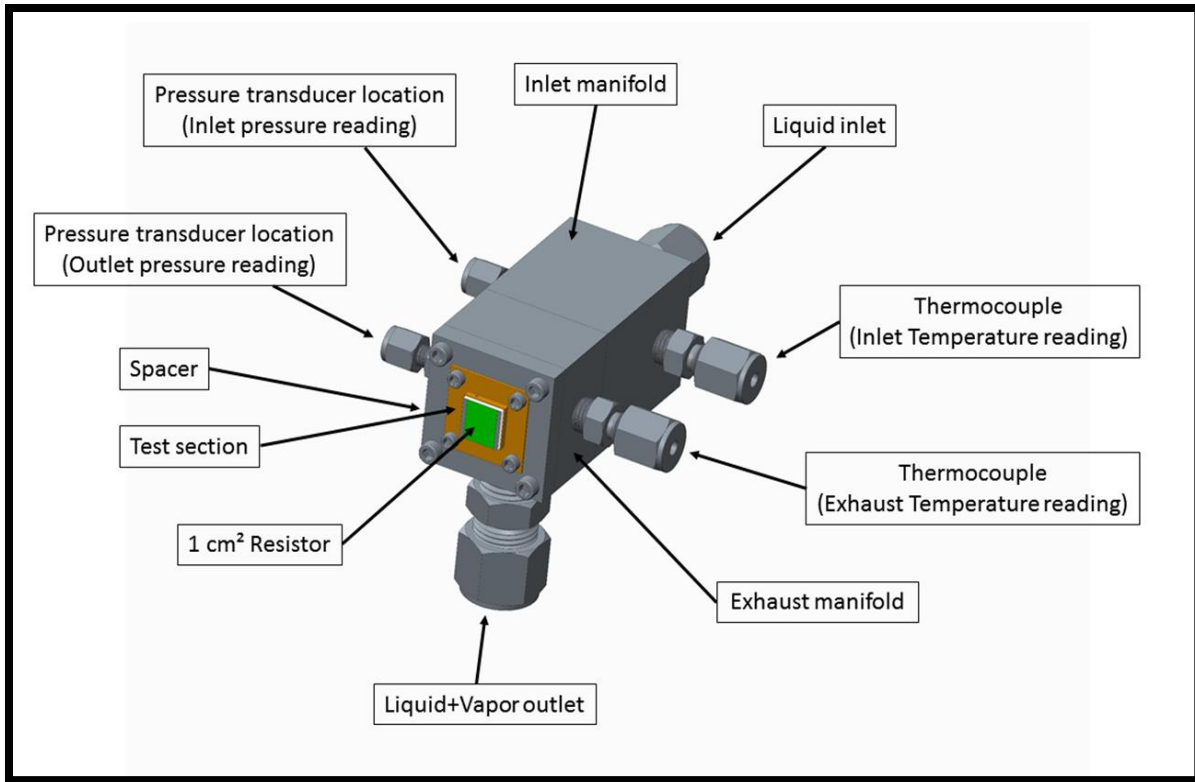
Figure 5: 3D model of the spray chamber parts (created using Creo 2.0).

Figure 6 includes the photographs of the experimental setup developed for continuous spray cooling. The pictures show all the equipment used in the setup. Out of three pressure transducers, one ranging from 0-50 psi is used at the inlet manifold of the spray chamber where the liquid pressure is high. The other two range from 0-15 psi, one is used at the exhaust manifold and the other is used at the reservoir. A programmable DC power supply (from Agilent Technologies) with a capacity of 1500 W (10 A, 150 V) is used to supply heat input to the test heater through a thick film resistor that simulates high heat flux generating device. One more DC power supply is used to supply power to the condenser fans and then to the gear pump. Two thermocouples are used to measure the heater temperature at two different locations on the heater as shown in the Figure 6. Two DAQ modules (National Instruments NI 9213 and 9201) are

used to read and record the temperatures and pressures from all the thermocouples and pressure transducers. These two modules are placed in chassis and is connected to the computer CPU and then powered to AC supply. A fully developed LabVIEW program is used to apply heat flux and record the data in a spreadsheet.
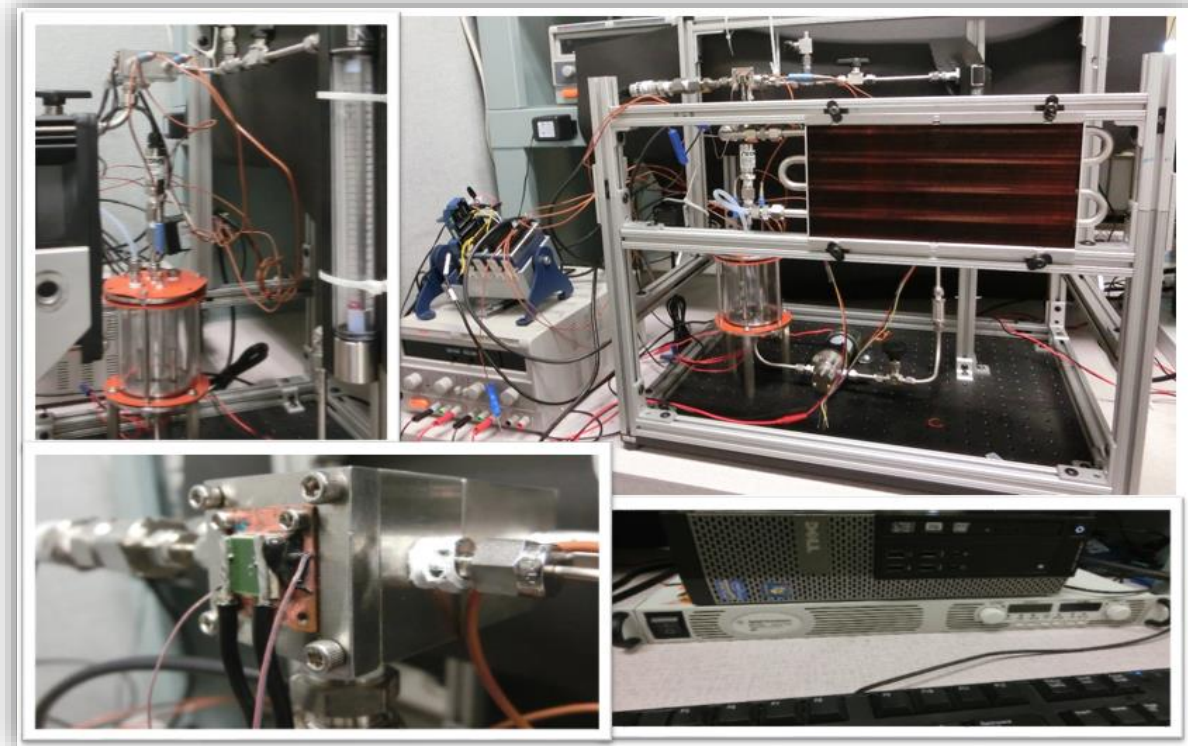
Figure 6: Developed experimental setup for steady flow spray cooling.

3.2 Variable Flow Spray Cooling Setup

The variable flow spray cooling setup is essentially same as the steady flow spray cooling setup. However, the variable flow spray cooling approach requires careful control of the pump. A LabVIEW program is developed to use the PID controller. This controller controls the pump by reacting to the surface temperature of the heater. The only major change in the setup involves

the power supply of the pump. Instead of a standard DC power supply, a programmable DC power supply is used in the variable flow approach, and it is integrated to computer and the PID controller in the LabVIEW program.

A PID controller is used to generate a variable flow by controlling the pump voltage and current. In order to obtain set points and PID parameters for variable flow spray cooling test, a steady flow test was conducted using the microporous surface at a selected flowrate. At each heat flux the steady state surface temperature is recorded and those temperatures are used as set points for the same heat flux inputs. PID parameters are calculated based on a step response of the surface temperature and those calculations are presented in Appendix G.

Even though many advanced controllers exist, PID controllers have influenced all the industries due to their simplicity and easy tuning [37]. To investigate the proposed cooling approach, a simple closed loop spray cooling system with PID controller is designed using Ziegler Nichols [38, 39] open loop tuning rule and experimentally realized the temperature control. It is noted here that since the main technical contribution of this study is to investigate the alternative techniques to implement in spray cooling systems, a simple but very effective PID controller which dominates the industrial applications is adopted [40, 41].

3.2.1 PID Controller

The Proportional Integral Derivative (PID) controller is one of the simplest and widely used controllers today. In process industries, more than 95% of the control loops are of PI or PID type. The controllers come in many different forms. PID control is often combined with logic, sequential functions, selectors, and simple function blocks to build the complicated automation

systems and used for energy production, transportation, and manufacturing. In this study PID controlled is used for high heat flux thermal management. The closed loop system of the proposed variable flow spray cooling based thermal management approach with PID controller is shown in Figure 7.
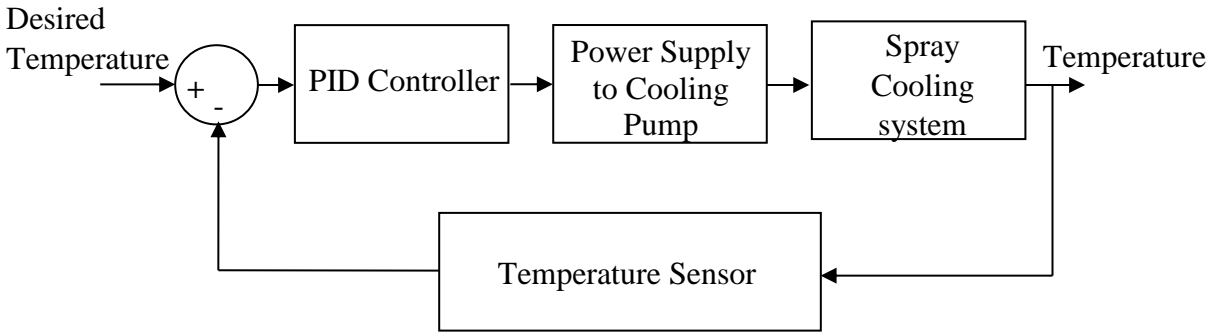
Figure 7: Block diagram of closed loop system for thermal management.

The closed loop system consists of spray cooling system, PID controller, power supply to cooling pump, temperature sensor and an error comparator. The voltage to the pump is varied in step manner, keeping the spray cooling system as a black box. The response of the spray cooling system is observed to be a first order with dead time whose transfer function model is given by

$$G_p(s) = \frac{K}{\tau s + 1} e^{-t_d s} \tag{1}$$

Where K is the system gain, τ is the time constant and t_d is the dead time of the cooling system. The PID controller is designed for the spray cooling system using Ziegler Nichols (ZN) tuning rule as given below.

$$K_p = \frac{1.2\tau}{Kt_d} \tag{2}$$

$$T_i = 2t_d \tag{3}$$

$$T_d = 0.5t_d \tag{4}$$

Where K_p is the proportional gain, T_i is the integral time constant and T_d is the derivative time constant. The law of the PID controller is given by

$$\frac{u(s)}{e(s)} = K_p + \frac{K_p}{T_i s} + K_p T_d s \tag{5}$$

Where, u is the PID controller output, which will vary the manipulated variable, i.e. voltage to the pump, and e is the error. Based on the controller parameters obtained using equations (2), (3) and (4), the closed loop thermal management system is designed with PID controller and temperature sensor (type T thermocouple).

The open loop response of the cooling system is obtained by applying a step input of 0-5V as shown in Figure 8. From the temperature response, the transfer function model of the spray cooling system is found to be

$$G_p(s) = \frac{-2.6}{3.285s + 1} e^{-1.505s} \tag{6}$$

Based on the ZN tuning rule given by equations (2), (3) and (4), the PID controller parameters are computed and are given by: $K_p = -1.007$, $T_i = 0.301$ and $T_d = 0.7525$.
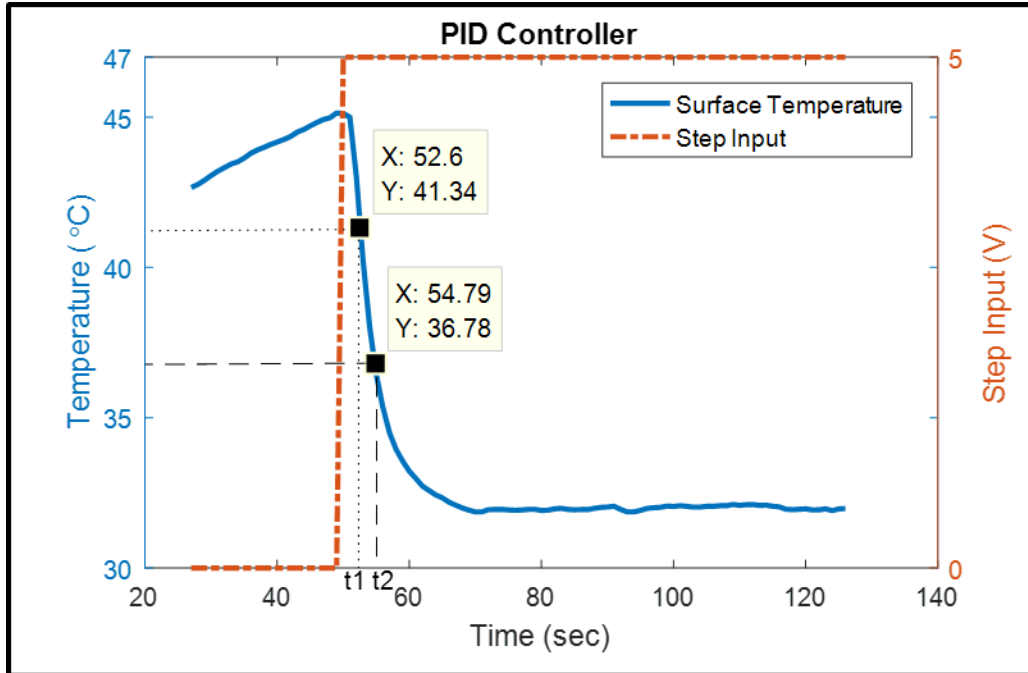
Figure 8: Open loop response of thermal management system.

3.3 Intermittent Flow Spray Cooling Setup

Figure 9 shows the schematic view of intermittent spray cooling setup. This setup is the modified version of the steady flow spray cooling setup where a miniature solenoid valve (Parker, Series 99) is added just before the inlet manifold to create the intermittent spray conditions by regulating the frequency and duty cycle depending on the varying heat load. The response time for this valve is around 5 milliseconds. DAQ NI 9401 module is used to generate a TTL signal necessary to operate the solenoid valve, and NI 9474 module is used to control the TTL signal where the frequency and duty cycle of the spray can be varied. Both of these modules can be fixed into the same chassis used in the continuous spray cooling setup. Few modifications were made to the existing LabVIEW program to control the spray frequency and duty cycle by controlling the solenoid valve.
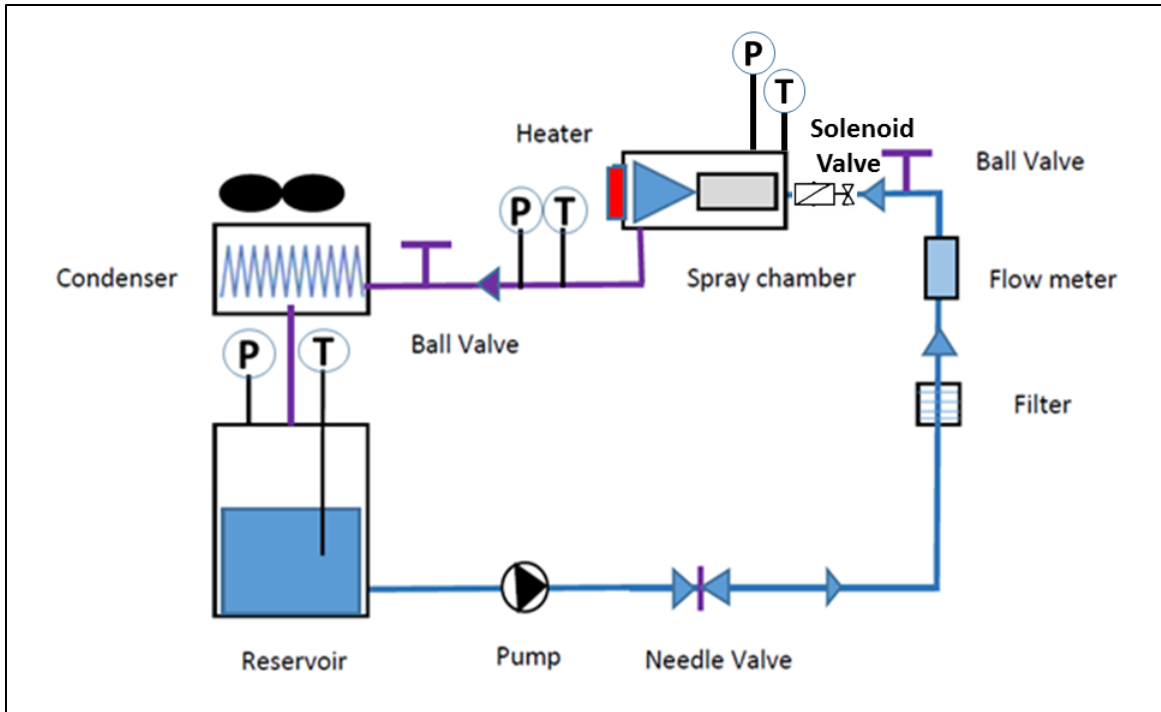
Figure 9: Schematic view of intermittent spray cooling setup.

3.3.1 Peak and Hold Driver Circuit

Solenoid valves are made of electric coils and need to be actuated by providing power supply. As a result, the coil acts as a magnet and pulls the armature to allow fluid flow, and when there is a break in the power supply, it releases the armature which stops the fluid flow through the valve. These electric coils get heated up due to their resistance and overheating can damage the coils. In order to avoid this issue and ensure a reliable valve operation, the rated voltage is supplied for a certain peak time and then the voltage is dropped to hold voltage, which is the minimum voltage required to keep the valve actuated. In this study, the selected solenoid valve has recommended rated (peak) and the hold voltages of 24 V and 5 V, respectively. The peak time is limited to 25 milliseconds.
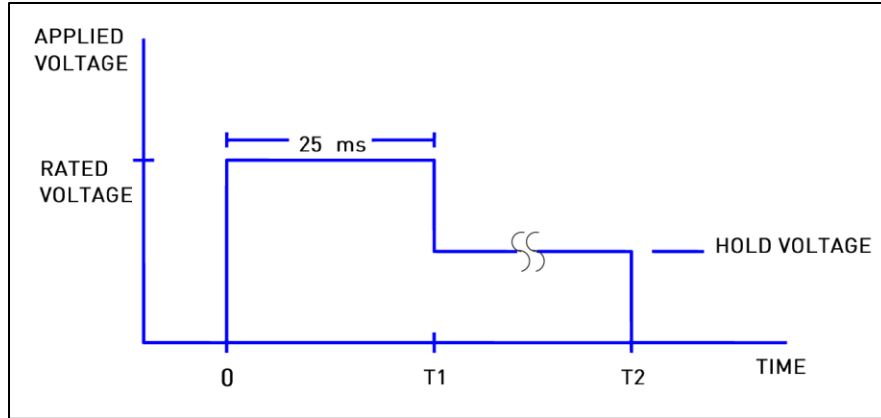
Figure 10: Peak and hold pattern followed by solenoid valve [42].

Peak and hold pattern is created using a peak and hold driver circuit (Applied Processor and Measurement, Model 500) which provides flexibility to adjust the peak time as necessary. The connection diagram is shown in Figure 11.
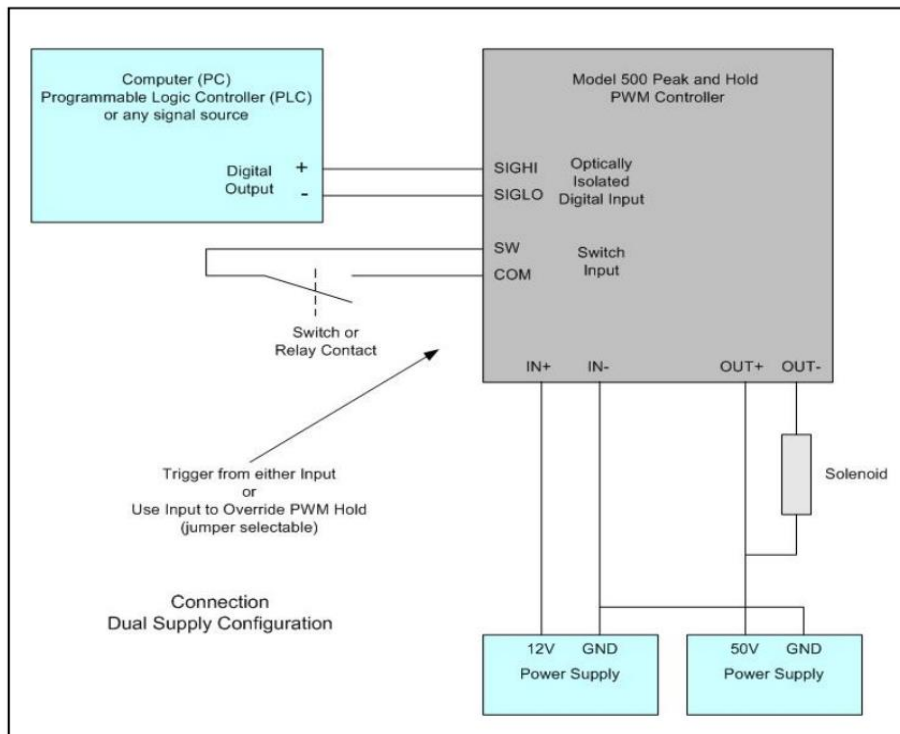

Figure 11: Peak and hold driver connection diagram [43].

3.4 Working Fluid

3M's Novec HFE-7100 methoxy-nonafluorobutane ($C_4F_9OCH_3$) was selected as a working fluid for this research. This is a dielectric liquid and the main reason for choosing this coolant is if needed, dielectric liquids can be directly sprayed on to electronic devices and can eliminate the intermediate layers that are normally used to insulate the electronic devices from coolants. This helps in improving the cooling performance and also enables to design more compact and light weight systems. Additionally, the HFE-7100 has advantages over other dielectric coolants.

HFE-7100 is a clear, colorless and low-odor fluid which is intended to replace ozone-depleting substances (ODSs) and compounds with high global warming potential (GWP) in many applications. This fluid has zero ozone depletion potential and other favorable environmental properties such as chemical and thermal stability, non-flammability and low toxicity that make it useful for many other industrial applications.

Table 2 lists the thermophysical and environmental properties of HFE-7100 dielectric fluid and compares them to those of HFE-7000 dielectric fluid and water. The properties listed in the table are defined at atmospheric pressure of 101.3 kPa. In Denton, TX, the location of this study, the local atmospheric pressure is slightly lower than 101.3 kPa due to its altitude above the sea level.

Table 2: Coolant properties [44], [45]

Saturation thermophysical properties (at 101.3kPa)	HFE - 7100 ($C_4F_9OCH_3$)	HFE-7000 ($C_3F_7OCH_3$)	Water (H_2O)
Ave. molecular weight (g/mole)	250	200	18
Boiling Point (° C)	61	34	100
Freeze Point (° C)	-135	-122.5	0
Latent heat of vaporization (kJ/kg)	111.6	142	2256.7
Liquid thermal conductivity (W/m-K)	0.062	0.075	0.68
Liquid surface tension (N/m)	1.019×10^{-2}	1.24×10^{-2}	5.9×10^{-2}
Liquid specific heat(J/kg-K)	1253	1300	4220
Liquid density (kg/m^3)	1370.2	1400	958
Vapor density (kg/m^3)	9.87	8.17	0.6
Liquid viscosity (kg/m-s)	3.70×10^{-4}	3.2×10^{-4}	2.8×10^{-4}
Environmental Properties			
Ozone Depletion Potential - ODP (yr)	0	0	0
Global warming Potential - GWP (yr)	320	530	0
Dielectric strength (kV)	28	40	-
Dielectric constant	7.39	7.4	80
Flammability range in air	None	None	None

3.5 Test Section

The test section involves a 2 mm thick oxygen free copper piece with a 1 cm^2 (10mm x 10mm) protrusion that is exposed to spray from the nozzle as shown in Figure 12. A matching, 1cm^2-size, 10-Ohms, thick film resistor is soldered through its metallized surface onto the test section, simulating a high heat flux generating device. Heat flux is applied gradually to the heater using a DC power supply (Agilent Technologies) through the two power leads soldered to the thick film resistor. The holes provided on the either side of the projected test section accommodates two thermocouples to record temperatures at each step. These thermocouple readings are used to calculate the surface temperature of the heater. Both smooth and microporous surfaces are prepared on the other side of the test section.
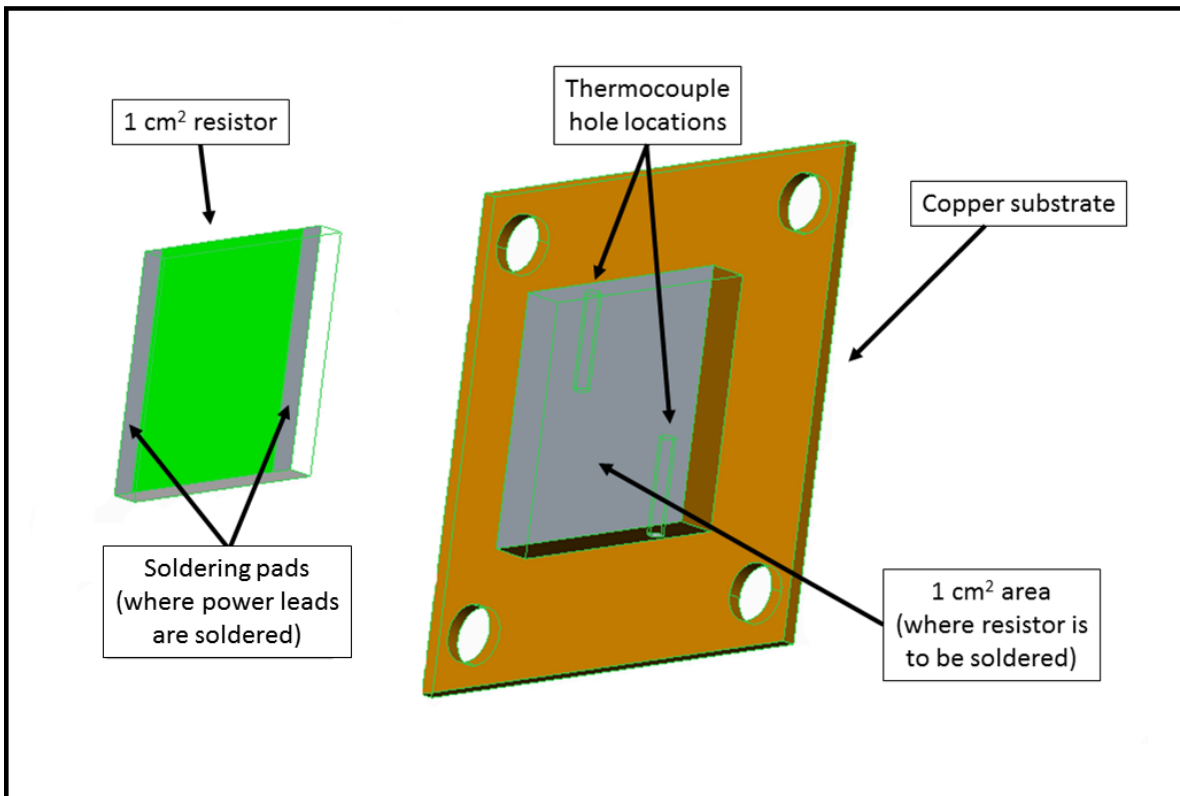

Figure 12: 3D model of the heater surface and resistor (created using Creo 2.0).

33

3.6 Test Surfaces

This section explains the step-by-step procedures in the preparation of test surfaces on 1-cm^2 copper test sections.

3.6.1 Reference Surface Sample Preparation [46]

Step 1: The sample is held down and sanded on 1200 grit sandpaper from left to right, applying medium pressure on the sample for 10 strokes.

Step 2: A polishing pad is mounted on the rotating drum at high speed. A slow and steady jet of water (typically 1 drop/sec) keeps the drum well lubricated.

Step 3: Aluminum oxide (Al_2O_3) solution of 5 μm is applied on the entire pad and the copper sample is held down on the polishing pad at medium pressure for about 30 seconds.

Step 4: Step 3 was repeated with the Al_2O_3 solution of 1 μm and rotating the sample by 90° clockwise directions.

Step 5: Step 4 was repeated with the Al_2O_3 solution of 0.05 μm.

Step 6: The copper sample is held under running water to remove the particles of the Al_2O_3 solution from the surface until a mirror surface finish is seen. This test section is then moved to fabrication process.

3.6.2 Microporous Surface Preparation Using Dual Stage Electroplating Process [20]

A chemical bath is prepared in a beaker using 250 ml of distilled water, 50 grams of cupric sulfate ($CuSO_4$), 17.5 grams of sulfuric acid (H_2SO_4), and 2.5 ml of 2% hydrochloric acid (HCl) and mixed well. To ensure high bonding strength of coatings, the surface of the test heater is rinsed with 2% hydrochloric acid. After the 1 cm^2 area of the test section which exposes to spray is identified and marked, the remaining area is masked to make sure that the metal deposition

34

takes place on the appropriate spray area. The target surface to be coated is then connected to

(-) terminal and a copper anode is connected to (+) terminal of a DC power supply as shown in

the Figure 13. This beaker is then placed on the magnetic stirrer, which helps generate uniform

coating by constantly circulating the chemical bath. The power supply is switched on and a

desired high current density of 0.5 A/cm^2 (area exposed to CuSO$_4$ solution) is maintained for a

fixed duration of 20-30 seconds to build dendrites and nodules, then a fixed low current density

of 0.05 A/cm^2 is supplied for 80 minutes to create the permanent bonding strength of

microporous structures. After completing the process, mask is removed from the test section,

then this microporous surface is rinsed with distilled water and acetone before mounting it on
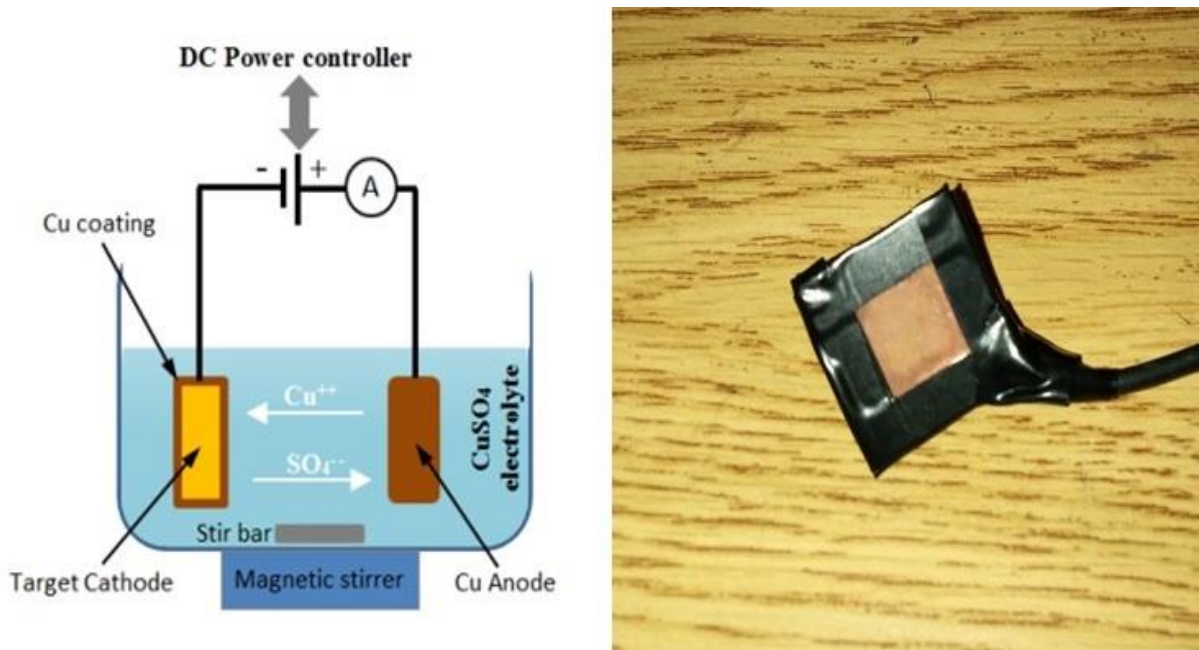
the spray chamber.

Figure 13: Schematic view of electroplating process [20] (a), a masked sample for electroplating

process.

Figure 14 shows the microporous structure prepared using the electroplating process. This picture was taken using a microscope with a magnification of 80x.
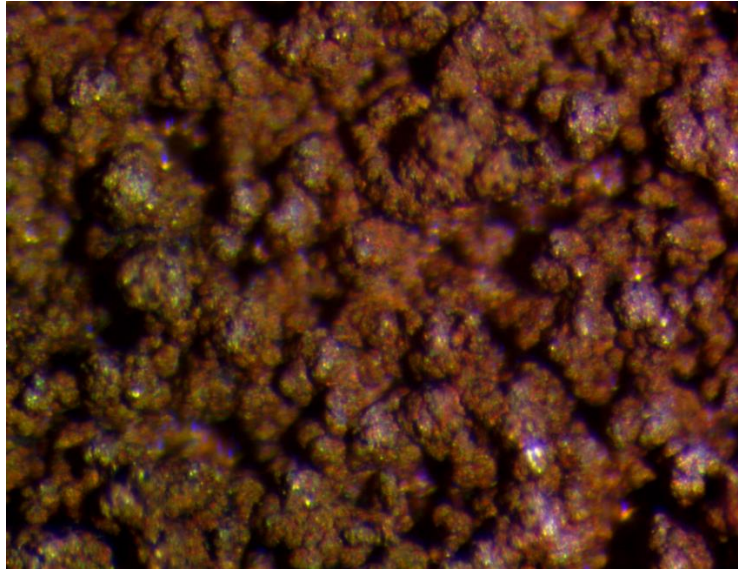

Figure 14: Microscopic view of electroplated microporous surface.

3.7 Test Conditions and Procedure

After building the spray cooling setup for steady flow, variable flow, and intermittent flow tests, the entire system is pressured and checked for leaks to avoid potential loss of working fluid during the tests. Before each test, a degassing procedure is conducted to purge air from the closed cycle. Vacuum is pulled out of the spray chamber by isolating it from the remaining sections, this process is carried out by a vacuum pump. Once the test is started, the heat flux is gradually increased in steps of 5-10 W/cm^2 until reaching CHF, and corresponding temperatures are monitored and recorded. The heat flux is determined from the total power supplied to thick film resistor per unit area as shown below.

$$q'' = \frac{V*I}{A} \qquad (6)$$

Surface temperature of the heater is calculated by extrapolating the average of two thermocouple (TC) readings through the known distance (1 mm) to the surface and assuming one dimensional (1D) steady state heat conduction through the heater wall as shown below.

$$T_{Surf} = TC_{avg} - (\frac{q''*x}{k}) \qquad (7)$$

Experimental setup enables to control the coolant flow rate, temperature, and pressure independently in order to conduct tests at various conditions. Test sections have two types of surface conditions, including reference smooth surface and microporous enhanced surface. The first phase of the study involves steady flow spray cooling, and investigates the effects of flow rate and subcooling on the performance.

The second phase of the study involves variable flow spray cooling, and aims to maintain the set surface temperatures, determined based on steady flow tests, by controlling the pump speed and therefore the liquid flow rate. The implemented PID controller varies flow rate between the maximum level (corresponding to steady flow condition) and the minimum level (corresponding the pump actuation), when the surface temperature goes above and below the set value, respectively.

Third phase of the study involves the intermittent flow spray cooling, and also aims to maintain the set surface temperatures, determined based on steady flow tests, by controlling the spray frequency and duty cycle using a solenoid valve before the spray chamber inlet.

Spray cooling performance is mainly characterized with HTC and CHF values. The experimental data are used to generate cooling curves in the form of surface superheat (ΔT_{sat}) vs. heat flux. Three separate LabVIEW programs were developed as shown in the appendix A through F for steady flow spray, intermittent flow spray and variable flow spray cooling experiments. These are used in conjunction with a DAQ system and programmable DC power supply in order to accurately monitor and record experimental data.

3.8 Experimental Uncertainties

Experimental uncertainties were estimated for temperature and heat flux measurements, which are critical in performance evaluation. In the steady state the error in temperature measurements through embedded T-type thermocouples in the test section was calibrated to be ±0.2°C. Error in heat flux measurement (considering the variations in voltage, current, thermal conductivity and thermocouple readings) at 150 W/cm² was ±2.1%. Uncertainty in spray surface temperature was ±0.3°C involving uncertainty in temperature extrapolation thermocouple hole location to heater surface at 150 W/cm². All uncertainties were estimated with a 95% confidence level.

CHAPTER 4

RESULTS AND DISCUSSION

In this chapter, experimental results obtained in steady flow spray cooling, variable flow spray cooling and intermittent flow spray cooling experiments were discussed. The spray characteristics were discussed based on the flow rates, subcooling level and type of test surface. Thermal management for variable heat loads were addressed and discussed briefly. The use of PID controls in controlling the surface temperature of the heat generating device was discussed. All tests used HFE-7100 as the coolant and TG0.5 as the spray nozzle. This nozzle size was selected based on an earlier study [47] with refrigerant HFC-134a that compared three pressure atomized nozzle types. As shown in Figure 15, using a constant flowrate, TG0.5 provided better HTC and CHF than TG0.3 and TG0.7 that feature smaller and larger orifice sizes, respectively.
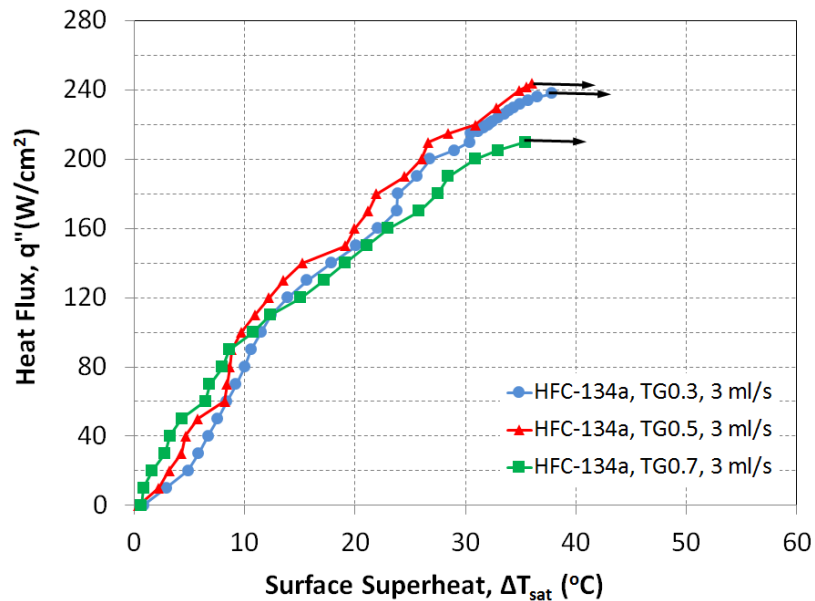
Figure 15: Spray nozzle comparison with HFC-134a [47].

4.1 Results for Steady Flow Spray Cooling

Initial tests were conducted on a reference surface (plain smooth copper surface) using a flow rate of 4 ml/cm².s at 30°C subcooling. Results were plotted for surface superheat versus heat flux as shown in Figure 16. CHF attained with this flowrate was 145 W/cm² at a surface superheat of 31.2°C and the surface temperature of the heater was 91.8°C. To make sure that results are repeatable with this surface, a similar test was conducted up to 120 W/cm² as shown in the same plot. In the second test, the cooling curve followed a nearly same trend as the previous test. Results with the reference surface are therefore repeatable.
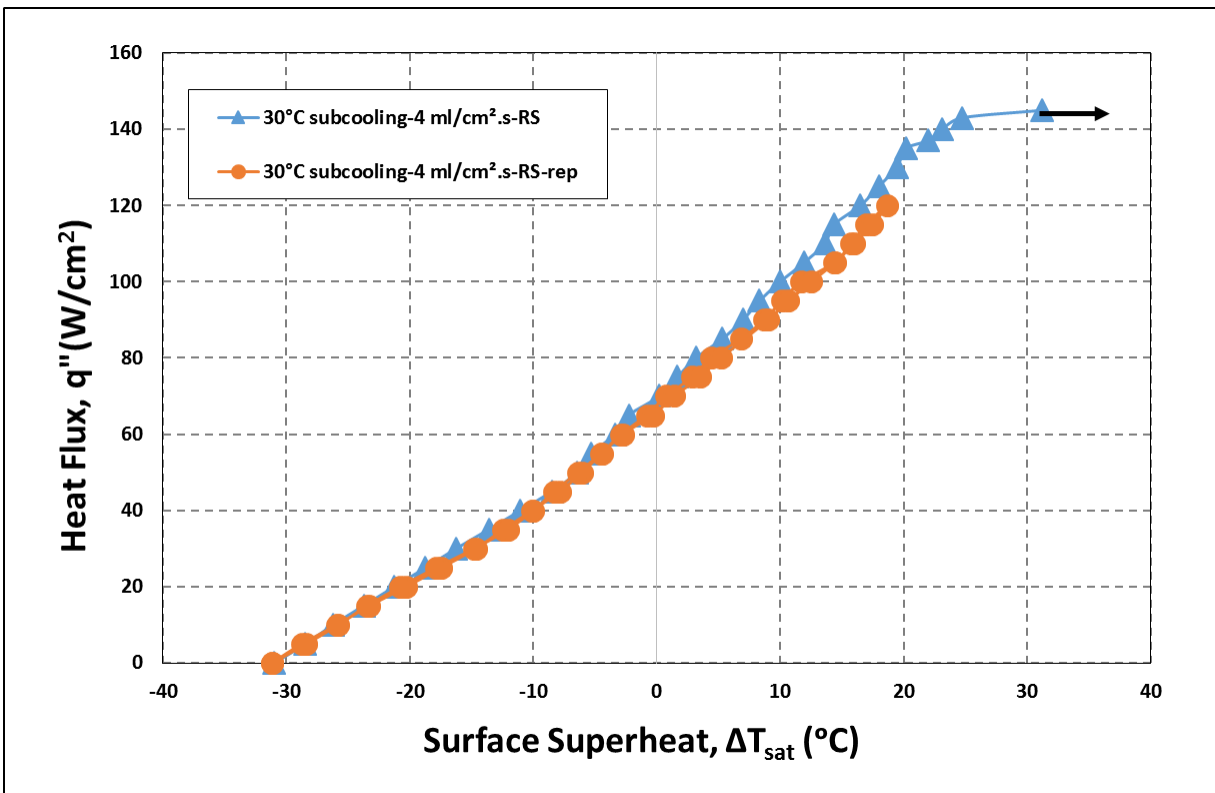

Figure 16: Repeatability of spray cooling performance with reference surface at a flow rate of 4 ml/cm².s and 30°C subcooling.

A series of tests were performed with the reference surface at 30°C subcooling on the same day to test the effect of flow rate. Along with 4 ml/cm².s, 2 and 3 ml/cm².s flowrates were tested and the results were plotted in Figure 17. As explained earlier the test conducted with 4 ml/cm².s provided a CHF of 145 W/cm², whereas 2 ml/cm².s provided a CHF of 95 W/cm², and 3 ml/cm².s provided a CHF of 125 W/cm² with corresponding surface temperatures of 91.8 °C, 91.5 °C and 89.5 °C, respectively. Test conducted with a flow rate of 4 ml/cm².s showed an increase of 52.6% in CHF when compared with 2 ml/cm².s and 16.0% when compared with 3 ml/cm².s. Test conducted with a flow rate of 3 ml/cm².s showed an increase of 31.5% in CHF when compared with 2 ml/cm².s. CHF increase with the flowrate and higher flow rates resulted in lower surface superheats which is desirable for a heat generating device.

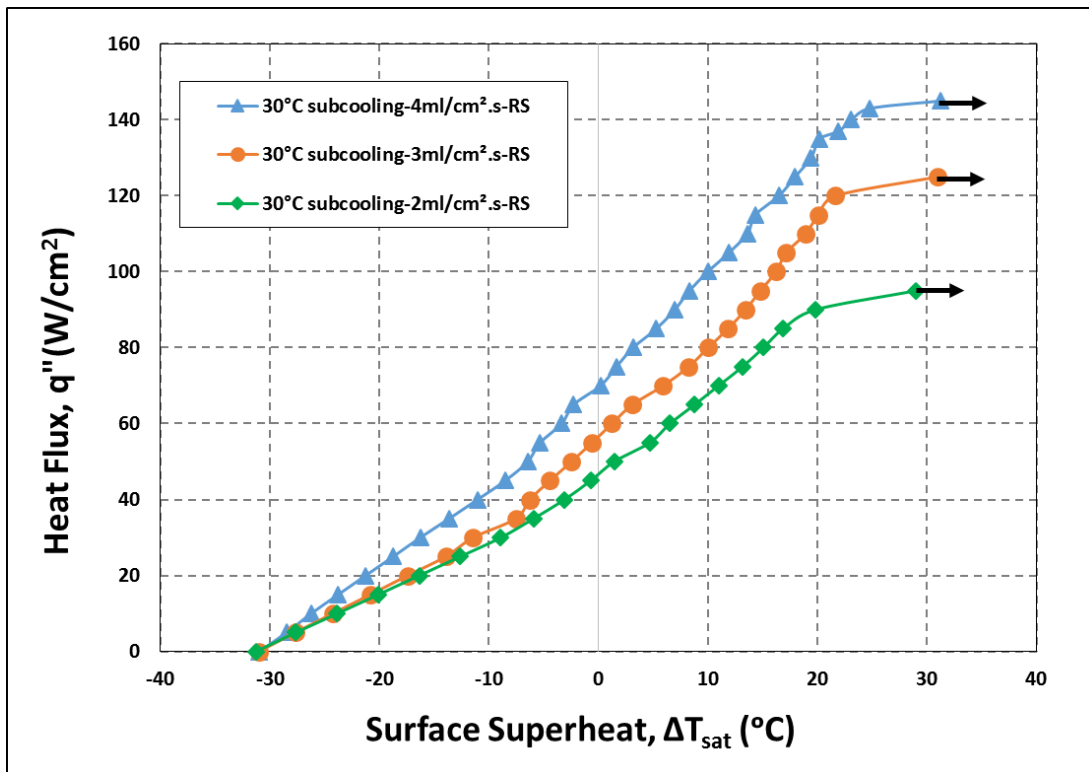
Figure 17: Heat transfer performance of RS at flowrates of 2, 3, 4 ml/cm².s and 30°C subcooling.

After evaluating the performance of reference surface, a similar test was conducted to evaluate the performance of electroplated microporous surface. A test was conducted with the surface MS-E using a flow rate of 4 ml/cm^2.s at 30°C subcooling and the results were plotted as shown in Figure 18. CHF reached at 216 W/cm^2 at a surface superheat of 45.9°C and the surface temperature of the heater was 106.5°C. Again to make sure that the results with the MS-E are repeatable, a similar test was conducted up to 200 W/cm^2 and it can be observed from the same plot that the cooling curve followed a nearly same trend as the previous test. Results with this MS-E are also repeatable.
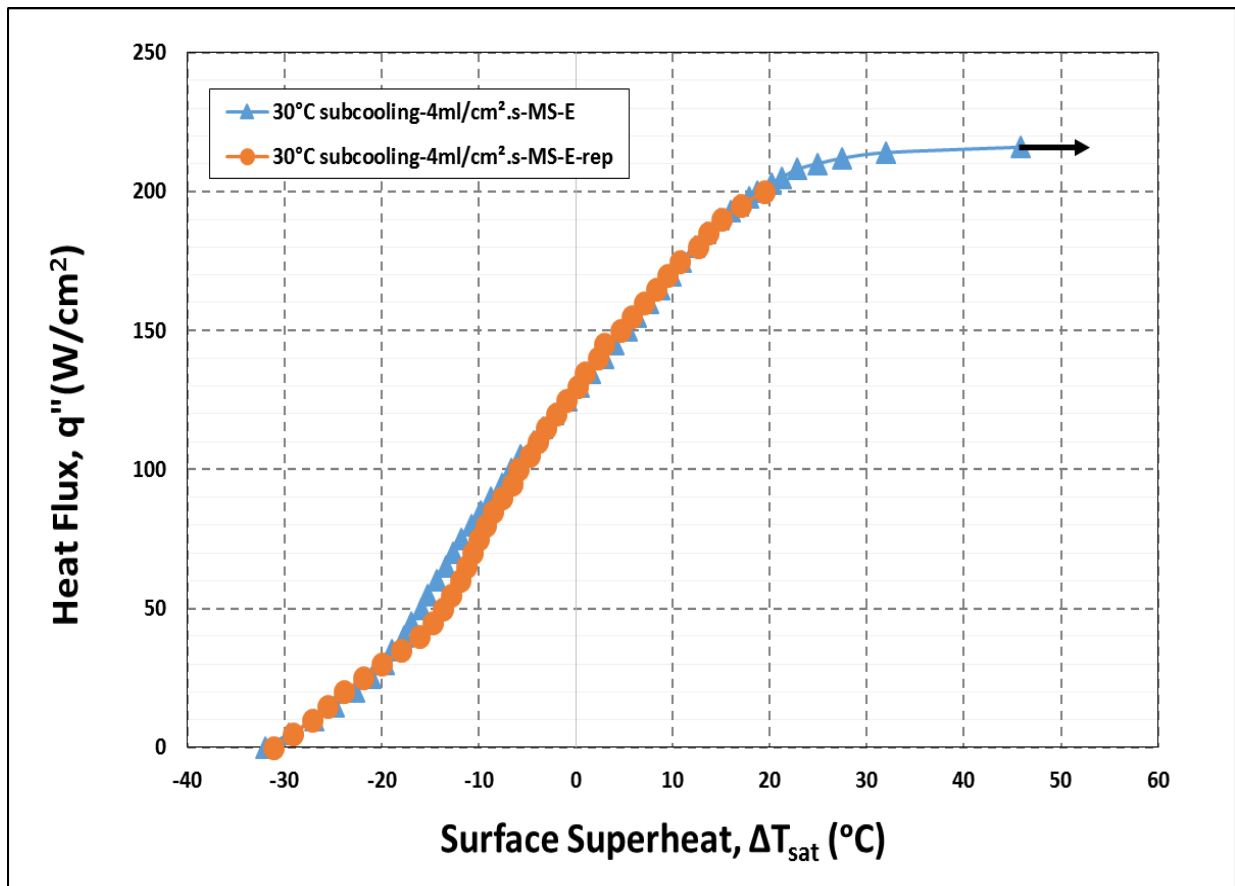

Figure 18: Repeatability of spray cooling performance with MS-E at a flow rate of 4 ml/cm^2.s and 30°C subcooling.

A series of tests were also performed with the surface MS-E at 30°C subcooling and at varying flow rates of 2, 3, 4, 5 ml/cm^2.s on the same day and the results were plotted as shown in Figure 19. Increase in the flow rate showed an increase in CHF similar to the results obtained with the reference surface. Test conducted with the flow rate of 5 ml/cm^2.s showed an increase of 35.3%, 27.7%, 21.0% in CHF when compared to tests with the flowrates of 2, 3, 4 ml/cm^2.s, respectively. The surface temperatures recorded at the flowrates of 2, 3, 4, and 5 ml/cm^2.s were 81.4°C, 73.1°C, 81.2°C, and 81.2°C, respectively.
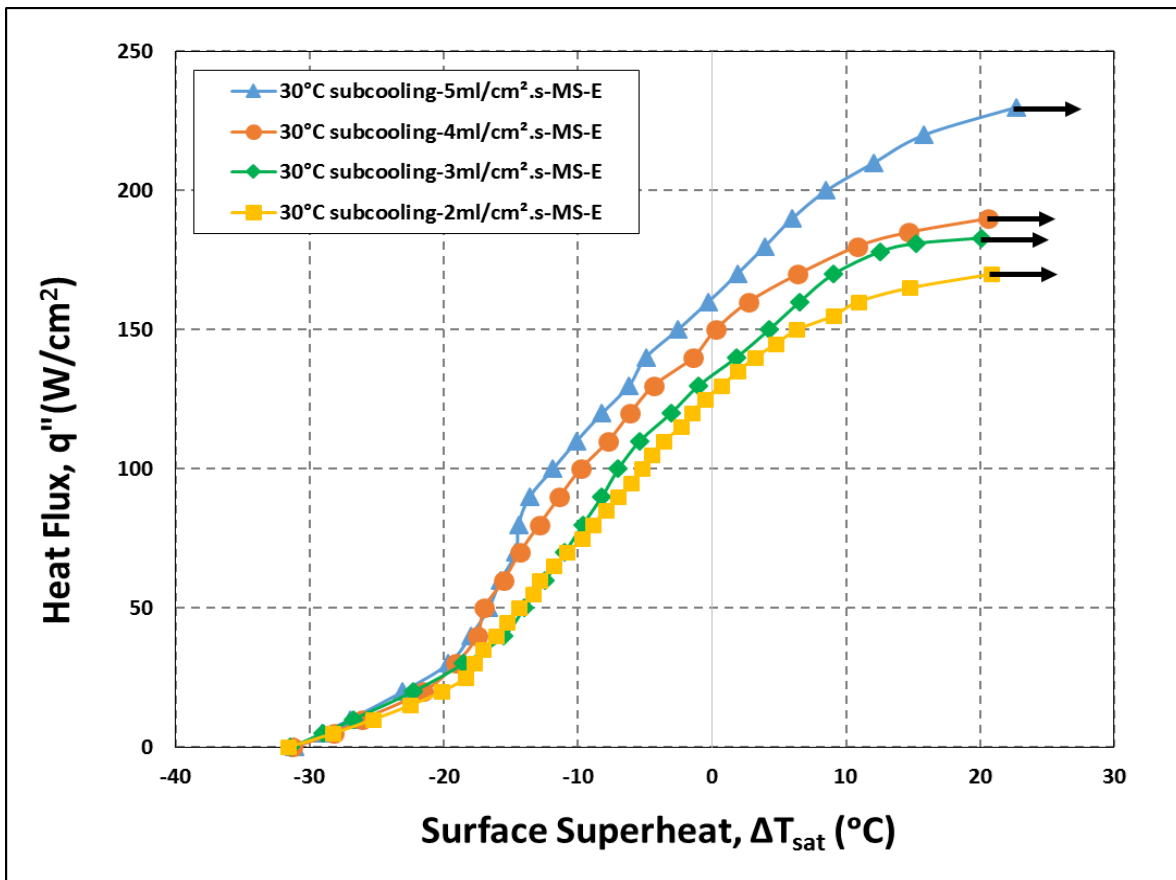

Figure 19: Heat transfer performance of the surface MS-E at flowrates of 2, 3, 4, 5 ml/cm^2.s and 30°C subcooling.

Figure 20 shows a plot for flowrate versus pressure at the inlet of the spray chamber. It can be clearly observed that the higher liquid flowrates requires higher inlet pressures, as expected. For the highest flowrate of 5 ml/cm^2.s, the average inlet pressure reached to 306.2 kPa (44.4 psig), representing an increase of 79.6% of inlet pressure when compared to a flowrate of 4 ml/cm^2.s. Such significantly increased pressure levels require correspondingly higher pumping power when compared to the other flowrates. Furthermore very high pressures can create back pressure on pump and more fluctuation of pressure resulting in overheating and damaging the pump. It is therefore advised to use a different nozzle with larger orifice size, if a higher flowrate is needed. For the selected TG0.5 type nozzle in this study, the flowrate of 5 ml/cm^2.s was eliminated in the upcoming tests.
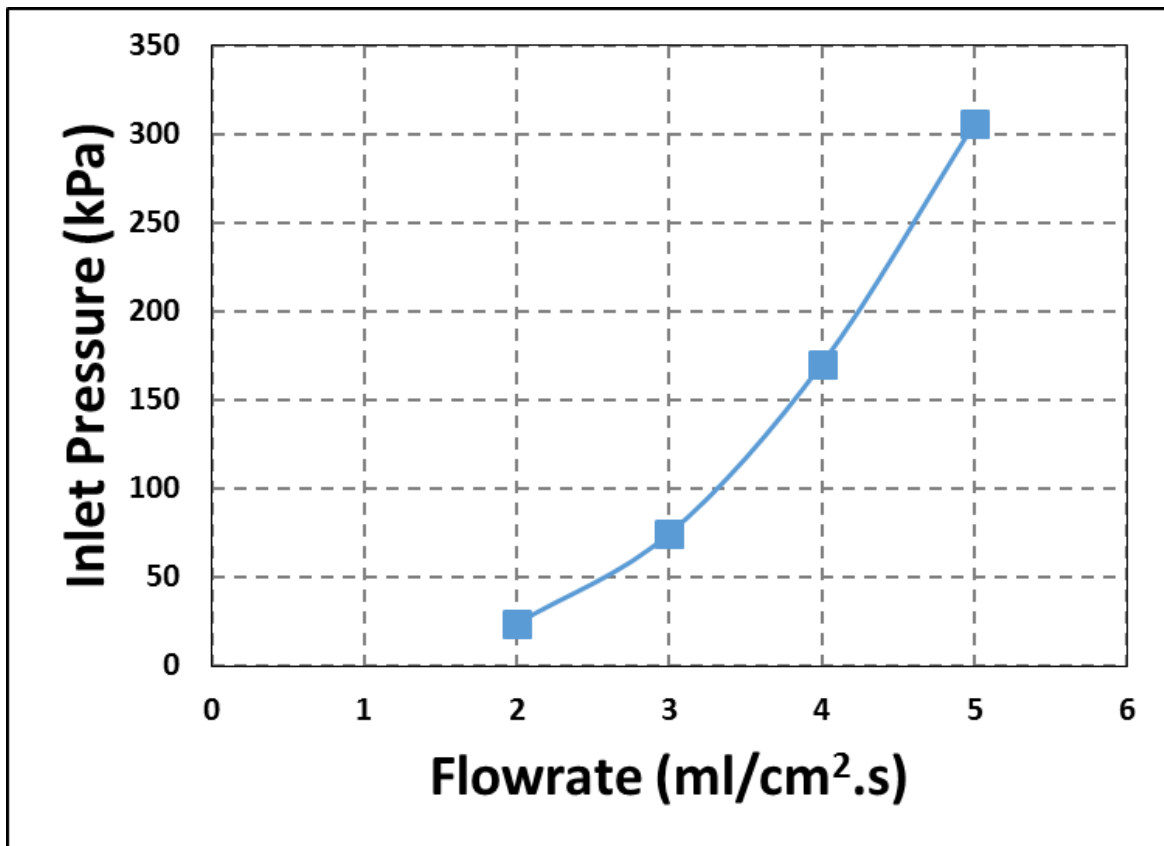

Figure 20: Inlet pressure values as a function of liquid flow rate.

Figure 21 combines earlier data and shows the effect of flowrate and the surface enhancement on spray cooling performance. It was observed that, at a given surface superheat, higher heat fluxes can be removed with increasing flowrates; or alternatively, at a given heat flux level, surface can be maintained at a lower temperature with increasing flowrates. Increasing the flowrate increases the droplet velocity and flux (number of droplets per unit area) and improves the spray cooling performance in terms of higher HTC and CHF. This prevents the number of dry-out spots resulting in more heat absorption from the heater enhancing CHF. It can be clearly observed that, not only the flowrate, but also surface enhancement enhances the CHF.
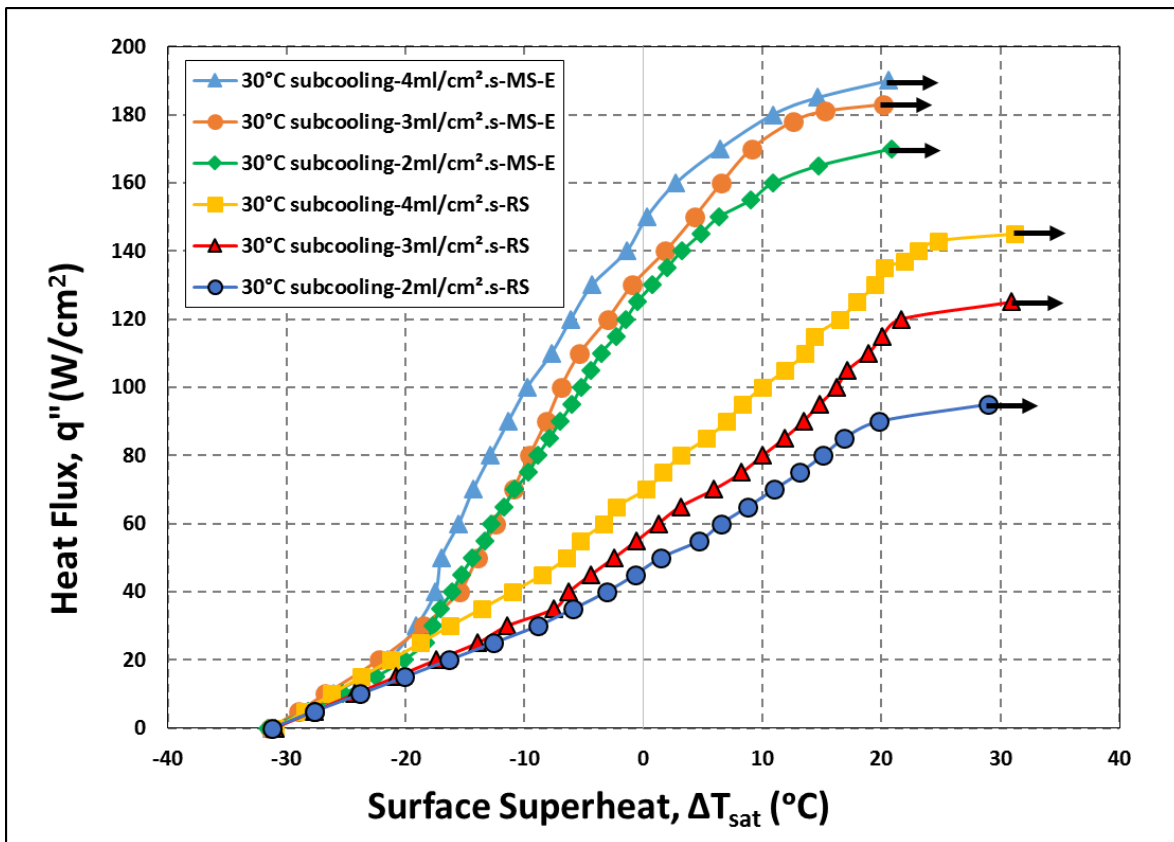

Figure 21: Effect of liquid flowrate and surface enhancement on spray cooling performance at 30°C subcooling.

Basically enhanced surface greatly improves boiling through surface nucleation, one of the heat transfer mechanisms in spray cooling. Enhanced surface showed an increase in CHF and the decrease in surface superheat at a given heat flux. In the test conducted using 4 ml/cm^2.s with RS and MS-E, CHF increased by 31.03% in MS-E compare to RS. For a given heat flux of 100 W/cm², surface superheat in MS-E test is -10°C where as it is 10°C in RS test. There is difference of 20°C between the two tests at the same flowrate and at 100 W/cm² heat flux. Microporous surface showed enhancement in both CHF and surface superheat.

Figure 22 shows the effect of surface enhancement at 10°C subcooling. This test is performed at a much lower subcooling level compared to earlier tests, at 10°C subcooling, using the selected flow rate of 4 ml/cm^2.s. Similarly, the surface MS-E provided improved spray cooling performance compared to the surface RS, in terms of both HTC and CHF. The surface MS-E achieved a CHF of 230 W/cm^2, representing a significant increase of 105.7% compared to that of the surface RS at 105 W/cm^2. At 100 W/cm^2 heat flux, surface superheats for the surfaces MS-E and RS were 5°C and 25°C, respectively. Therefore, at this heat flux, enhanced surface can maintain the surface at 20°C lower temperature compare to a plain, smooth surface.
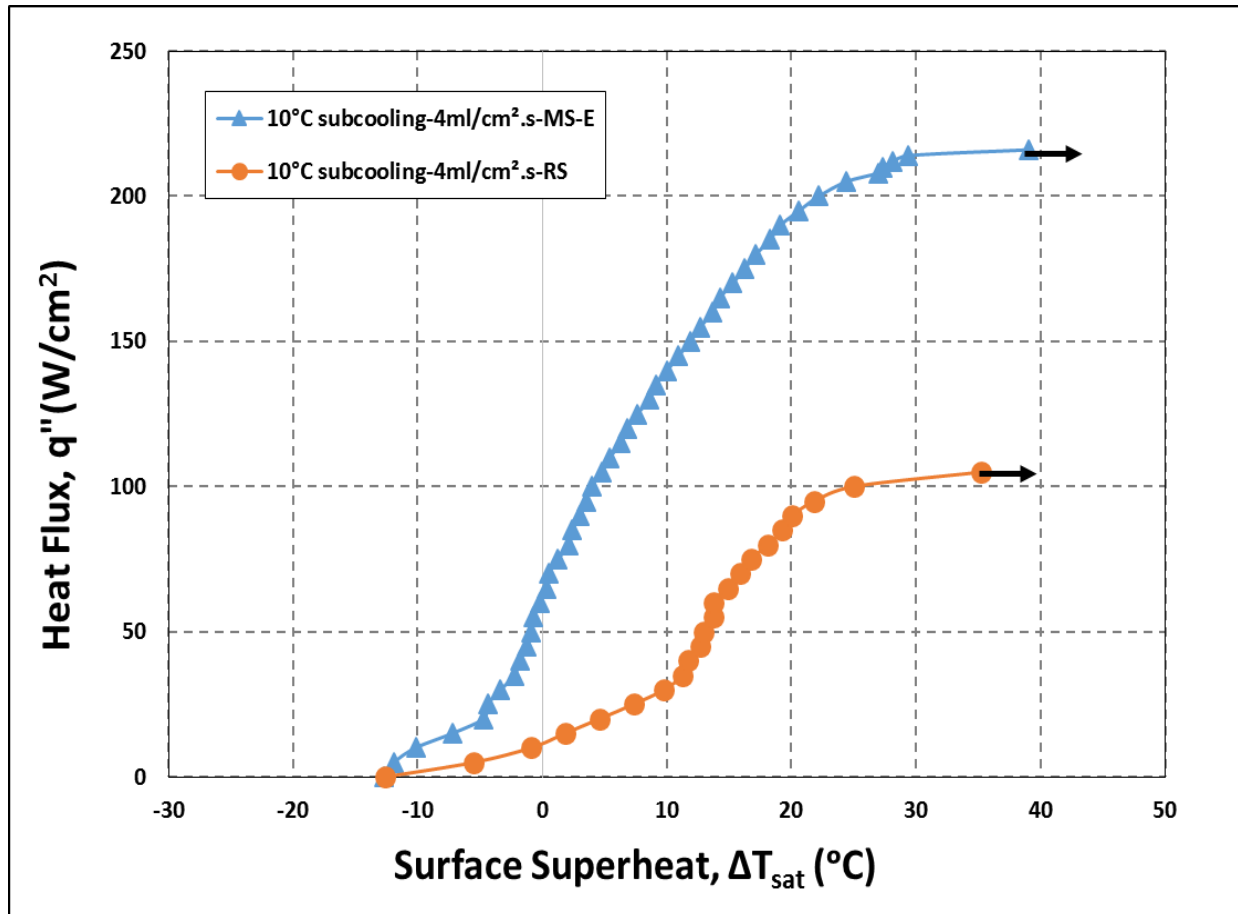
Figure 22: Effect of surface enhancement on spray cooling performance at 10°C subcooling.

Figure 23 shows the effect of subcooling and surface enhancement on spray cooling performance. Slope of the cooing curves are significantly different indicating different HTC levels. For the surface RS, 30°C subcooling provides lower surface superheats throughout although the initial ~20°C difference diminishes as heat flux increases. Higher subcooling also provides higher CHF due to a larger contribution of sensible heat. For the surface MS-E, higher subcooling also provides lower surface superheats at low and moderate heat flux levels, but at high fluxes near CHF 10°C subcooling achieves a lower surface superheat (e.g., at 190W/cm^2, surface superheat for 30°C and 10°C subcooling tests were 20.5°C and 19°C, respectively). This can be attributed to the contribution of different heat transfer mechanisms. For 30°C subcooling, enhanced surfaces

would mainly improve heat transfer due to increased surface area. However, for 10°C subcooling, when the supplied liquid is much closer to the saturation condition (or boiling point), enhanced surfaces greatly improve heat transfer due to boiling through surface nucleation, as can be seen with an immediate increase in the slope of the curve right after zero surface superheat. The microporous structures on the surface coating provide many active nucleation sites and help promote boiling in this case. Better utilization of two-phase heat transfer mechanisms eventually help 10°C subcooling condition to achieve a higher HTC, as well as higher CHF, compared to 30°C subcooling condition. In two therefore, it can be concluded that the mechanisms are different.
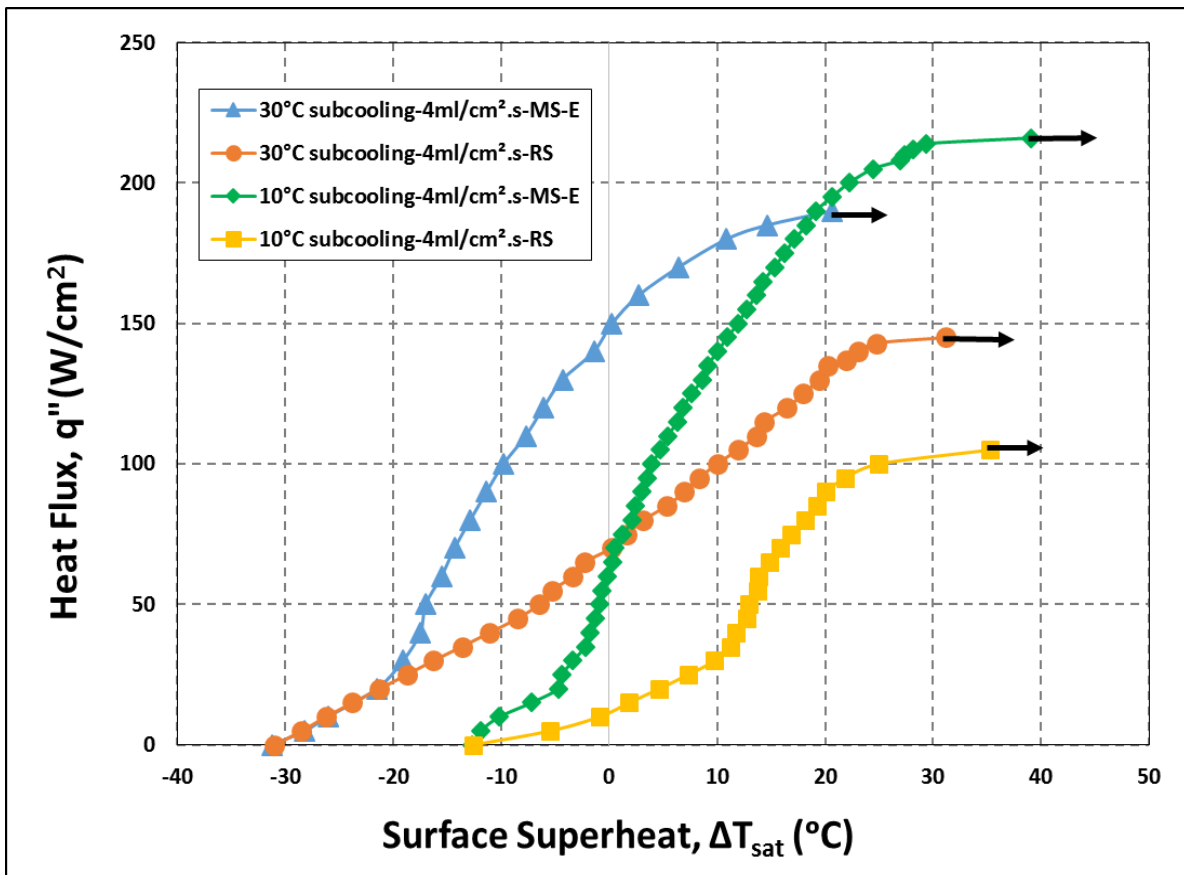

Figure 23: effect of surface enhancement and subcooling.

Figure 24 shows how HTC varies as a function of heat flux, and incorporates the effects of flowrate, subcooling and surface enhancement on the performance. HTC (or h) is calculated using the following equation, where the temperature of incoming liquid stream is taken as the reference. In general, HTC increased with the flow rate, subcooling and surface enhancement at a given heat flux.

$$h = \frac{q''}{(T_{Surf} - T_{in})} \qquad (8)$$

For the surface RS, it can be observed that the HTC values linearly increased with the heat flux up to near CHF. At 10°C subcooling, contribution of the two-phase processes were much more pronounced and the HTC increased with heat flux at a higher rate compared to 30°C subcooling tests. Highest HTC values observed at the flowrates of 2, 3 and 4 ml/cm².s were 18.5, 24.1 and 28.5 kW/m²°C, respectively, at 30°C subcooling, while the highest HTC at 4 ml/cm².s was 28.9 kW/m²°C at 10°C subcooling.

For the surface MS-E, it can be observed that the HTC values linearly increased with the heat flux up to near CHF. At 10°C subcooling, contribution of the two-phase processes were much more pronounced and the HTC increased with heat flux at a higher rate compared to 30°C subcooling tests. Highest HTC values observed at the flowrates of 2, 3, 4 and 5 ml/cm².s were 43.9, 47.7, 50.0 and 57.0 kW/m²°C, respectively, at 30°C subcooling, while the highest HTC at 10°C subcooling and a flowrate of 4 ml/cm².s was 69.7 kW/m²°C. Highest HTC values are recorded in the mid-range of heat fluxes. At 10°C subcooling, HTC was increased by 140.3% in microporous surface when compared with reference surface at a flowrate of 4 ml/cm².s, it can be observed that the highest increment in HTC with was observed in 10°C subcooling test. Whereas the

increment in HTC with 30°C subcooling test was 75% which is almost half the value obtained in 10°C subcooling test.
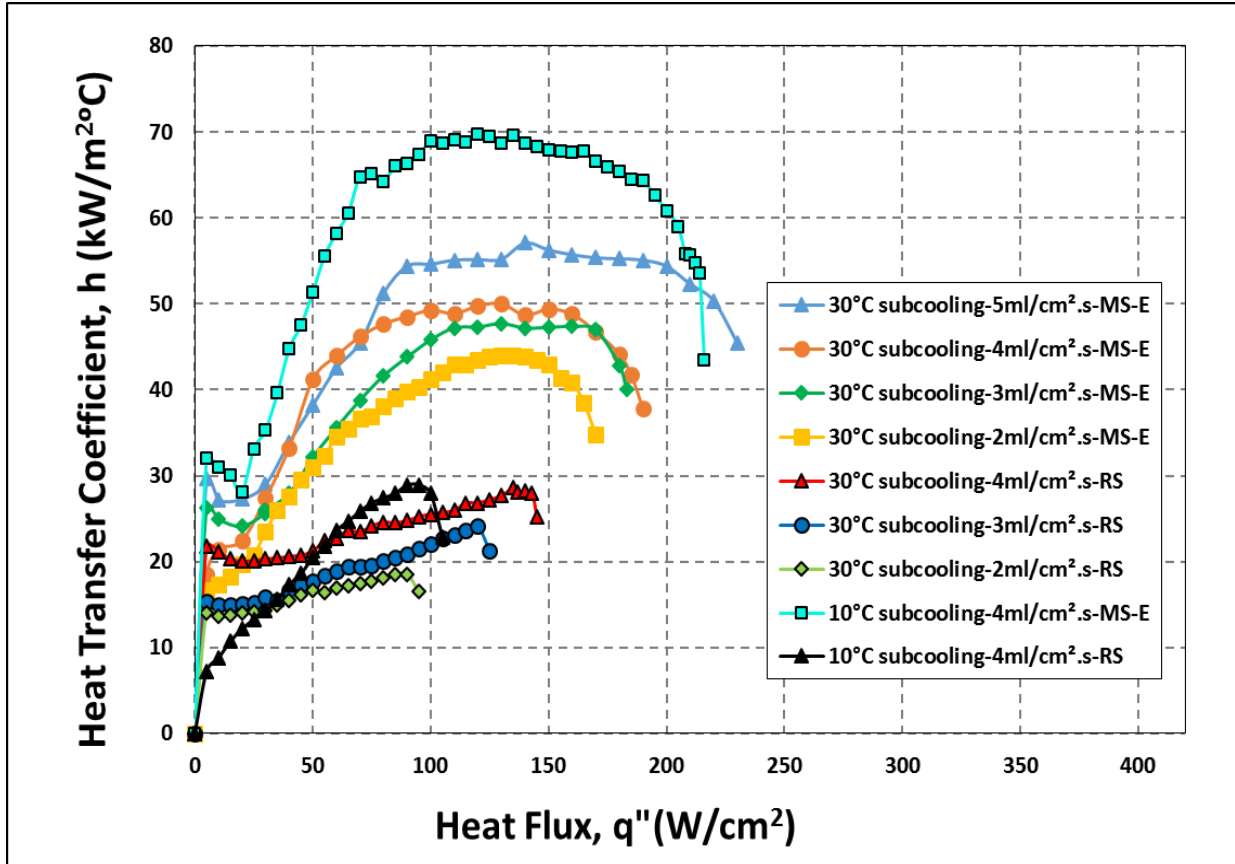

Figure 24: HTC as a function of heat flux at different flowrate, subcooling and surface conditions.

Figure 25 shows the effect of flowrate and surface enhancement on CHF. In the case of CHFs, 10°C subcooling achieved a higher CHF compare to 30°C subcooling. The results therefore indicate that the improvement due to surface enhancement is greater at low subcooling. The microporous structures on the surface coating provide many active nucleation sites and help promote boiling in this case. Better utilization of two-phase heat transfer mechanisms eventually help 10°C subcooling condition to achieve a higher HTC, as well as higher CHF.
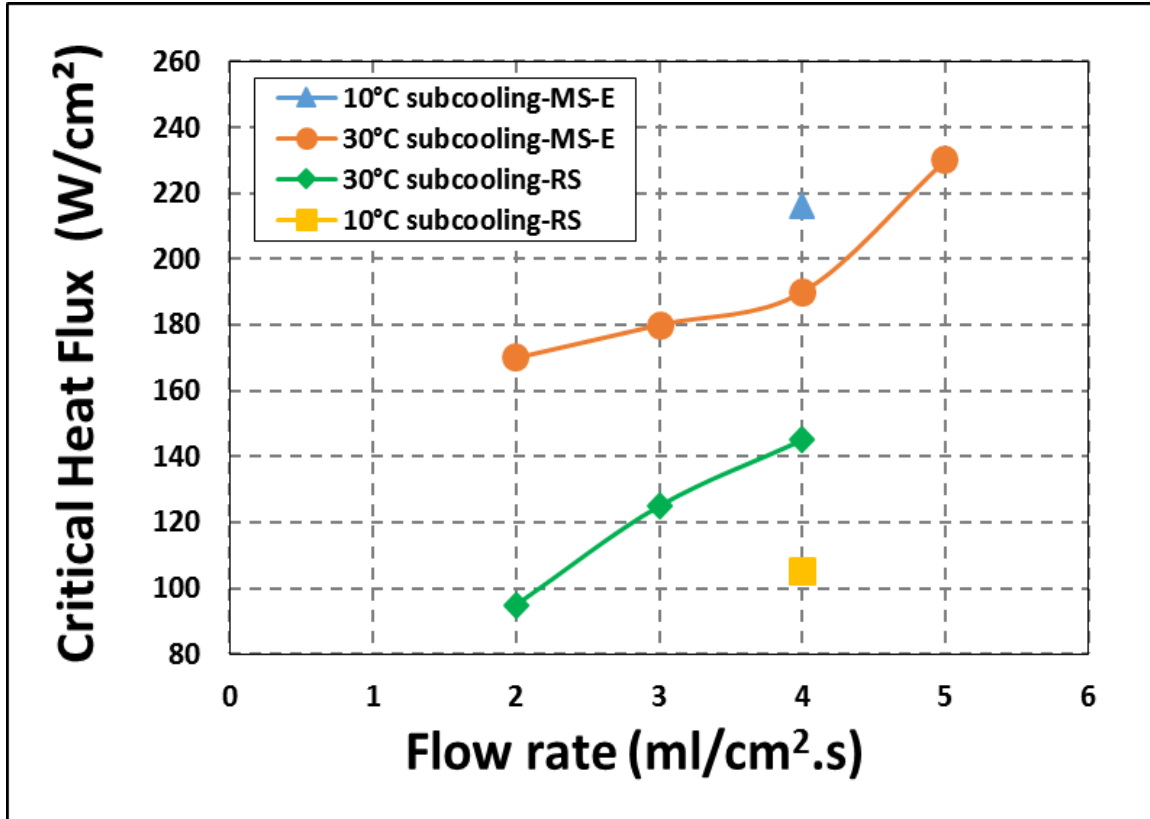
Figure 25: CHF as a function of liquid flowrate at different subcooling and surface conditions.

Figure 26 shows the effect of flowrate on spray cooling efficiency. This performance aspect represents the liquid usage efficiency, and that is defined as the ratio of the actual heat removed to the total heat capacity of the liquid used, including the required heat to bring the liquid from subcooled to saturation condition (sensible heat), and then to complete vaporization (latent heat) [48]. The spray cooling efficiency (η) can be found out using the following equation.

$$\eta = \frac{q''*A}{Q_{pf}*(c_p \Delta T_{sub} + h_{fg})} \qquad (9)$$

It can be observed from the plot that in both subcooling levels efficiency decreases as the flowrate increases, since the increase in CHF is not proportional to the increase in flow rate. The spray cooling efficiency at CHF on the surface MS-E is in the range of 56.9 - 30.8% whereas, it is

31.8 – 21.1% on the surface RS based on the tested range of subcooling levels and flowrates. Efficiency decreases linearly in the reference surface tests and decreasing exponentially in the microporous surface tests at 30°C subcooling. Observing the efficiencies in all tests clearly indicates that not all liquid sprayed on the heater surface is effective in removing heat. With the higher flowrates, only a small portion of liquid evaporates and the remaining liquid favors in delaying CHF without participating in two-phase heat transfer process, and a portion of spray scatters off the surface in liquid state. In the case of lower flowrates, the opposite trend can be observed, where larger fraction of liquid hitting the surface participates in two-phase heat transfer process and results in higher efficiency. In practical applications, lower liquid usage efficiency translates into high pumping power, and therefore liquid flow rate should be carefully determined to optimize the overall system performance.

One interesting case can be observed at a flowrate of 4 ml/cm^2.s, where lower subcooling decreases efficiency for reference surface by 12.9%, and increases efficiency for microporous surface by 36.6%. As explained earlier, this can be attributed to the better utilization of two-phase heat transfer mechanisms at lower subcooling levels.
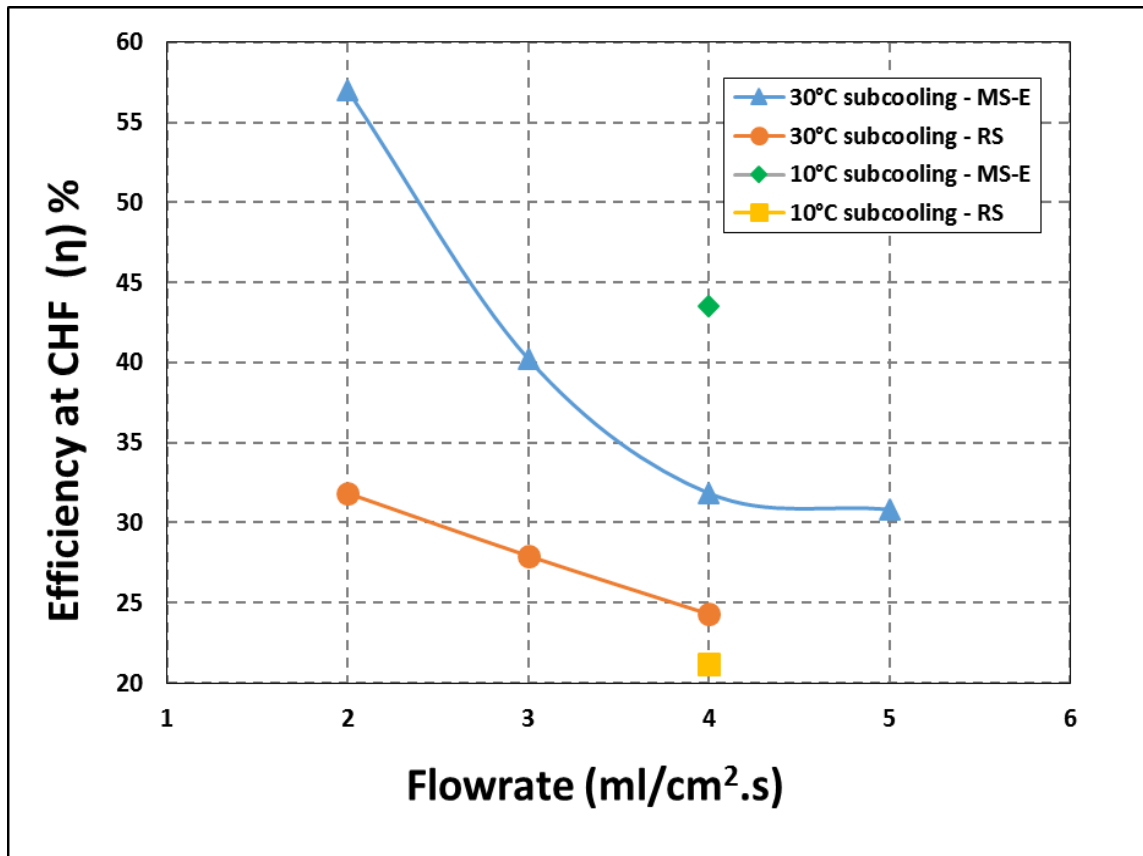
Figure 26: Spray cooling efficiency (η) at CHF as a function of liquid flowrate at different

subcooling and surface conditions.

4.1.1 Evaluation of Experimental Results Using Finite Element Analysis

A commercial finite element analysis software, ANSYS, was used to evaluate some of the key experimental results. The 3D model generated using Creo 2.0 software is imported in to ANSYS steady state thermal analysis module. The heater material was defined as copper, and the model was meshed using tetrahedral element with the size of 2.0 e[-004] m as shown in the Figure 27.
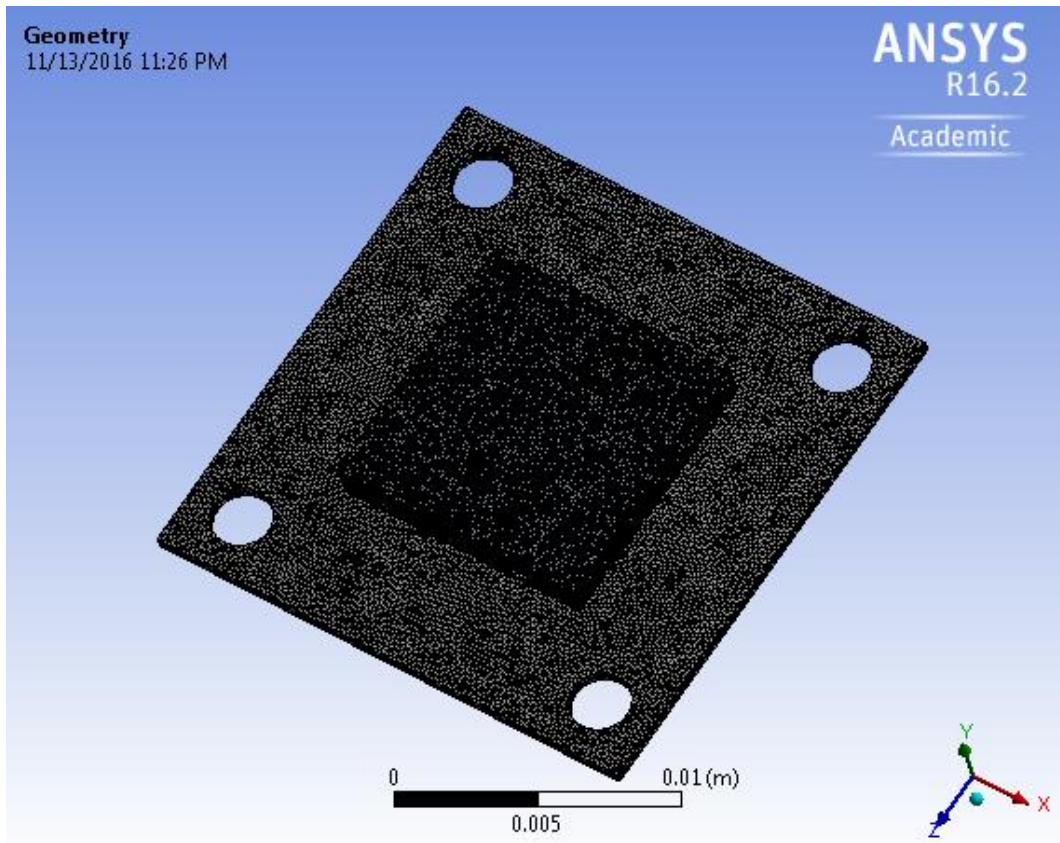
Figure 27: Finite element mesh on model geometry.

After meshing the steady state heat flux, convection heat transfer coefficient, ambient temperature, and remaining parameters were plugged in from microporous test conducted using a flowrate of 5 ml/cm^2.s and 30°C subcooling according to test conditions. Solutions are prepared for temperature and total heat flux. Thermocouple and surface temperatures were measured using a probe and compared with the experimental results at CHF.

Figure 28 shows the measurement of thermocouple temperature and it was found to be 87.20°C whereas the average thermocouple reading obtained in the experiment was 87.09°C. The difference of 0.11°C contributes to heat loss from the heater and this is explained in experimental uncertainties.
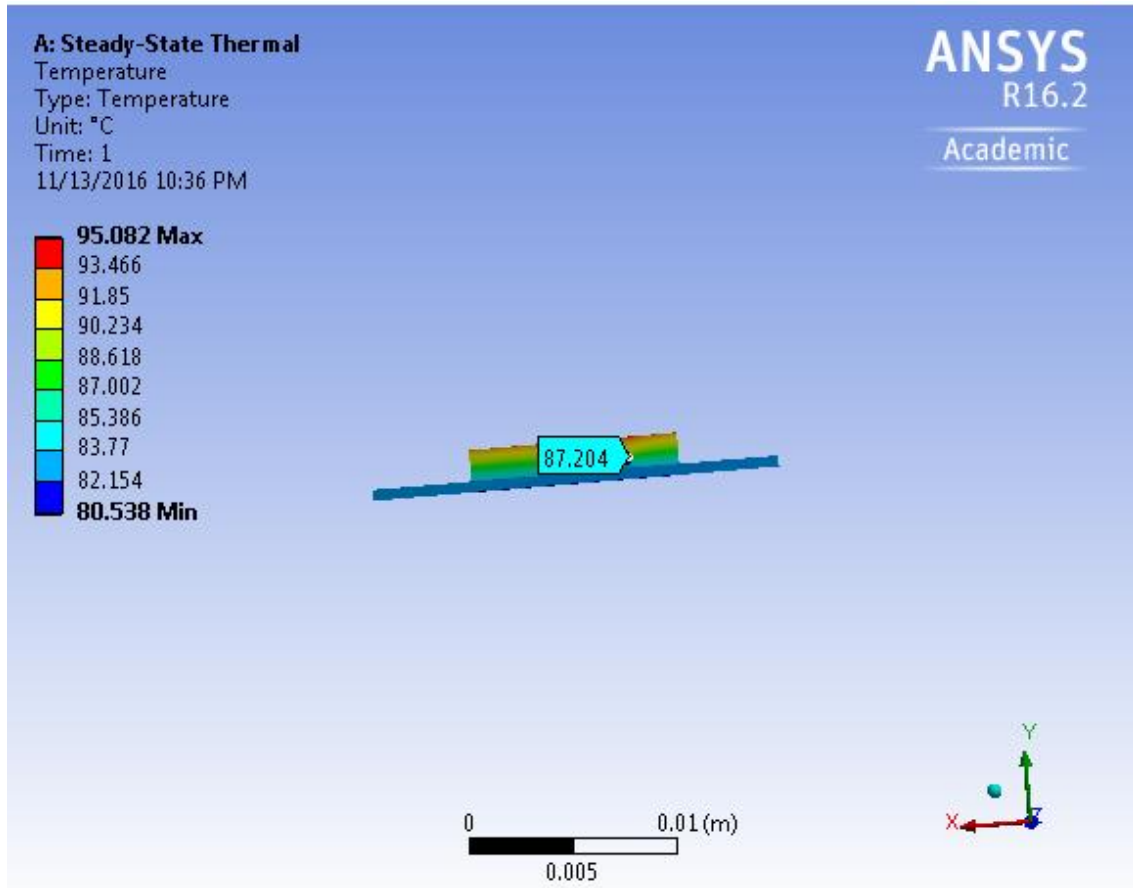
Figure 28: Thermocouple reading at CHF.

Figure 29 shows the temperature distribution from surface 1 to surface 2. The temperature at the resistor - heater interface was found to be 94.17°C, and the temperature at the spray surface was shown as 81.28°C.

Figure 29: Temperature distribution from surface 1 to surface 2.
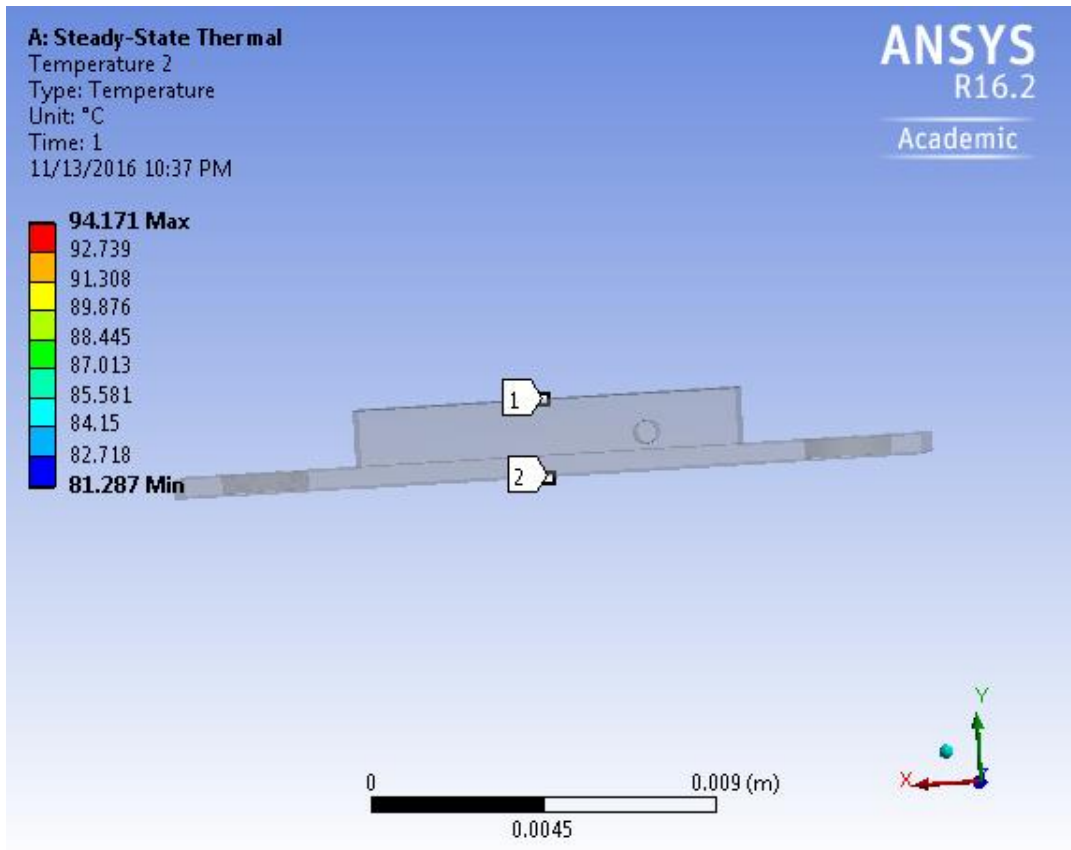
Figure 30 shows the temperature distribution diagonally, at the mid-section of the heater, where thermocouple holes lie, particularly between the two thermocouple holes, and it can be observed that, there is a nearly uniform temperature distribution across the two thermocouple holes. It can also be assumed that the temperatures across that layer are fairly uniform.
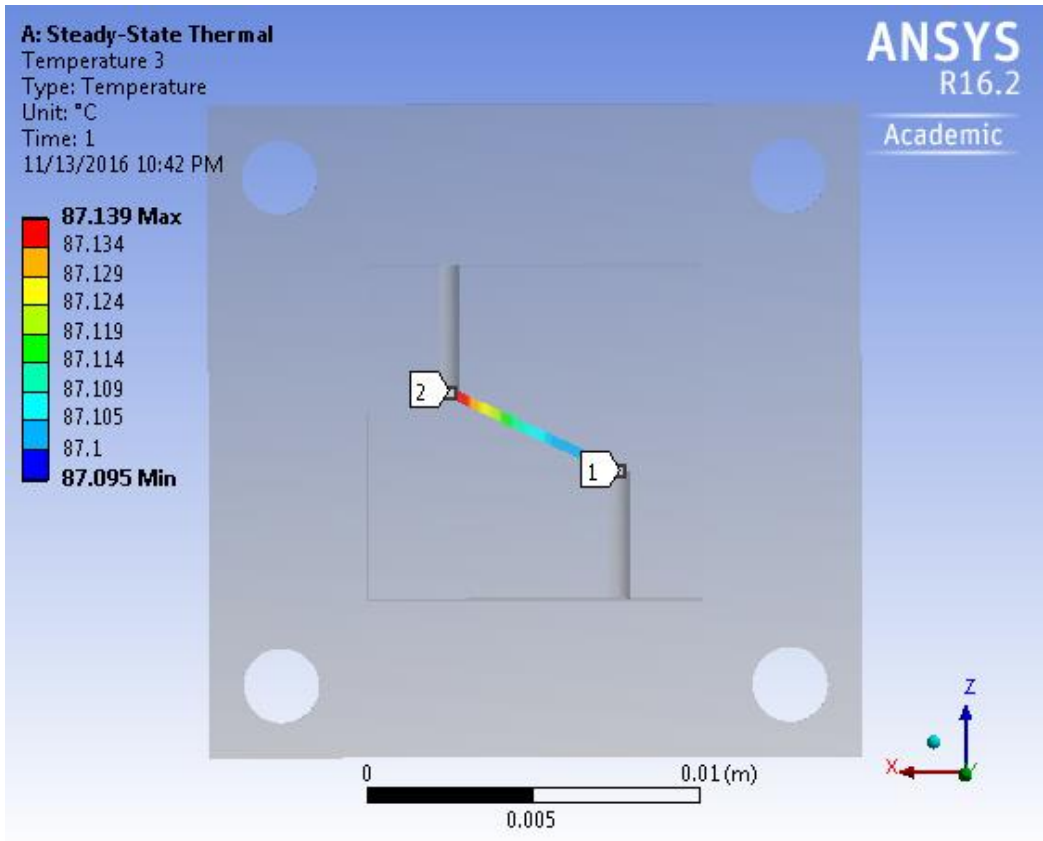
Figure 30: Temperature distribution between two thermocouple holes.

Figure 31 shows the surface temperatures at 6 different locations on the spray surface, and they are found to be around 81.25°C whereas the experimental value is 81.23°C. Thus the temperatures match very well and the results are verified.
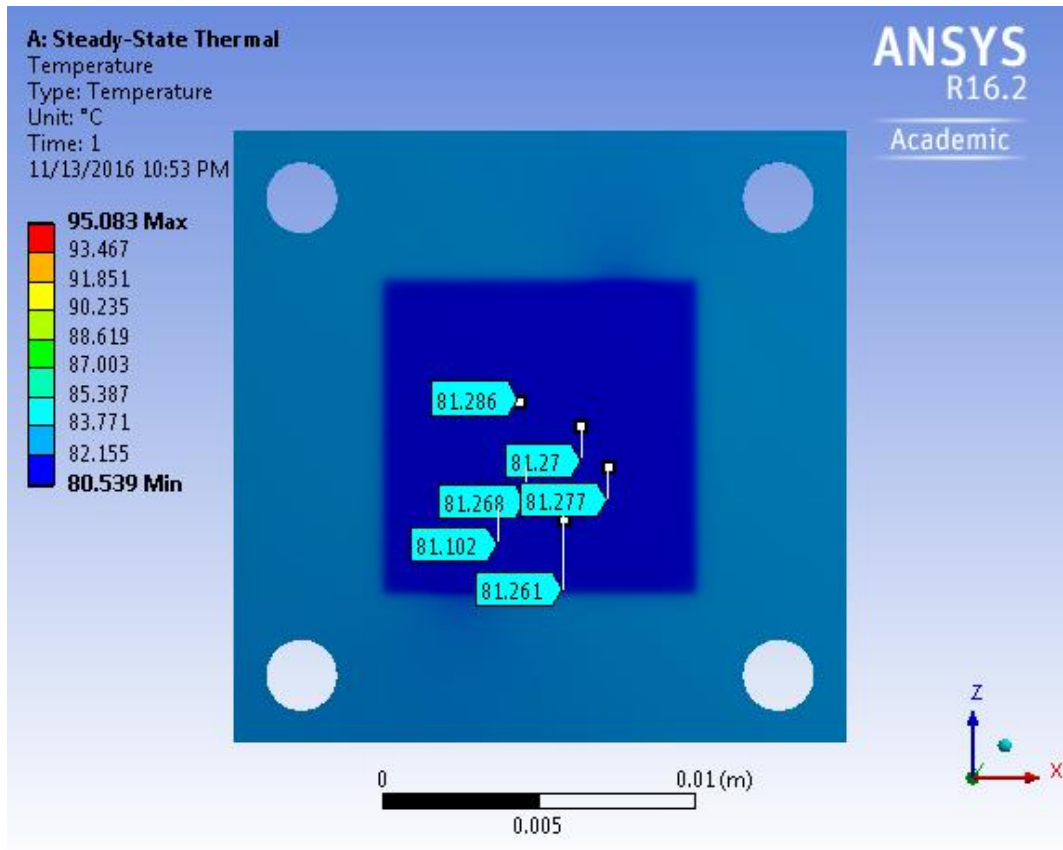
Figure 31: Spray surface temperatures.

Similar analysis was done to verify the surface temperatures at moderate heat fluxes of 70 and 150 W/cm². At 70 W/cm² heat flux, average surface temperature from the experimental results was 45.9°C whereas it is 46.2°C in FEA analysis. At 150 W/cm² heat flux, average surface temperature from experimental results was 58.07°C, whereas it is 58.6 in FEA analysis. The results were matching at these heat flux levels.

4.2 Results for Variable Flow Spray Cooling

Variable flow spray cooling approach aims to adjust the flow rate based on the monitored surface temperature by varying the pump dc voltage that indirectly dictates the flow rate through the spray nozzle. This process is carried out by a PID controller.

Before conducting the variable flow test, PID parameters were determined and a steady flow spray cooling test was conducted with the surface MS-E at a flowrate of 4 ml/cm^2.s and 30°C subcooling. Based on this test, surface temperatures at each heat flux value were recorded and these were used as the set points for PID controller in this setup. The maximum pumping power was 5.512 W (5.3 V and 1.04 A), representing the pumping power required to deliver 4 ml/cm^2.s liquid flow rate in steady flow spray cooling. The minimum pumping power was 1.8 W (3.3 V and 0.6 A), representing the pumping power required to actuate the pump. These two values were plugged into PID controller. Variable flow test was conducted similar to steady flow test by increasing the heat flux gradually until CHF. For each heat flux step, the surface temperature obtained from the steady flow test was used as the set point, so that if the surface temperature in the variable flow test was above the set point pumping power was increased to maximum that can provide 4 ml/cm^2.s liquid flow rate, and if the surface temperature was below the set point then the pumping speed was decreased to minimum, i.e. 1.8 W.

Figure 32 compares the performance of steady flow and variable flow spray cooling tests in terms of surface superheat vs. heat flux with the surface MS-E at a flowrate of 4 ml/cm^2.s and 30°C subcooling. In this plot the data from the steady flow test were compared to the variable flow test in two ways, (i) using the average of last 20 seconds of data at each heat flux, and (ii) using the average of overall data at each heat flux that typically lasted 2-3 minutes.
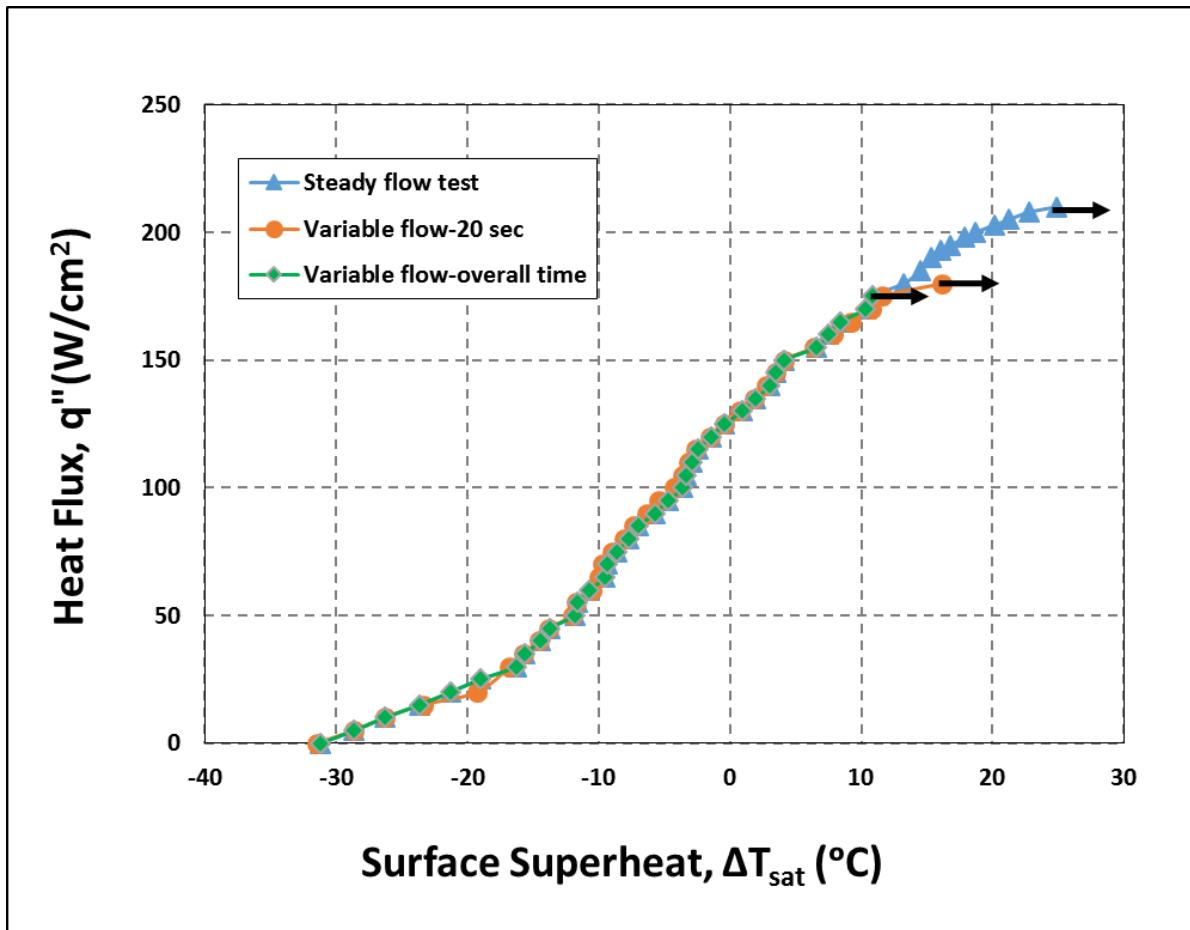
59

Figure 32: Spray cooling performance comparison of steady and variable flow tests with the surface MS-E, at a flowrate of 4ml/cm².s and 30°C subcooling.

As it can be seen from the plot, the three curves align very closely, and it can be stated that the variable flow test showed a similar cooling performance when compared to the steady flow test. The data indicate that the variable flow approach with PID controller can successfully maintain the set surface temperature value at low and moderate heat flux levels. However, at high heat fluxes the current variable flow approach resulted in early CHF at 180 W/cm², while the steady flow approach provided a higher CHF at 208 W/cm². At high heat fluxes, when the surface temperature drops below the set point, the variable flow approach decreases the pumping speed

(or flow rate) to a minimum that can quickly initiate a local dry out and lead to an early CHF before the system can react and increase the pumping speed.

Furthermore, nearly identical surface superheats from the average of last 20 seconds and from the overall period reveals that the surface temperatures in variable flow approach quickly reach steady state condition.

Figure 33 shows how HTC is varies with heat flux in both cases. It can be seen from the plot that variable flow plot exhibited slightly better HTC values when compared with the steady flow test. The highest HTC value in variable flow test is 49.92 kW/m^2°C achieved at 150 W heat flux, whereas it is 48.65 kW/m^2°C achieved at 175 W. It can be seen from the plot that the HTC values in both the tests are achieved in the mid-range heat fluxes.
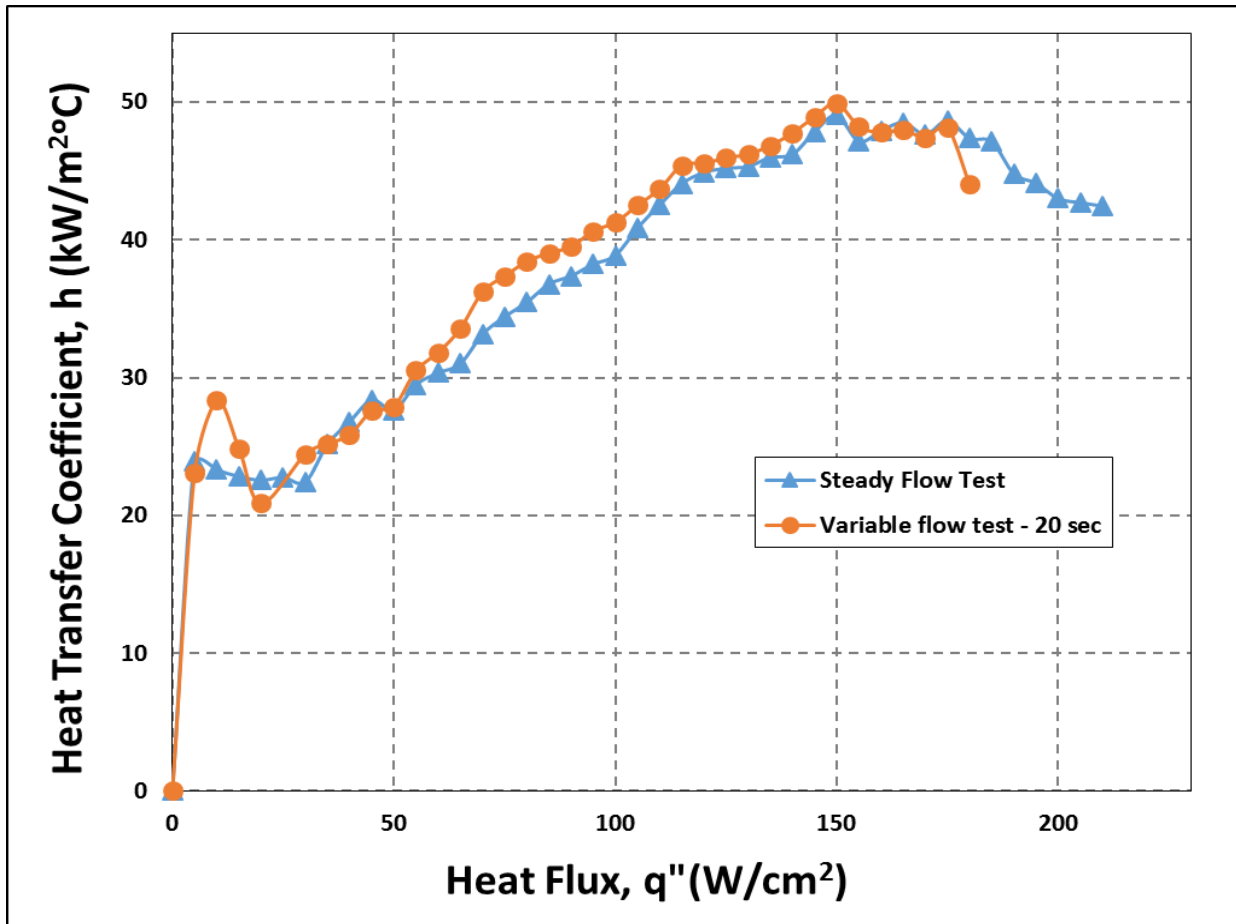
Figure 33: Plot for HTC versus heat flux.

Figure 34 shows the variation of surface temperature with heat flux and time for both variable flow and steady flow tests. It can be observed from the plot that the surface temperature increased with the increase in heat flux and that increase in steps can be clearly seen for the flow initial steps of heat flux increment where it keeps on varying, then after in the variable flow test, and this variation is less in the steady flow test. Since the surface temperature varies above and below the set point for each heat flux range for variable flow test hence the variation in the plot, whereas due to steady flow of coolant in the steady flow test this variation is minimum.

As discussed earlier, surface temperature increases with heat flux and the variation of this surface temperature is increasing at high heat fluxes whereas this variation is even high near the CHF in both the cases. This is because, when the surface is at high temperature it tends to increase its temperature to the maximum value and the coolant provided may not be sufficient to drop the temperature hence the variation and then it attains CHF.

Figure 34: Surface temperature variation with time and heat flux.
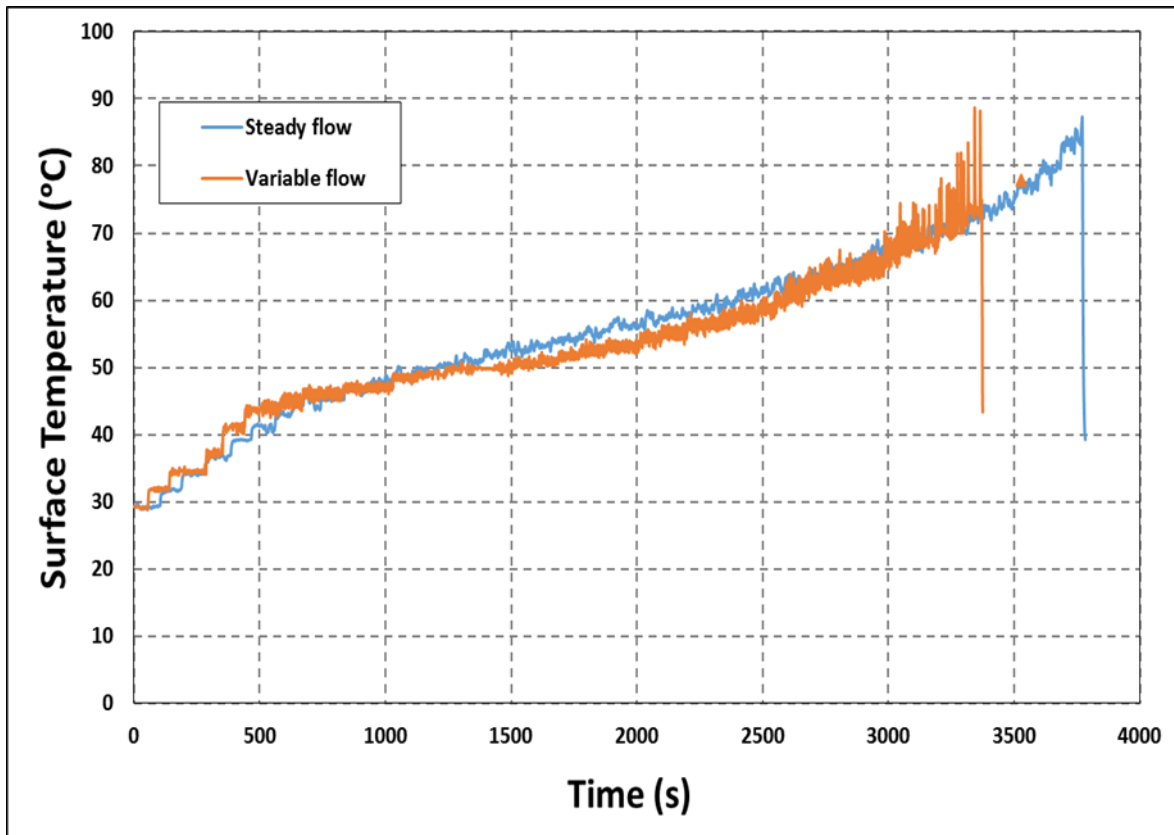
Figure 35 shows the deviation of surface temperature around the set points with time at varying heat flux levels. Whenever the surface temperature is above the set point for each heat flux, pumping power increases increasing the flowrate due to this more amount of liquid is available to absorb heat from the heater surface reducing the surface temperature value below

the set point then the surface temperature tries to increase and goes above set point. The time for which the surface temperature values to remain below the set point depends on the surface behavior at that heat flux. For certain heat fluxes (low and medium), the surface temperature values try to remain below the set point with minimum fluctuation, but at the high heat fluxes this variation is high. Hence the usage of PID is good for low and medium heat flux ranges, and it can be good for high heat fluxes as well, but PID tuning has to be done for those heat flux ranges.

All the surface temperature values falling below the set point indicates the power savings. The increase in surface temperature fluctuation which can damage the electronic component. The usage of PID as high heat fluxes is not advisable as of now until the suitable parameters were found out for that heat flux range.
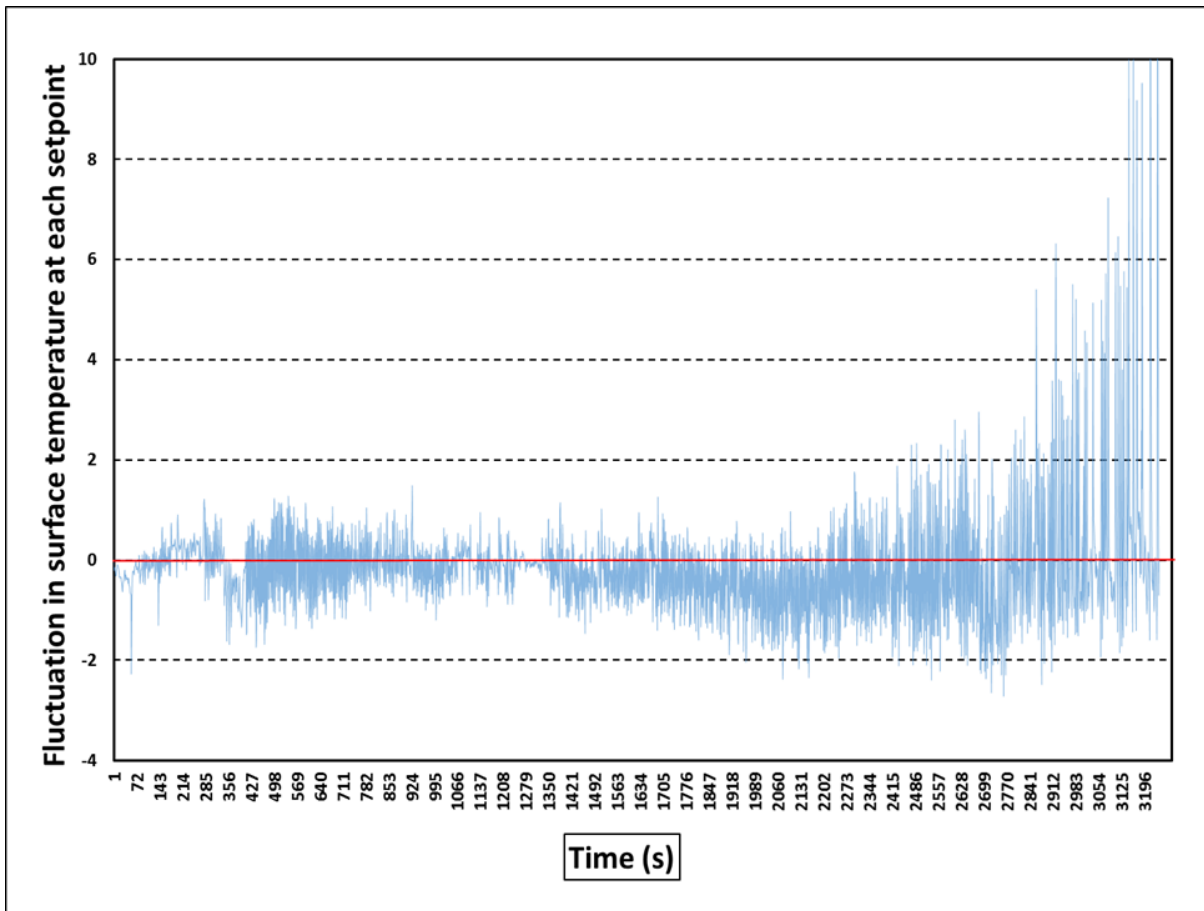
Figure 35: Fluctuation of surface temperature with time and heat flux.

Figure 36 shows the time-averaged pumping power at each heat flux throughout the test at varying heat fluxes. It can be seen from the plot that the pumping power falls below the pumping power required for 4 ml/cm^2.s steady flow test. This indicates that the more amount of pumping power can be saved in a variable flow test. When compared both the last 20 seconds data and the overall data for each heat flux has an increasing trend from 0 W heat flux to the CHF, this is expected because the increase in heat flux increases the surface temperature and it tends to increase to higher value but the spray pattern remains same from 0 W heat flux to CHF. Here the maximum flowrate the pump can reach is 4 ml/cm^2.s, this value is restricted in to

compare it with the steady flow test conditions. The pumping power variation may be different if the maximum power limit is changed. When compared the last 20 second data for each heat flux needed more power than the overall data.
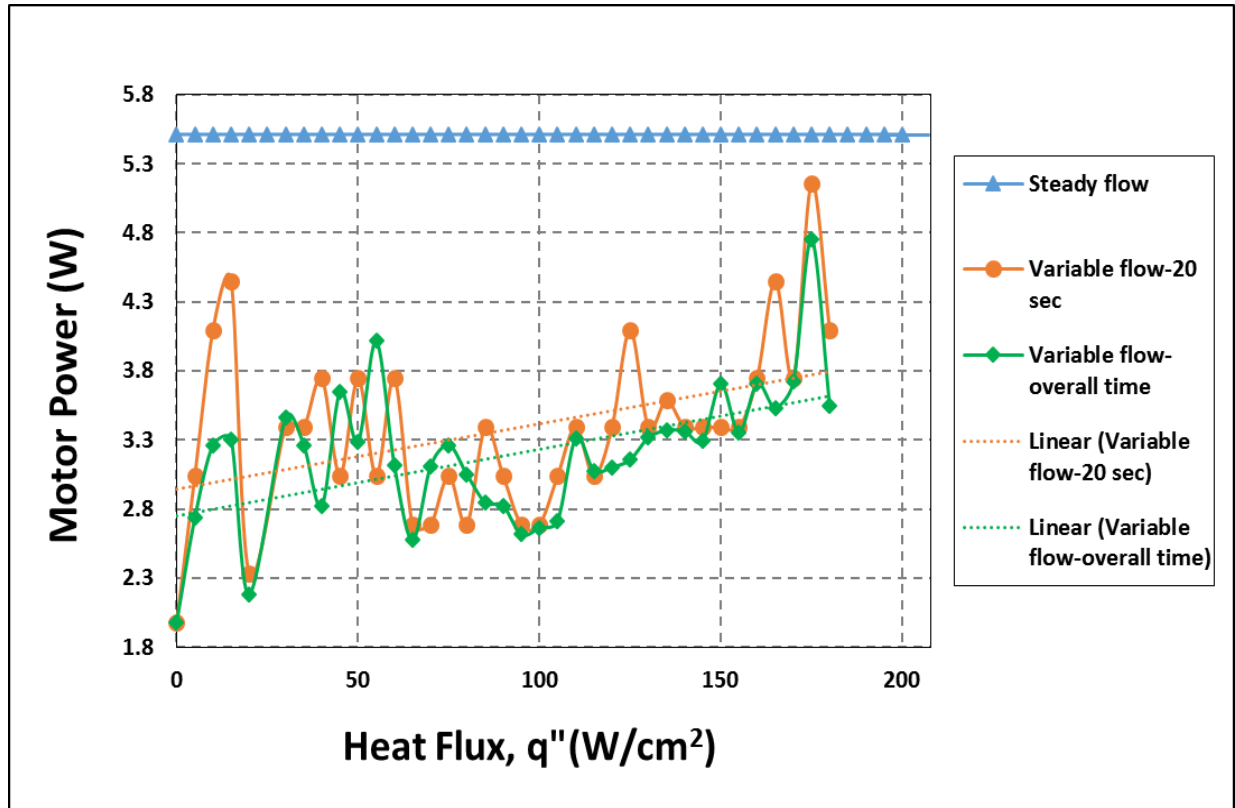

Figure 36: Variation of pumping power with heat flux.

Figure 37 shows the variation of average pumping power at each heat flux level with heat flux in steps. If observed it can be observed from the plot that, for the last 20 seconds data, the pumping power is 3.35 W for up to 50 W heat flux and then it decreased to 3 W for 55 W to 100 W heat flux after that it keep on increasing with heat flux. This is because of the initiation of nucleate boiling in the range of 55 W to 100 W heat flux where the two phases of the coolant exist and evaporation if cooling starts this is where all the latent heat is removed maintaining uniform surface temperature probably most of the values fall below the set points.
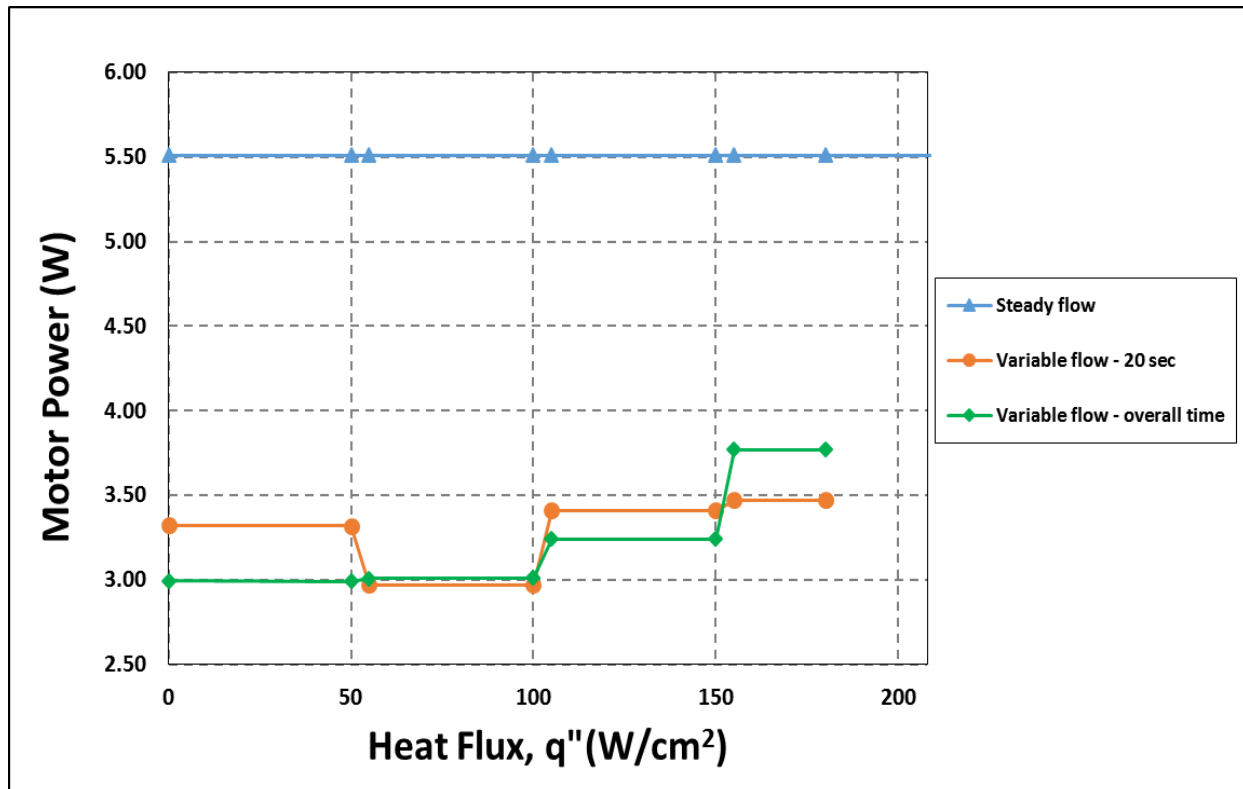
66

Figure 37: Variation of pumping power with heat flux in steps.

However when overall values are considered pumping power was uniform up to 100 W heat flux and then it kept on increasing, this is due to the existence of more initial numbers where pumping power consumed is different when compare to the last 20 second steady values. Table 3 shows the amount of pumping power utilization in both the cases, steady flow test consumes 5.512 W of average pumping power whereas 3.38 W for last 20 seconds data points in variable flow setup i.e. 38.68% power savings and when overall data points are considered pump consumes an average of 3.2 W pumping power i.e. 41.98% savings. The usage of PID controller is saving pumping power whenever the surface temperature falls below set points.

Table 3: Pumping power variation and savings.

Pumping power for steady Flow spray cooling test.	Pumping power for variable Flow spray cooling test	
	Last 20 seconds data	Overall data
5.512 W	3.38 W	3.2 W
Power savings up to	38.68 %	41.98 %

Figure 38 shows the variation of average flowrate at each heat flux with heat flux. Actually flowrate varies in proportion with the pumping power i.e. when the surface temperature goes above the set point pumping power increases, increasing the flowrate and when the surface temperature falls below the set point pumping power decreases, decreasing the flowrate. This flowrate is calculated form the flowmeter reading, the maximum flow that the pump can take is 4 ml/cm².s and the minimum is 2.53 ml/cm².s. The average flowrate for the last 20 second data and the overall data is taken and compared with the steady flow results.

It can be seen from plot that the trend line increases from 0 W to 180 W heat flux. Thus, it can be stated that the flowrate increases with heat flux. This is expected since the surface temperature tries to increase continuously it requires more time to cool it down below the set point hence the increase in flowrate. The flowrate is more in 20 seconds data when compared with the overall data. It can also be noticed that the average flowrate is below 4 ml/cm².s.
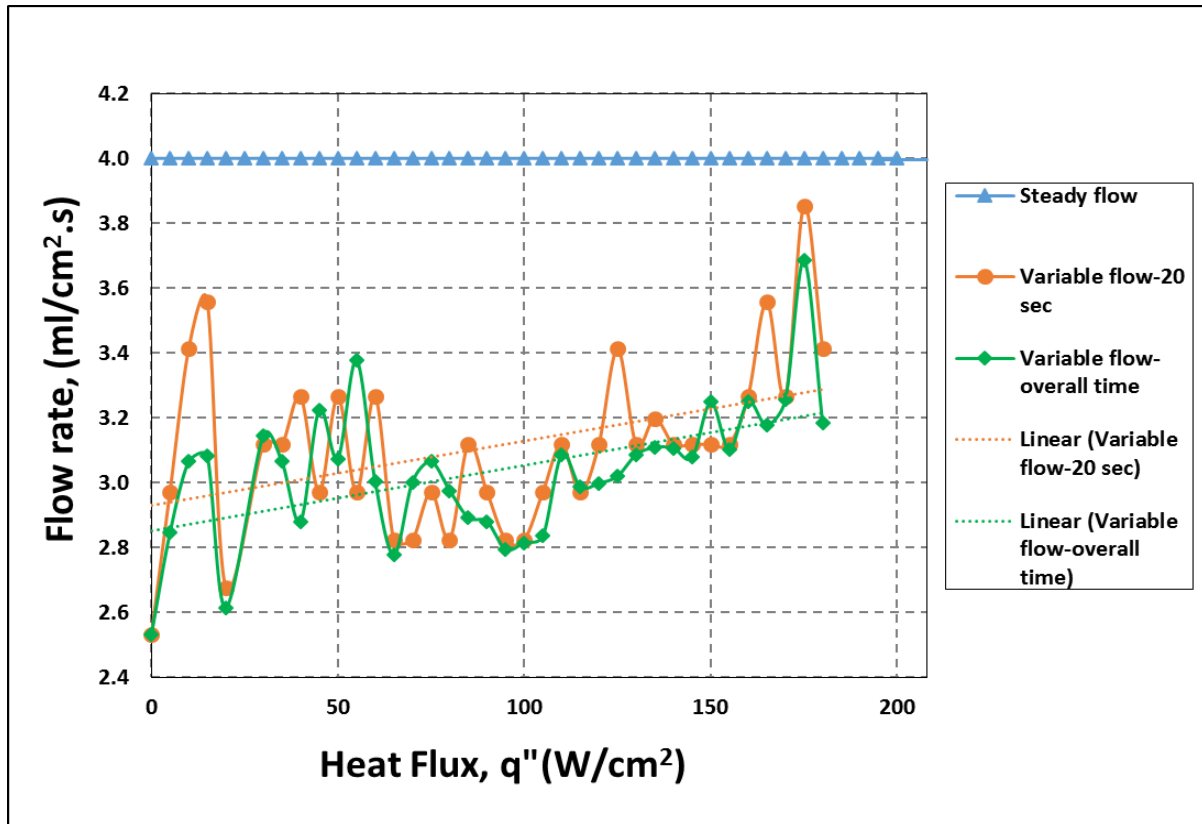
Figure 38: variation of flowrate with heat flux.

Figure 39 shows the variation of average flowrate at each heat flux level with heat flux in steps. It can be observed that when last 20 seconds data are considered, flowrate is around 3 ml/cm^2.s for the heat flux of up to 50 W and it decreased to 2.92 ml/cm^2.s in the next 50 W range of heat flux. Then the flowrate keep on increasing with the heat flux. In the heat flux range if 55 W to 100 W nucleate boiling initiates and the two phase liquid exists. In this range, the surface temperature of the heater remains uniform probably most of the time below set point. Hence the low flowrate. When the overall flowrate values are considered the flowrate constantly increases with heat flux.
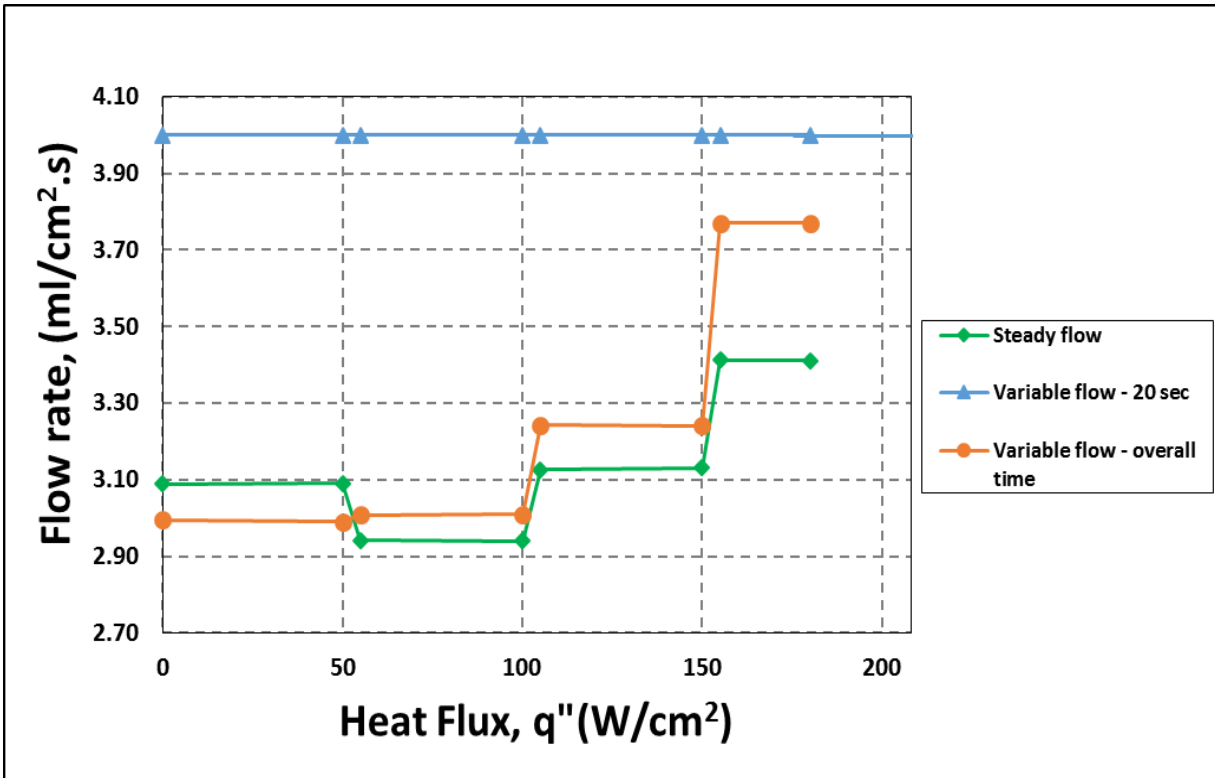
Figure 39: Variation of flowrate with heat flux in steps.

Table 4 shows the amount of coolant utilized in both the cases, steady flow test consumes coolant at an average of 4 ml/cm^2.s whereas 3.11 ml/cm^2.s for last 20 seconds data points in variable flow setup i.e. 22.25% coolant savings, and when overall data points are considered average flowrate of the coolant is 3.04 ml/cm^2.s, i.e. 24% savings. The usage if PID controller is saving coolant usage by decreasing the flowrate whenever the surface temperature falls below the set points.

Table 4: Flowrate variation and coolant savings.

Flowrate for steady Flow spray cooling test.	Flowrate for variable Flow spray cooling test	
	Last 20 seconds data	Overall data
4 ml/cm^2.s	3.11 ml/cm^2.s	3.04 ml/cm^2.s
Coolant savings up to	0.89 ml/cm^2.s (22.25 %)	0.96 ml/cm^2.s (24%)

4.3 Results for Intermittent Flow Spray Cooling

A series of tests were conducted to investigate the effect of intermittent flow spray cooling characteristics with the surfaces RS and MS-E at 30°C subcooling. For intermittent flow, spray frequency was varied between 5-10 Hz, and spray duty cycle was varied between 60-75%, as the two main parameters, to investigate their effect on HTC and CHF.   The results are plotted in the form of surface superheat versus heat flux.

Figure 40 shows the effect of spray frequency on reference surface. These tests were conducted at frequencies of 5 and 10 hz at a constant duty cycle of 60%. It can be observed from the plot that as the frequency of spray increases from 5 hz to 10 hz, there is an improvement in surface superheat and increase in CHF at heat fluxes >60 W/cm^2. Both curves followed the same trend until 30 W/cm^2 heat flux and then the test with 10 hz frequency showed lower surface super heat as the nucleate boiling started.
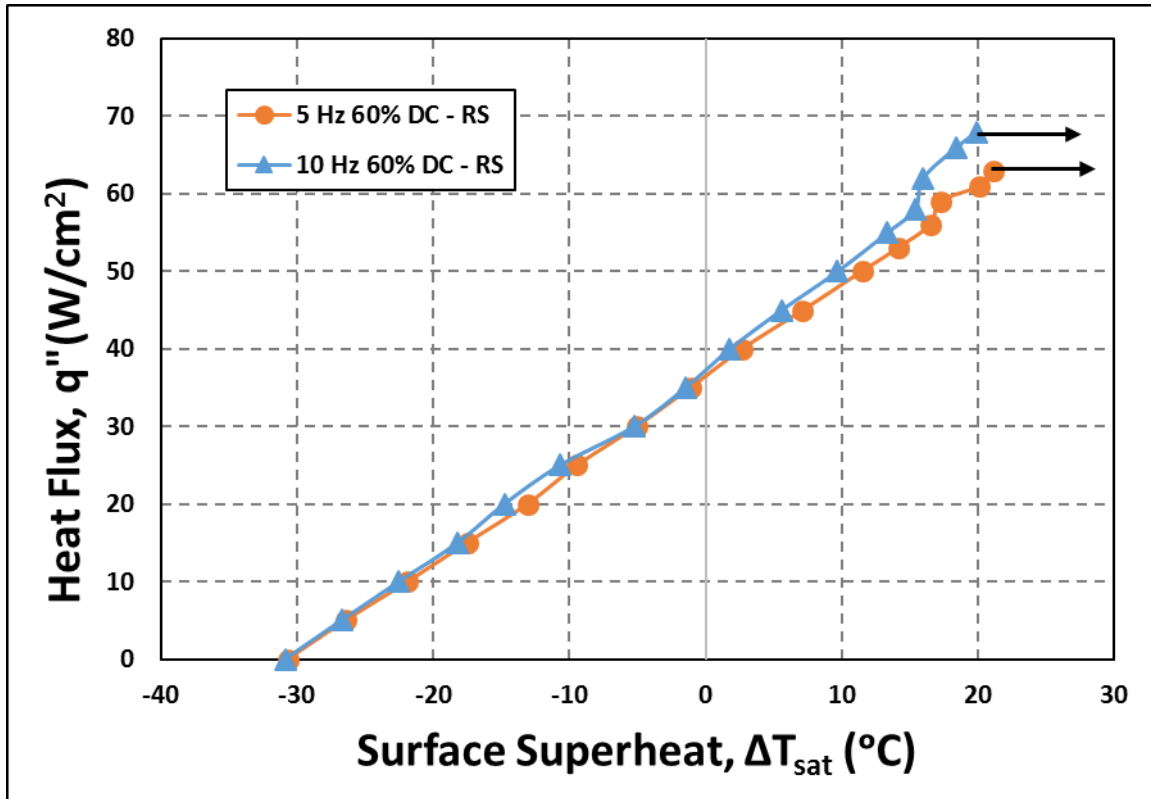
Figure 40: Effect of spray frequency on heat transfer performance of reference surface at 60% duty cycle and 30°C subcooling.

Figure 41 shows the effect of spray frequency on electroplated microporous surface. These tests were conducted at frequencies of 5 and 10 hz at a constant duty cycle of 60%. Both tests showed similar performance up to 80 W/cm² heat flux but the CHF increased from 85 W/cm² to 90 W/cm² with the frequency of spray. There is an increase of 5.8% CHF in 10 hz test when compared to 5 hz test. Comparison of data in Figure 41 and 42 shows that CHF increases with the spray frequency at a given duty cycle.
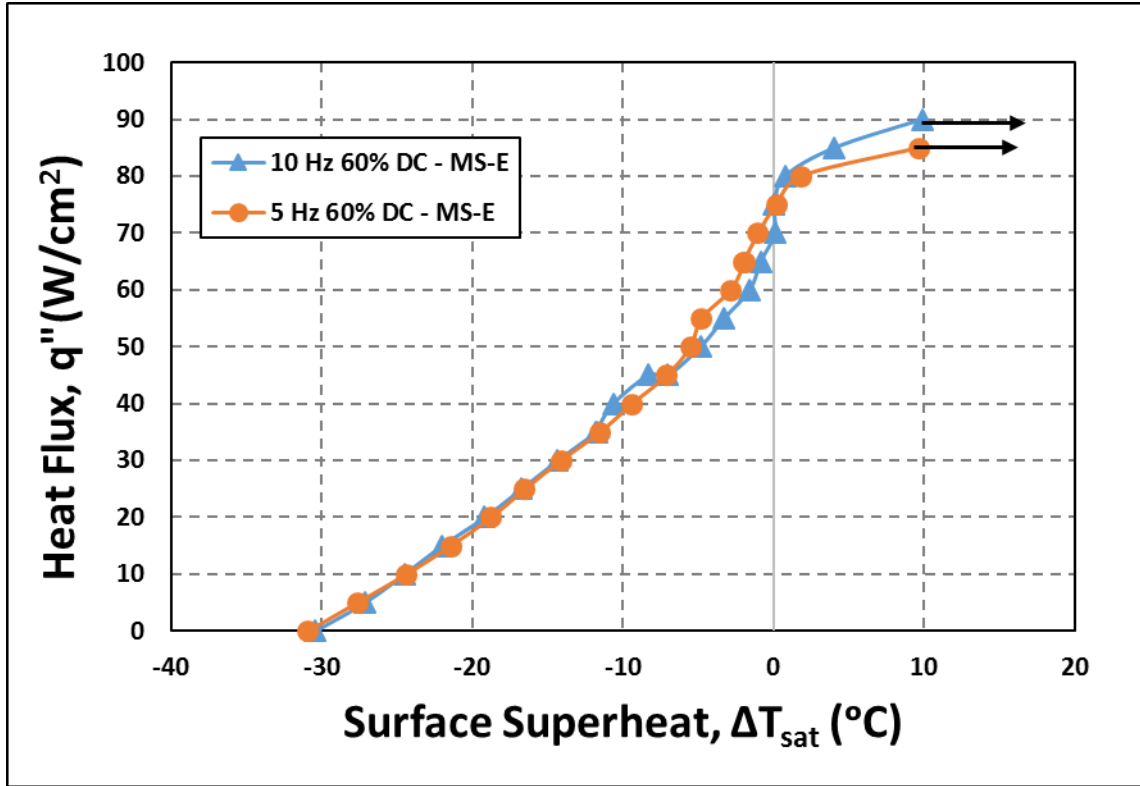
Figure 41: Effect of spray frequency on heat transfer performance of MS-E at 60% duty cycle and 30°C subcooling.

Figure 42 also shows the effect of spray frequency on electroplated microporous surface at an increased duty cycle. These tests were conducted at frequencies of 5 and 10 hz at a constant duty cycle of 75%. Both plots followed a similar trend in general, although at heat flux range of 30-70 W/cm², the test with 5 hz frequency showed lower surface superheat. As expected the CHF increased by 4.7% with 10 hz frequency compared to 5 hz. From all the above three plots we can conclude that CHF increased when the spray is more frequent for the same duty cycle. This can be explained with the better chance of keeping the surface wet at high heat fluxes by using more frequent sprays.
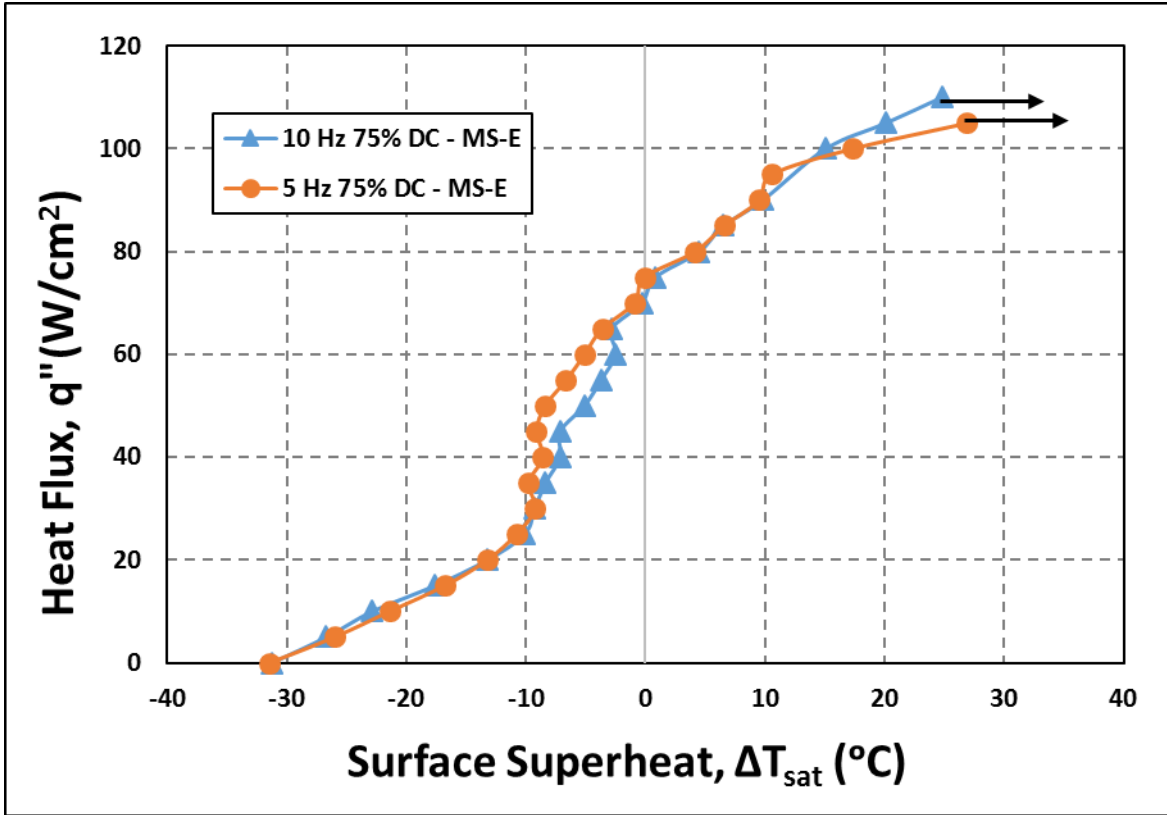
Figure 42: Effect of spray frequency on heat transfer performance of MS-E at 75% duty cycle and 30°C subcooling.

Figure 43 shows the effect of surface enhancement on intermittent flow spray characteristics, by comparing the data from the surfaces RS and MS-E at spray frequency of 5 hz and duty cycle of 60 %. From these data, it can be clearly observed that, there is much lower surface superheat and a significant enhancement in CHF with the surface MS-E over the surface RS. At 60 W/cm² heat flux the surface temperature of MS-E is 57.7°C whereas, it is 80.7°C for RS. Additionally, with the surface MS-E, CHF increased from 63 W/cm² to 85 W/cm² when compared to the surface RS, representing 35% enhancement. Similar to steady and variable flow tests, intermittent flow tests also showed enhancement in CHF and surface temperature with microporous surfaces, as expected.
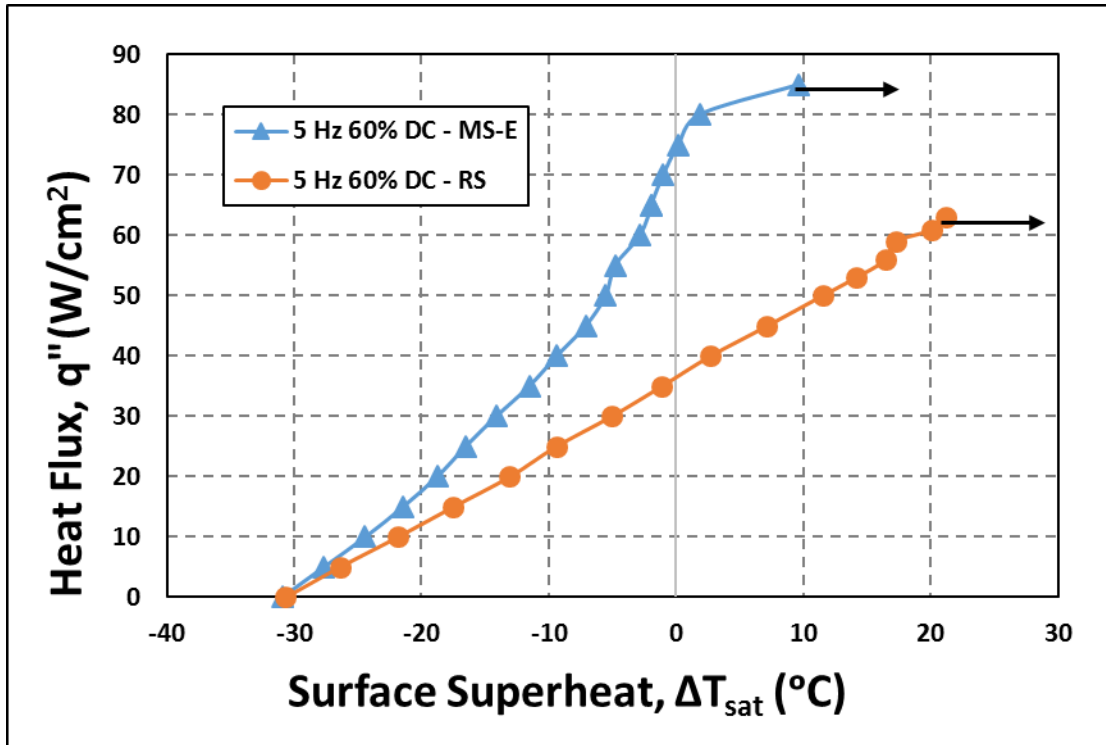
Figure 43: Effect of surface enhancement on heat transfer performance at 5 hz frequency, 60% duty cycle and 30°C subcooling.

Figure 44 shows the effect of spray duty cycle on intermittent flow spray characteristics. These tests were conducted at duty cycles of 60% and 75% and constant frequency of 10 hz. Test with the duty cycle of 60% showed lower surface superheat until 45 W/cm² heat flux, and then followed a similar trend. CHF increased from 90 W/cm² to 110 W/cm² when the duty cycle increased from 60% to 75%, representing 22.2% enhancement. The data show that as the duty cycle (and overall flow rate) increases, CHF increases as expected, and improves the performance towards the benchmark performance of steady flow spray cooling.
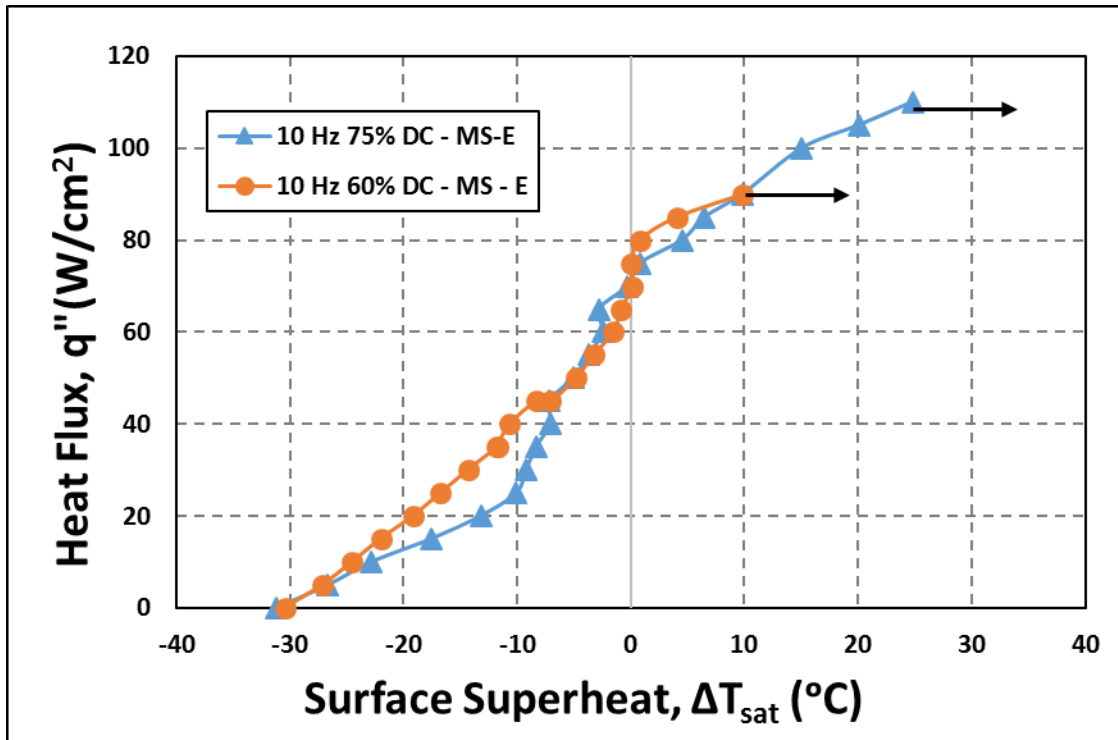
Figure 44: Effect of spray duty cycle on heat transfer performance of MS-E at 10 hz frequency and 30°C subcooling.

Figure 45 compares the steady flow test at a flow rate of 4ml/cm².s and intermittent flow test at 30°C subcooling using both surfaces RS and MS-E. Steady flow test conducted using microporous surface showed best performance with a CHF of 208 W/cm².s whereas, intermittent flow test conducted at a spray frequency of 10 hz and 60% duty cycle using RS showed a least CHF of 68 W/cm².

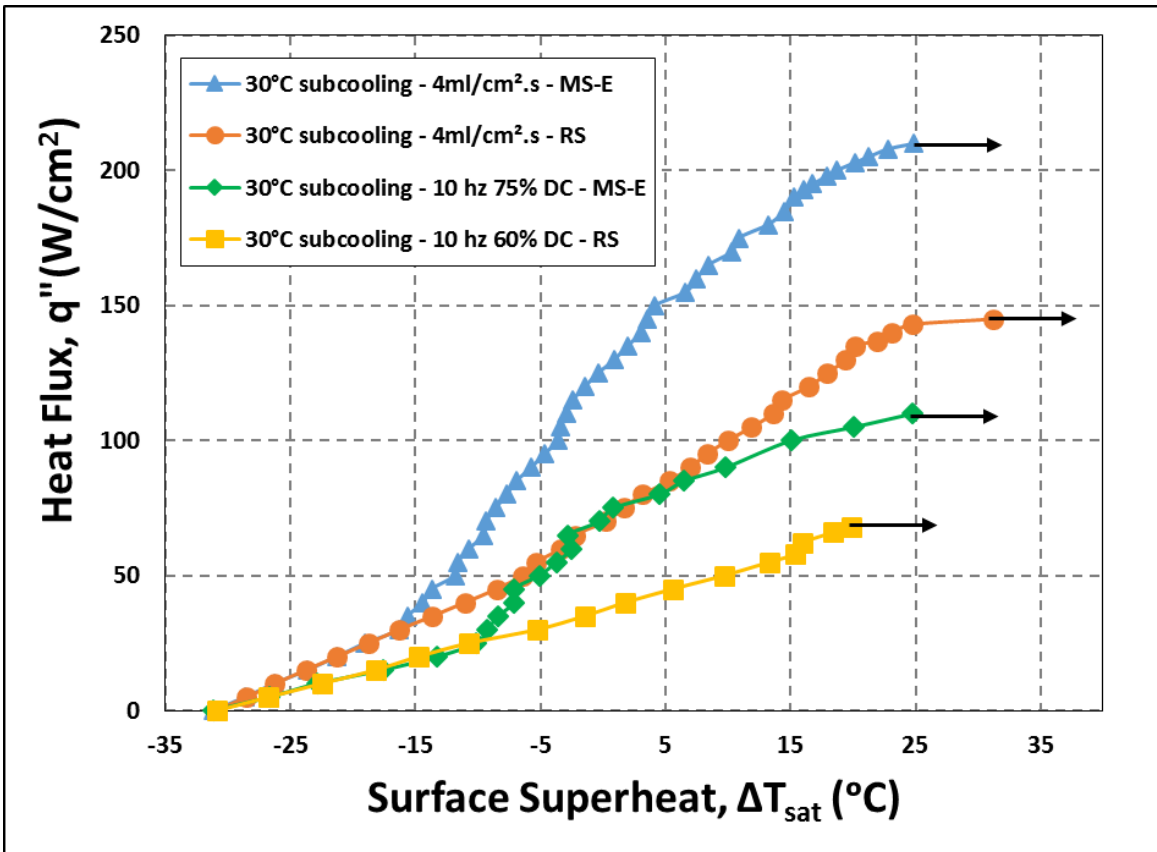Figure 45: Comparison of steady flow at 4 ml/cm².s and intermittent flow at different

frequencies and flowrates at 30°C subcooling.

CHAPTER 5

CONCLUSIONS AND RECOMMENDATIONS

5.1 Concluding Remarks

This study experimentally investigated the performance of spray cooling schemes for dynamic thermal management applications. Tests were conducted using HFE-7100 dielectric liquid as the coolant, a TG0.5 type pressure atomized spray nozzle, and smooth and microporous heat transfer surfaces. The cooling performance was identified in terms of HTC and CHF based on two types of flow conditions, namely, steady flow and dynamic flow (including variable and intermittent flows). The following conclusions were drawn from the obtained results.

- From steady flow, continuous spray cooling experiments, it can be concluded that CHF and HTC values increases with the increase in flowrate for both of the test surfaces. The electroplated microporous surface provides a significant performance enhancement compared to smooth (reference) surface. Spray cooling efficiency decreases as the flowrate increases.

- From variable flow spray cooling experiments, it can be concluded that, an average of 40% pumping power as well as an average of 22% coolant can be saved. Use of PID control in variable flow tests can achieve comparable cooling performance up to 150 W/cm^2 heat flux with electroplated microporous surfaces.

- From intermittent flow spray cooling experiments, it can be concluded that, CHF values increase with spray frequency and duty cycle. Use of intermittent flow approach can save coolant with manageable temperature increases at low to moderate heat flux levels.

5.2 Future Recommendations

Several topics can be recommended for relevant future studies.

- Similar experiments can be conducted to expand the experimental database to include low subcooling and saturated test conditions to better investigate the effects of two-phase heat transfer related mechanisms on dynamic thermal management approaches.

- Additional experiments can be conducted to test the effect of other enhanced surfaces such as hydrophilic, hydrophobic, mixed hydrophilic/hydrophobic, sintered microporous, and particle blasted heater surfaces.

- Variable flow spray cooling approach involving PID controller can be improved through a more comprehensive tuning process that can improve cooling performance at high heat flux ranges.

- Heater aging for the microporous surfaces can be studied, since the heater performance might change over time.

APPENDIX A

FRONT PANEL OF LABVIEW PROGRAM FOR STEADY FLOW SPRAY COOLING SETUP
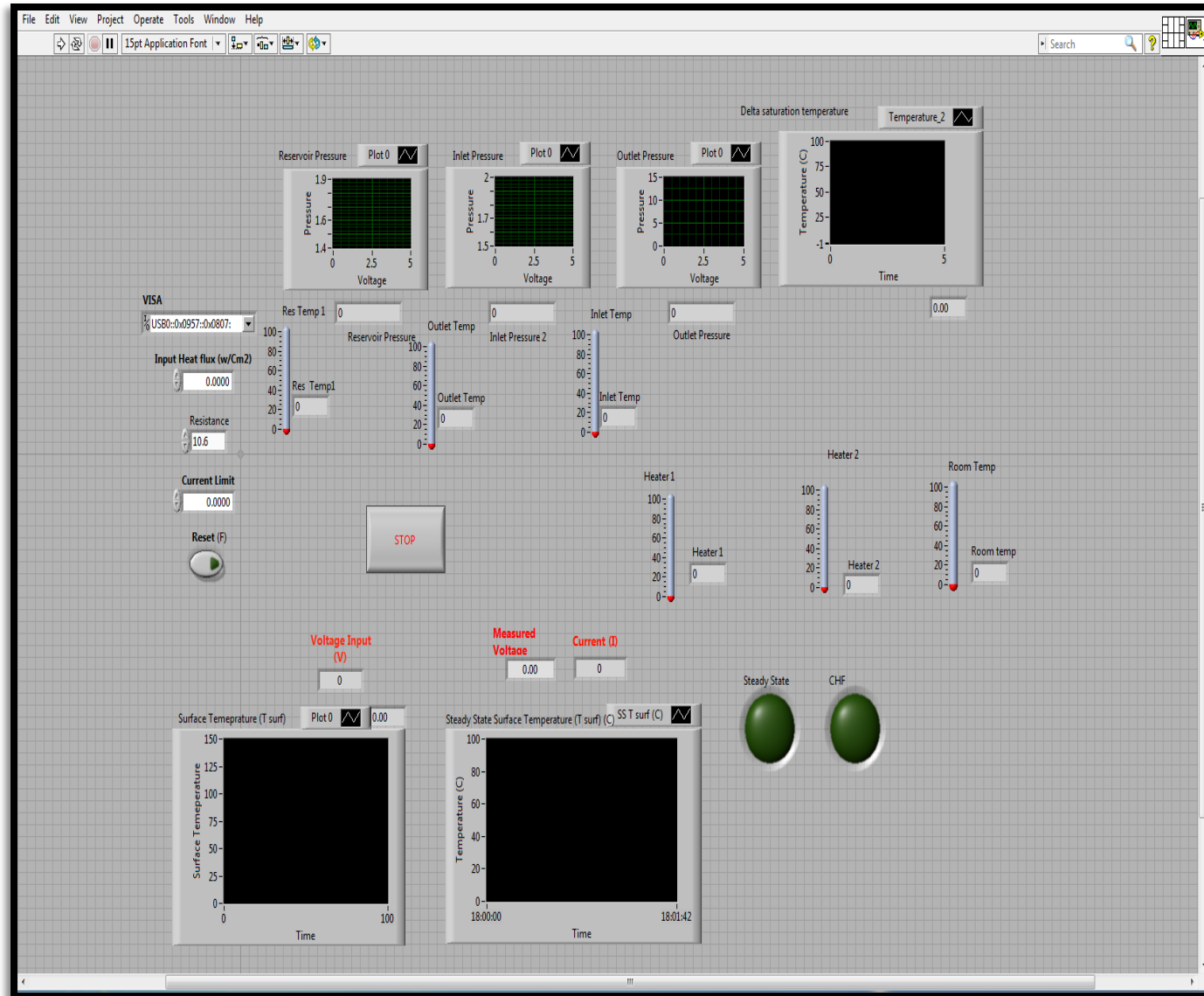
APPENDIX B

BLOCK DIAGRAM OF LABVIEW PROGRAM FOR STEADY FLOW SPRAY COOLING SETUP
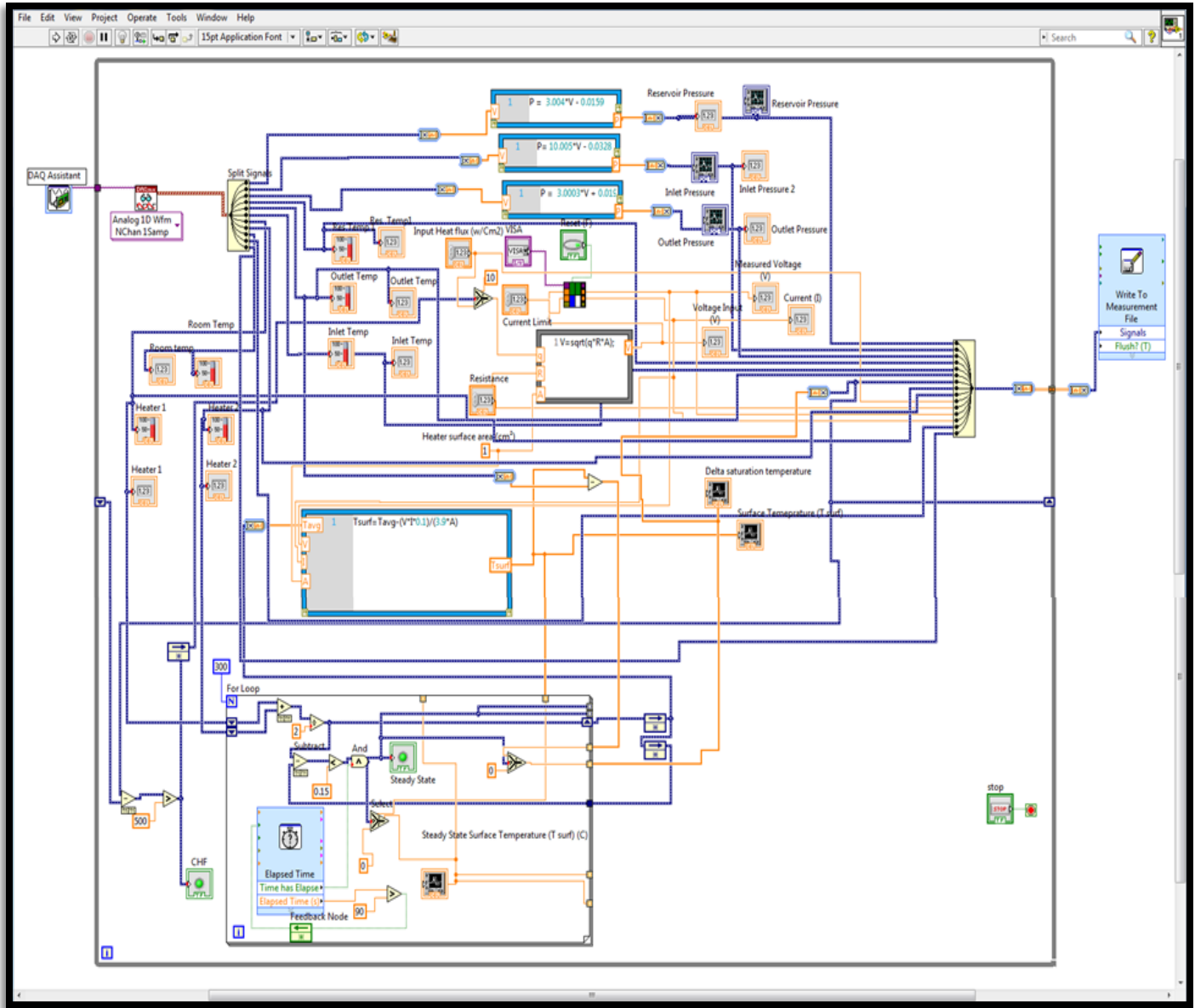
APPENDIX C

FRONT PANEL OF LABVIEW PROGRAM FOR INTERMITTENT FLOW SPRAY COOLING SETUP
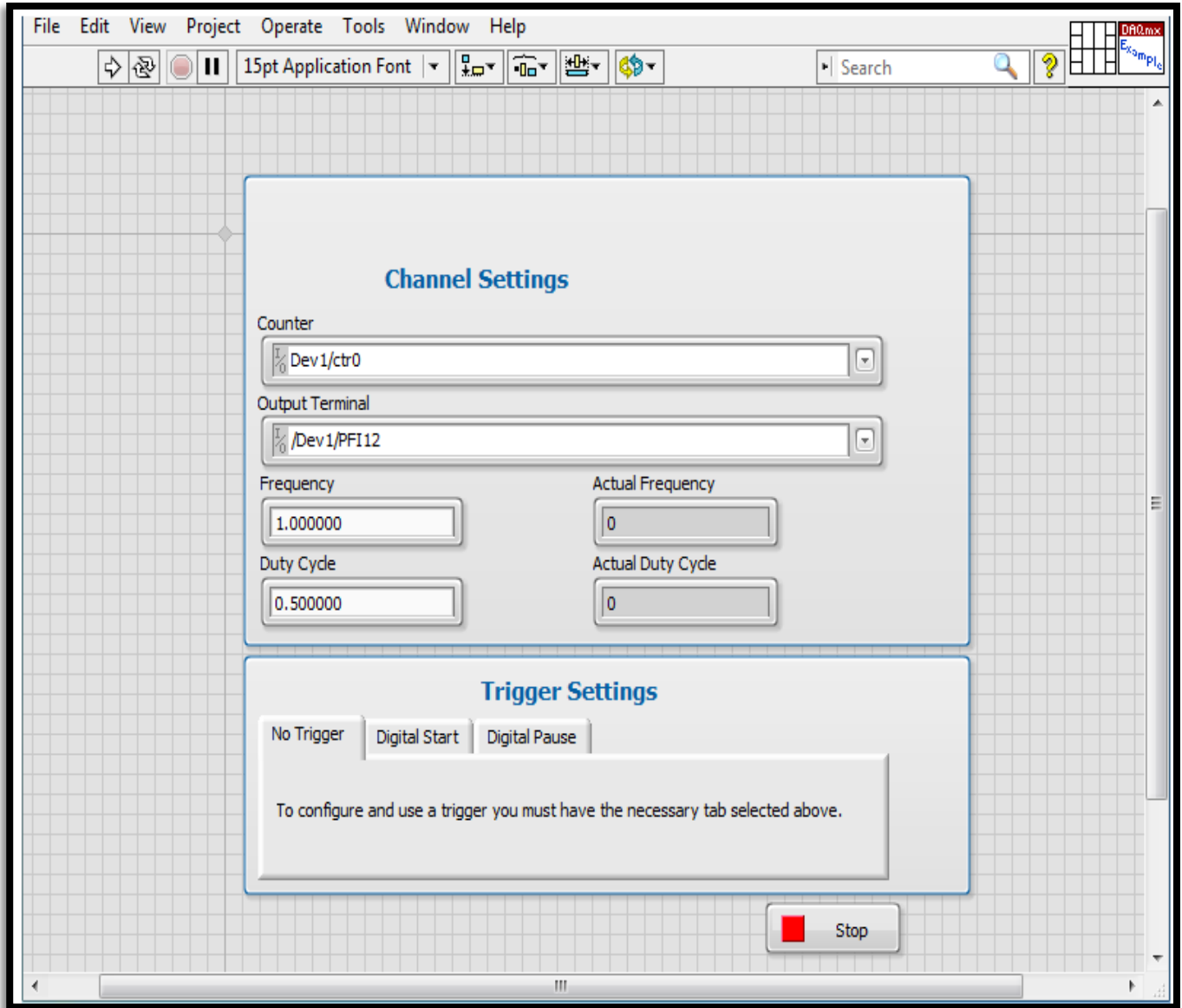
APPENDIX D

BLOCK DIAGRAM OF LABVIEW PROGRAM FOR INTERMITTENT FLOW SPRAY COOLING SETUP
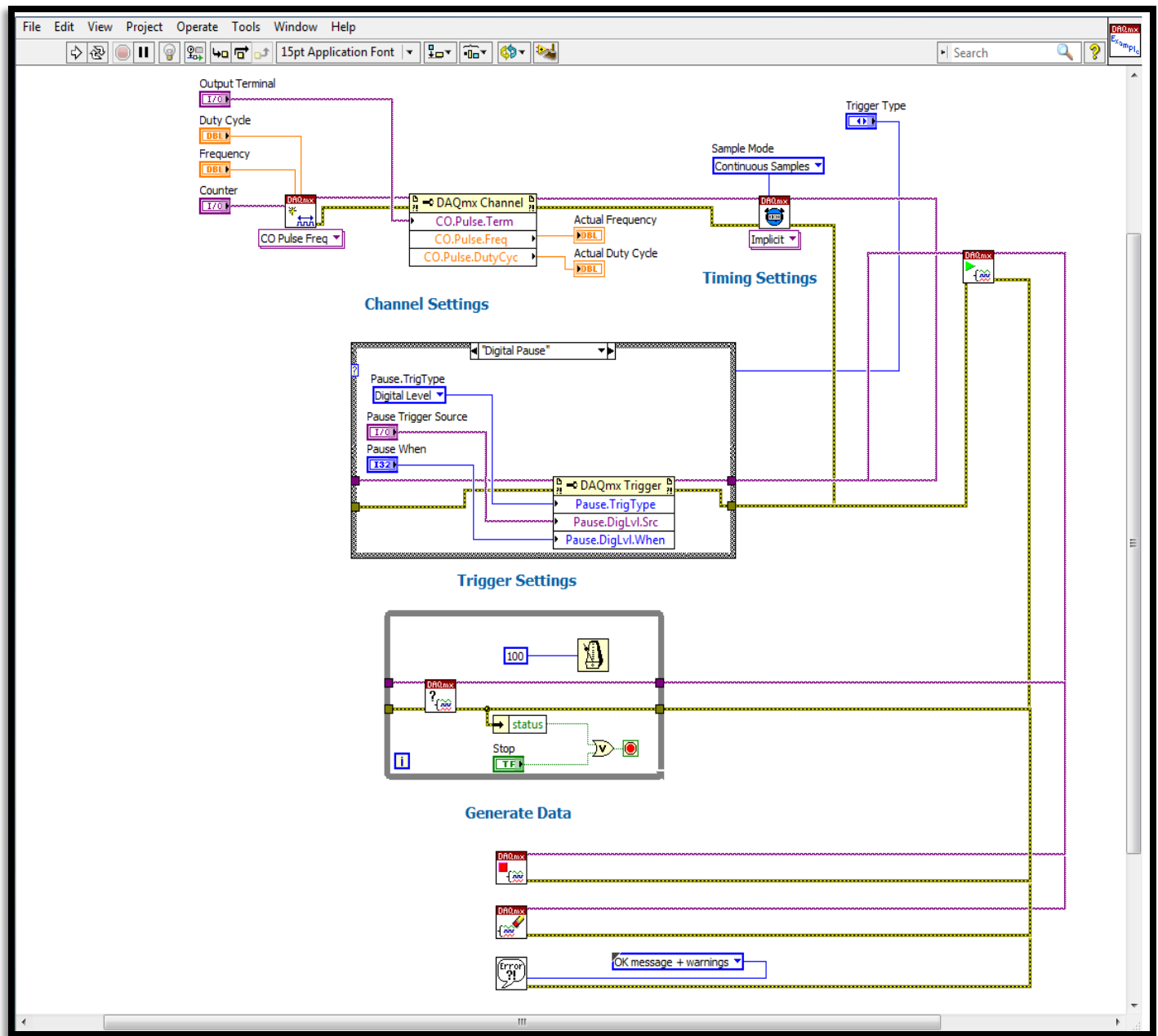
APPENDIX E

FRONT PANEL OF LABVIEW PROGRAM FOR PID CONTROLLED VARIABLE FLOW SETUP

An addition to the program in Appendix A.
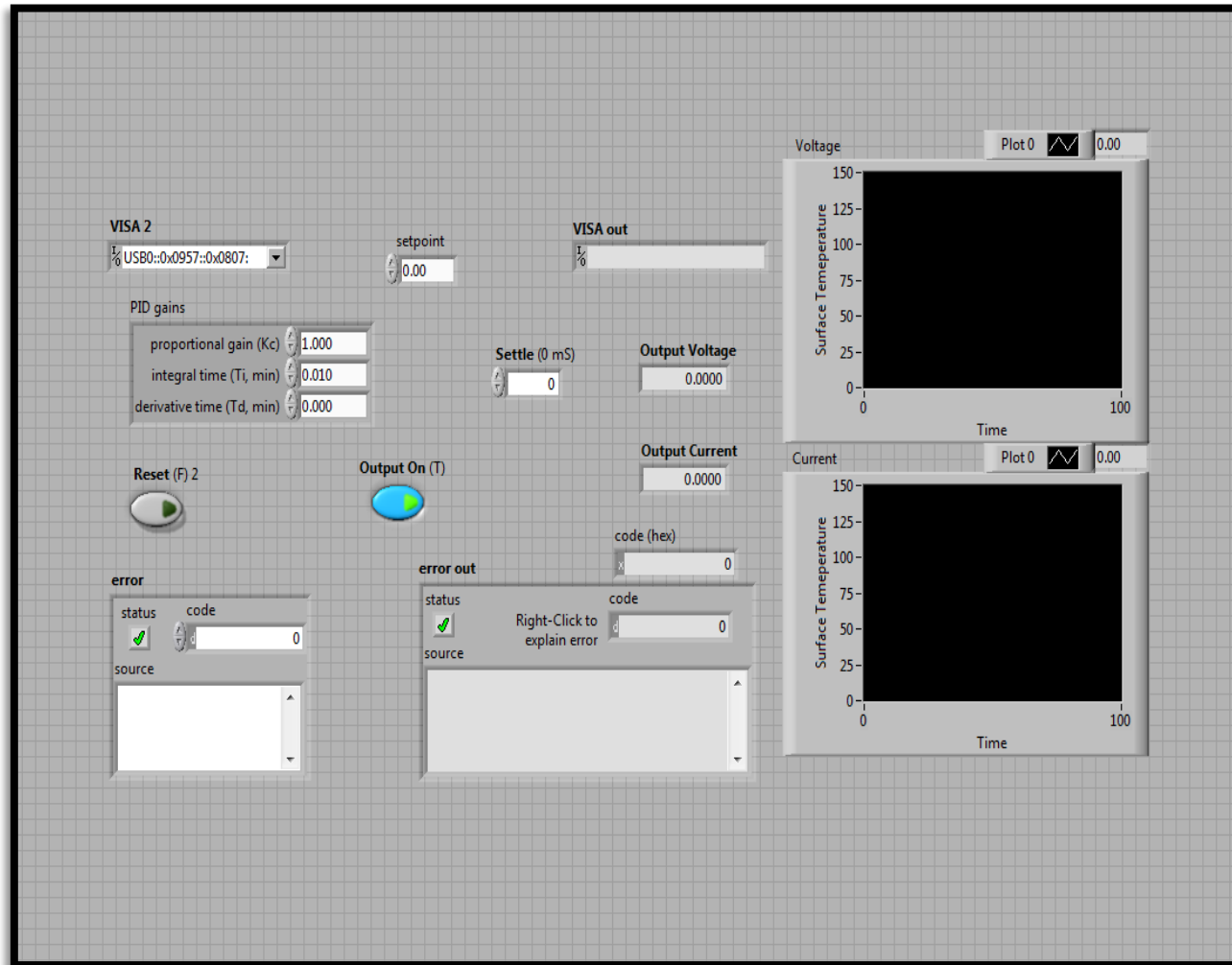
APPENDIX F

BLOCK DIAGRAM OF LABVIEW PROGRAM FOR PID CONTROLLED VARIABLE FLOW SETUP

An addition to the program in Appendix B.
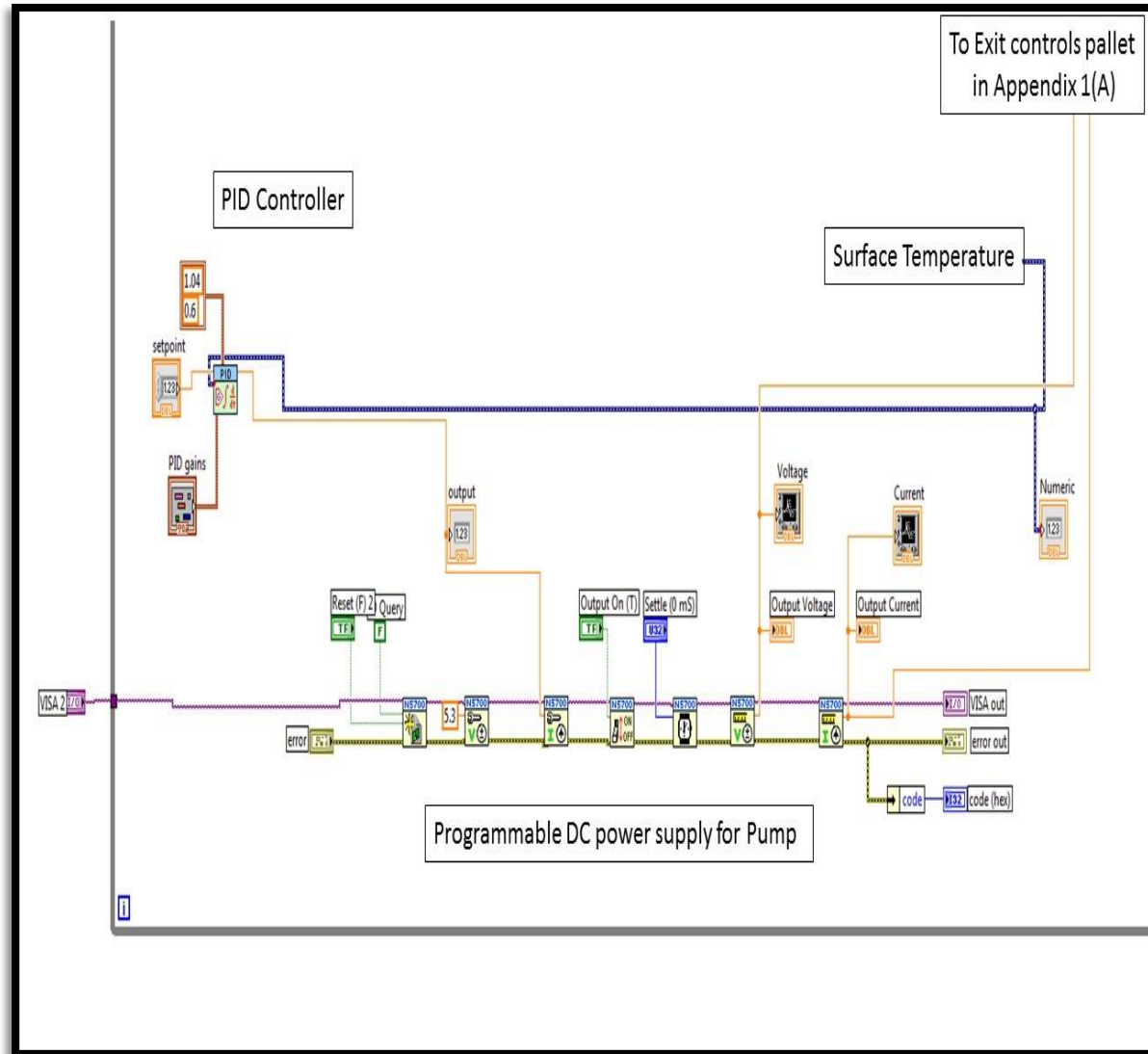
APPENDIX G

PID PARAMETERS

PID Controller
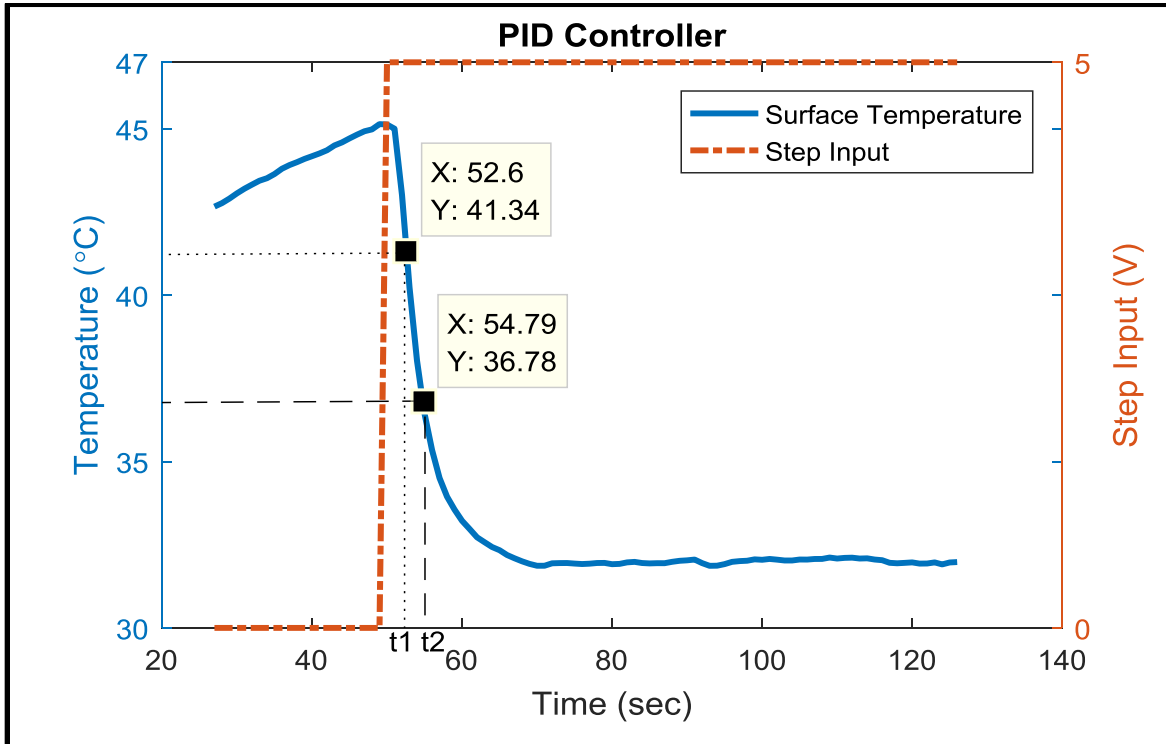
$$K = \frac{m-o}{u-o} = \frac{45-32}{0-5} = \frac{13}{-5} = -2.6$$

$$t_2 = T_{36.78} = 54.79 - 50 = 4.79 \,\text{sec}$$

$$t_1 = T_{41.32} = 52.6 - 50 = 2.6 \,\text{sec}$$

$$\tau = 1.5(t_2 - t_1) = 1.5(4.79 - 2.6) = 3.285 \,\text{sec}$$

$$t_d = t_2 - \tau = 4.79 - 3.285 = 1.505 \,\text{sec}$$

Gain = $K_p = \dfrac{1.2\tau}{Kt_d} = \dfrac{1.2*3.285}{-2.6*1.505} = -1.007$

Integral Time = $T_i = 0.2t_d = 0.301\,\text{sec}$

Derivative Time = $T_d = 0.5t_d = 0.7525\,\text{sec}$

REFERENCES

[1] http://betanews.com/2013/10/15/breaking-moores-law/ (accessed on 10/30/2016).

[2] http://www.gadgetsnow.com/tech-news/By-2040-computers-may-need-more-electricity-than-the-world-can-generate-Report/articleshow/53378223.cms (accessed on 07/25/2016).

[3] http://interestingengineering.com/wont-enough-power-computers-2040/ (accessed on 07/29/2016).

[4] Shabany. Y., "Heat transfer: Thermal management of electronics." Published by Taylor & Francis, Dec 2009.

[5] Glassman, Brian, "Spray cooling for land, sea, air and space based applications, a fluid managment system for multiple nozzle spray cooling and a guide to high heat flux heater design," (2005). Electronic Theses and Dissertations. Paper 327. Department of Mechanical Material and Aerospace Engineering in the College of Engineering and Computer Science. University of Central Florida.

[6] Kim. J. H., "Spray cooling heat transfer: The state of art." International Journal of Heat and Fluid Flow 28, (2007) 753-767.

[7] H. Bostanci, D. P. Rini, J. P. Kizito, V. Singh, S. Seal , L. C. Chow, "High heat flux spray cooling with ammonia: Investigation of enhanced surfaces for HTC." International Journal of Heat and Mass Transfer 75 (2014) 718–725.

[8] Yaddanapudi, Satvik Janardhan. "Spray cooling with Hfc-134a and Hfo-1234yf for thermal management of automotive power electronics," thesis, December 2015; Denton, Texas.

(digital.library.unt.edu/ark:/67531/metadc822762/: accessed July 20, 2016), University of North Texas Libraries, Digital Library, digital.library.unt.edu; .

[9] Issam Mudawar, Desikan Bharathan, Kenneth Kelly, and Sreekant Narumanchi, "Two-phase spray cooling of hybrid vehicle electronics." Components and Packaging Technologies, IEEE Transactions on, 2009. 32(2): p. 501-512.

[10] Mudawar, I. "Assessment of high-heat-flux thermal management schemes." IEEE Transactions on Components and Packaging Technologies, vol. 24, no. 2, June 2001.

[11] L. Lin, R. Ponnappan, "Heat transfer characteristics of spray cooling in a closed loop." International Journal of Heat and Mass Transfer 46 (2003) 3737–3746.

[12] El-Genk, M.S., Bostanci, H. "Saturation boiling of HFE-7100 from a copper surface, simulating a microelectronic chip." International Journal of Heat and Mass Transfer 46 (2003) 1841–1854.

[13] B. Horacek, Kenneth T. Kiger, J. Kim, "Single nozzle spray cooling heat transfer mechanisms." International Journal of Heat and Mass Transfer 48 (2005) 1425–1438.

[14] A. L. N. Moreira, Ana S. Moita, E. Cossali, M. Marengo, M. Santini, "Secondary atomization of drop impactions onto heated surfaces." 13th International Symposium on Applications of Laser Techniques to Fluid Mechanics Lisbon, Portugal, 26-29 June, 2006.

[15] J.H. Kim, S.M. You, Stephen U.S. Choi, "Evaporative spray cooling of plain and microporous coated surfaces." International Journal of Heat and Mass Transfer 47 (2004) 3307–3315.

[16] Mohamed S. El-Genk, Amir F. Ali, "Enhanced nucleate boiling on copper micro-porous surfaces." International Journal of Multiphase Flow 36 (2010) 780–792.

[17] S. J. Thiagarajan, S. Narumanchi, R. Yang, "Effect of flowrate and subcooling on spray heat transfer on microporous surfaces." International Journal of Heat and Mass Transfer 69 (2014) 493 – 505.

[18] S. J. Thiagarajan, R. Yang, C. King, S. Narumanchi, "Bubble dynamics and nucleate pool boiling heat transfer on microporous copper surfaces." International Journal of Heat and Mass Transfer 89 (2015) 1297 – 1315.

[19] C. M. Patil, K.S.V. Santhanam, S. G. Kandlikar, "Development of a two-step electrodeposition process for enhancing pool boiling." International Journal of Heat and Mass Transfer 79 (2014) 989–1001.

[20] S. M. Kwark, J. H. Kim, S. M. You, "Microporous coating by dual-stage electroplating to enhance pool boiling performance of saturated R-123 and FC-72." International Mechanical Engineering Congress and Exposition, IMECE2014-36828.

[21] Arvind Jaikumar, S. G. kandlikar, "Enhanced pool boiling heat transfer mechanisms for selectively sintered open microchannels." International Journal of Heat and Mass Transfer 88 (2015) 652–661.

[22] Y. Zhang, L. Pang, M. Liu, Y. Xie, "Investigation of spray cooling: Effect of different heater surfaces under acceleration." International Communications in Heat and Mass Transfer 75 (2016) 223–231.

[23] T. M. S. Bica, "Thermal and dynamic behavior of drops incidents on micro-structured surfaces." Master's thesis, Department of Mechanical Engineering, Higher Technical Institute, Technical University of Lisbon, (2011).

[24] Wang Jin, Li Yunze, Wang Jun, "Transient performance and intelligent combination control of a novel spray cooling loop system." Chinese Journal of Aeronautics, (2013), 26(5): 1173–1181.

[25] K. M. Yu and J. A. Kim, "Model reference PID control and tuning for steam temperature in thermal power plant." 2011 11th International Conference on Control, Automation and Systems, Gyeonggi-do, 2011, pp. 415-419.

[26] Y. Ding, Y. Li, Y. Li, W. Chen, H. Zhang and D. Li, "Intensive cooling method for power electronic component with high heat flux." 2014 13th International Conference on Control Automation Robotics & Vision (ICARCV), Singapore, 2014, pp. 163-168. doi: 10.1109/ICARCV.2014.7064298.

[27] T. K. Sai and K. A. Reddy, "Design of fuzzy gain scheduler for superheater temperature control in power plant." 2016 2nd International Conference on Control, Instrumentation, Energy & Communication (CIEC), Kolkata, 2016, pp. 521-525. doi: 10.1109/CIEC.2016.7513817.

[28] M. R. O. Panao, A. L. N. Moreira, "Thermo and fluid dynamics characterization of spray cooling with pulsed sprays." Experimental Thermal and Fluid Science 30 (2005) 79–96.

[29] A. L. N. Moreira and M. R. O. Panao, "Heat transfer at multiple-intermittent impacts of a hollow cone spray." International Journal of Heat and Mass Transfer 49 (2006) 4132-4151.

[30] M. R. O. Panao, A. L. N. Moreira, "Two-phase cooling characteristics of a multiple-intermittent spray." 13th International Symposium on Applications of Laser Techniques to Fluid Mechanics.

[31] A. L. N. Moreira, J. Carvalho, M. R. O. Panao, "An experimental methodology to quantify the spray cooling event at intermittent spray impact." International Journal of Heat and Fluid Flow 28 (2007) 191–202.

[32] M. R. O. Panao, A. L. N. Moreira, "Intermittent spray cooling: A new technology for controlling surface temperature." International Journal of Heat and Fluid Flow 30 (2009) 117–130.

[33] M. R. O. Panao, A. M. Correia, A. L. N. Moreira, "High power electronics thermal management with intermittent multijet sprays." International journal of Applied thermal engineering 37 (2012) 293-301.

[34] S. Somasundaram and A. A. O. Tay, "Intermittent spray cooling — Solution to optimize spray cooling." Electronics Packaging Technology Conference (EPTC), 2012 IEEE 14th, Singapore, 2012, pp. 588-593. doi: 10.1109/EPTC.2012.6507150.

[35] S. Somasundaram, A. A. O. Tay, "An experimental study of closed loop intermittent spray cooling of ICs." International Journal of Applied Thermal Engineering 31 (2011) 2321-2331.

[36] B. Majaron, L. O. Svaasand, G. Aguilar, J. S. Nelson, "Intermittent cryogen spray cooling for optimal heat extraction during dermatologic laser treatment." Physics in Medicine and Biology 47 (2002) 3275–3288.

[37] K.J. Astrom, T. Hagglund, "Revisiting the Ziegler Nichols step response method for PID control." Journal of Process Control 14 (2004) 635–650.

[38] J.G. Ziegler, N.B. Nichols, "Optimum settings for automatic controllers." Transactions of ASME, 64 (1942) 759–768.

[39] Aidan O. Dwyer, "Handbook of PI and PID controller tuning rules." Third edition, Imperial College Press, 2009.

[40] M.T. Ho, A. Datta, S.P. Bhattacharyya, "Design of P, PI and PID controllers for interval plants." Proceedings of the American Control Conference (1998).

[41] Ming-Tau Ho, A. Datta and S. P. Bhattacharyya, "A new approach to feedback stabilization," *Proceedings of 35th IEEE Conference on Decision and Control*, Kobe, 1996, pp. 4643-4648 vol.4. doi: 10.1109/CDC.1996.577606.

[42]   http://aldax.se/wp-content/uploads/2012/07/Series-99-Data-Sheet.pdf   (accessed   on 02/10/2015).

[43]   http://www.appliedprocessor.com/pdf/APM_PWMC-500_datasheet.pdf   (accessed   on 04/12/2016).

[44]   http://multimedia.3m.com/mws/media/199818O/3mtm-novectm-7100-engineered-fluid.pdf (accessed on 06/14/2015).

[45]   http://www.me.umn.edu/courses/me4331/FILES/NOVEC7000.pdf   (accessed   on 04/07/2016).

[46] Joshua, Nihal E. Direct Immersion Cooling Via Nucleate Boiling of HFE-7100 Dielectric Liquid on   Hydrophobic   and   Hydrophilic   Surfaces, thesis, December   2014; Denton,   Texas. (digital.library.unt.edu/ark:/67531/metadc699916/: accessed   June   16,   2016), University   of North Texas Libraries, Digital Library, digital.library.unt.edu; .

[47] Satvik. Y. J, H. Bostanci, "Spray cooling with HFC-134a and HFO-1234yf for thermal management of automotive power electronics." International Mechanical Engineering Congress & Exposition, IMECE2015-52312.

[48] A. G. Pautsch, T. A. Shedd, "Spray impingement cooling with single and multiple nozzle arrays. Part I: Heat transfer data using FC-72." International Journal of Heat and Mass Transfer 48 (2005) 3167–3175.